九州大学学術情報リポジトリ
Kyushu University Institutional Repository

High-speed directly modulated lasers with photon-photon resonance (PPR) by utilizing active-multimode interferometer (MMI) laser diode

肖, 何

https://hdl.handle.net/2324/7329390

出版情報：Kyushu University, 2024, 博士（学術）, 課程博士
バージョン：
権利関係：

KYUSHU UNIVERSITY

High-speed directly modulated lasers with photon-photon resonance (PPR) by utilizing active-multimode interferometer (MMI) laser diode

Department of Applied Science for Electronics and Materials

Interdisciplinary Graduate School of Engineering Sciences

Kyushu University

Japan

He Xiao

March 2024

Abstract……1

Chapter 1 Introduction…….……...3

1.1 Background: optical connection for supercomputer system 3

1.2 Directly modulated lasers: State of the art 10

1.3 Photon-Photon resonance (PPR): state of arts 17

1.4 Outline of this thesis 21

Reference 23

Chapter 2 Photon-photon resonance phenomenon in active-MMI laser as Fabry-Perót (F-P) laser...……42

2.1 Introductory overview 42

2.2 Mode orthogonality in F-P laser 43

2.3 Non-orthogonality in active-MMI laser diode 46

Reference 56

Chapter 3 Theoretical analysis of Photon-photon-resonance in active-MMI lasers diode……...……. 62

3.1 Introductory overview 62

3.2 rate equation of PPR in active MMI LD 63

3.3 PPR frequency, width, and height control by using active-MMI laser diode 76

3.3.1 Coupling efficiency 76

3.3.2 Phase difference 79

Reference 82

Chapter 4 Overshoot affection in frequency response of photon-photon-resonance (PPR) on high-speed laser diode…….……...89

4.1 Introductory overview 89

4.2 Numerical calculation of large signal modulation response based on small signal modulation response 90

4.3 Simulation results 92

4.4 Discussion of overshoot to large signal modulation 96

Reference 100

Chapter 5 Active-MMI LD design for optimizing PPR utilization..102

5.1 Introductory overview 102

5.2 Theory of Multimode Interferometer 103

5.3 Coupling efficiency control scheme in active-MMI LD 110

5.4 Discussion of designed active-MMI LD 118

5.4.1 Affection of carrier plasma effect to active-MMI laser diode 118

5.4.2 Temperature 120

5.4.3 Fabrication tolerance 121

5.5 Modulation speeds over 100 Gbps 122

Reference 130

Chapter 6 Conclusion and outlook…….……132

6.1 Conclusion 131

6.2 Outlook 132

Acknowledgement …….……...135

Abstract

This thesis is about the research on high-speed modulation laser with photon-photon phenomenon (PPR). The PPR theory in small signal modulation response has been discussed. The affection of PPR to large signal modulation response has also been clarified. Based on the PPR principle in small signal modulation response and large signal modulation response, we proposed a special mode-selective active-MMI configuration to explore PPR phenomenon.

Not only does the computer processing speed rely on the processor performance, but also on the interconnection rate. It is forecasted that the interconnection speed in supercomputer will exceed 1 Tbps in the near future. For this reason, optical interconnection has been already deployed in supercomputer. And the similar performance of the supercomputer will be required in personal computer (PC) later after a few decades according to the past background. [5]. Optical interconnection, therefore, may be expected to be introduced also into mobile devices including PC, smartphone, and others. For these applications, directly modulated laser diode (DML) is one of the candidates with the merits of small footprint, and relatively low cost. The DML's modulation bandwidth is restricted in principle by the so-called relaxation oscillation frequency (or in other word, carrier photon resonance (CPR) frequency.

One possible way to overcome the restriction of relaxation oscillation is to

utilize PPR which is known to display higher frequency resonance compared to CPR. Another resonance peak in addition to CPR improves the damping at higher frequency. Therefore, the so-called -3 dB bandwidth is extended compared to the case without PPR. To achieve higher frequency response without -3 dB degradation in the bandwidth, one important thing is to optimize the peak position, width and height (i.e. the control scheme of PPR peak), however, it seems the investigation as to the control scheme is still not sufficient. And almost all the research on PPR are concentrated on its small signal modulation response that its affection to large signal modulation response has not discussed yet. In this work, the PPR control mechanism by utilizing active-MMI laser geometries. we also proposed a special active-MMI laser configuration to realize the control of PPR.

Chapter 1

Introduction

1.1 Background: optical inter-connection for supercomputer system

1.1.1 Interconnections in supercomputer

With the development of modern society, the demands for extremely high-speed computation for complicated scientific and engineering work such as testing mathematical models for complex physical phenomena or designs of climate and weather, the evolution of the cosmos, nuclear weapons and reactors, new chemical compounds (especially for pharmaceutical purposes), and cryptology [1-9] are rising rapidly. All such needs can be realized through supercomputer to process vast volumes of data quickly and efficiently. The performance of supercomputers has experienced steady growth in the last decade and has mainly kept up with the intensive computation needs of advanced scientific studies. Fig1.1 shows the trends of relative evolution of the average of the most powerful 10 supercomputers in terms of total computer power growth [10].

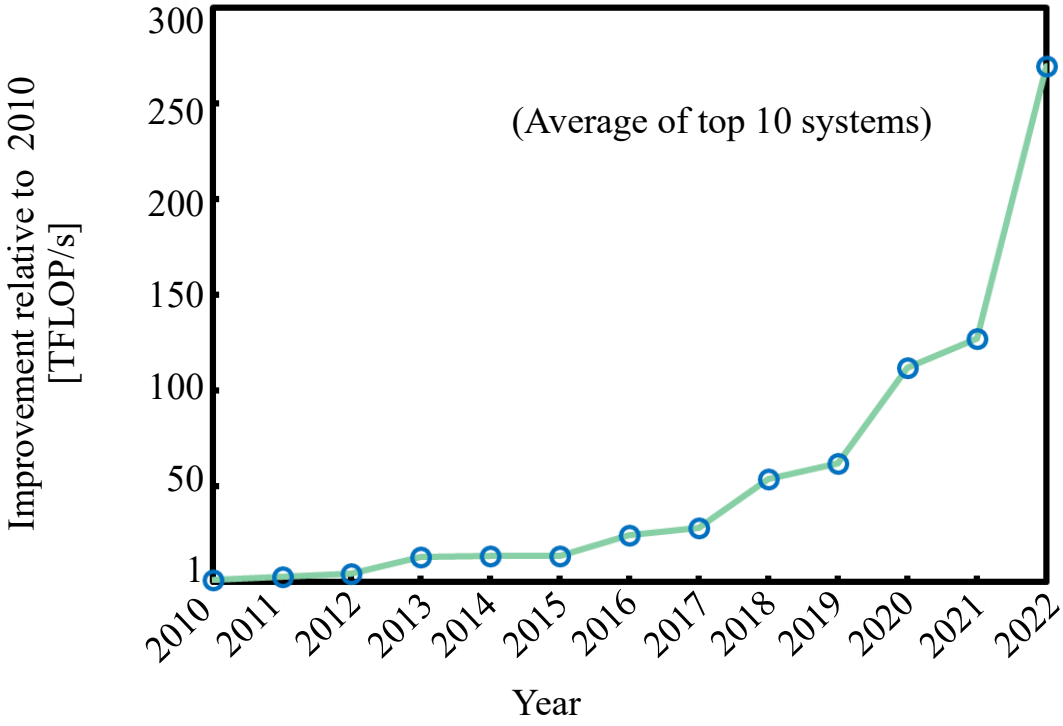

Fig.1.1 Computer power growth in past years [10]

It shows that the power of supercomputer dramatically. To achieve high-performance computers (HPC), large-scale multichip systems have been built and the number of cores in one computer has also been increased as shown in Fig 1.2 (Average of the top ten powerful computers from 2012-2022). This multicore approach, however, only makes sense if each core can receive and transmit large messages from all other cores simultaneously. In other words, bulk computing power requires adequate interconnection to become a real supercomputer. Each FLOP (floating point operations per second) on a chip has to be grouped with enough bandwidth for data exchange with other nodes.

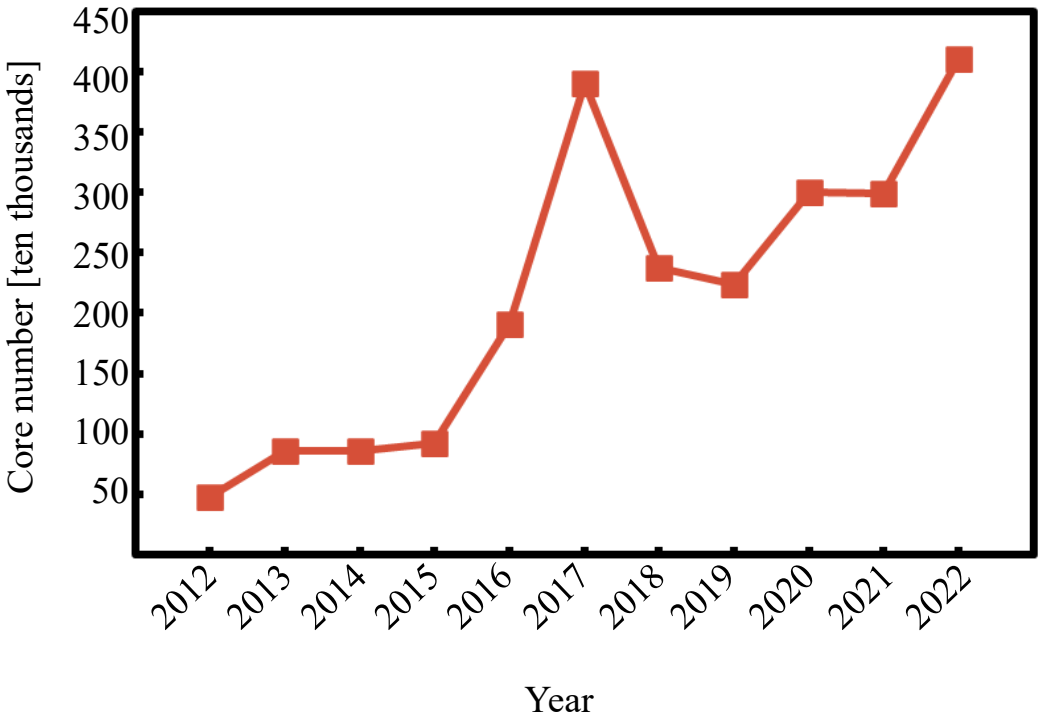

Fig.1.2 Computer core growth in last ten years [10]

Table 1.1 shows the capabilities of the main interconnects used in supercomputer.

Tab 1.1 Capabilities of main interconnects

Name	year	Node to node Bandwidth (GB/s)
Tofu [11]	2010	4.76
Infiniband QDR-4x [12,13]	2010	3.4
Infiniband FDR-4x [12,13]	2011	6.3
BlueGene/Q [14]	2012	1.75
TH express-2[15]	2013	11.8
Tofu 2[16]	2014	11.46
Infiniband EDR-4x [17]	2015	8
Tofu D [18]	2018	6.35
Slingshot-10 [19]	2020	12.5

In 2010, the typical interconnect was based on Infiniband QDR, which is providing MPI bandwidth of 3.4 GB/s. In 2020, the Slingshot was used in the world's first exascale and the most powerful supercomputer system in 2023 [20] offering 12.5 GB/s. The progress of bandwidth is appreciable, however, substantially slower than the one of the FLOPs/node. Small byte/FLOPs ratio tends to negatively impact the efficiency of supercomputer systems. This situation is able to be ameliorated by the development of optical transmission techniques [21].

1.1.2 Optical communication technology

Optical communication is an ancient technology for human beings. Lots of methods such as fire, and light reflected from the sun have been used to transfer information. It is rapidly modernized photonics that integrate optics and electronics in single devices with the development of science and technology. In this section, modern optic transmission techniques have been introduced.

Wavelength Division Multiplexing (WDM) is a fiber-optic transmission technique that enables the use of multiple light wavelengths (or colors) to send data over the same medium [22]. The scheme of WDM is shown in Fig. 1.3 modulated signal is generated by four laser diodes (LD) whose wavelengths are different from each other. all those lights would be transferred to the device called multiplexer respectively. The multiplexer

joins all the light together. When the lights propagate to Demultiplexer, all the light will be divided based on their wavelength and detected by the photon diode (PD). They are assuming that the frequency of the modulated signal is 50 Gbps for one channel. In the example in Fig.1.3, there are four channels. It means that the capability of this system is 200 Gbps. And if there are 20 channels in one system and the capacity for each channel is 50 Gbps too, 1 Tbps capacity will be achieved. it also suggests that with the increasing capacity of each channel and the number of channels, the capacity of this WDM system will grow.

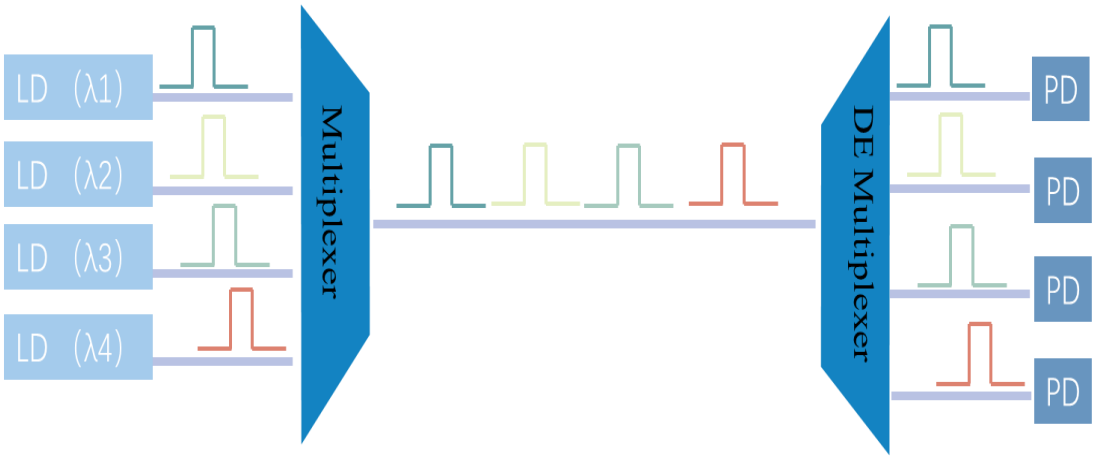

Fig.1.3 Scheme for WDM system

In WDM there are two categories, CWDM (coarse wavelength division multiplexing) and DWDM (dense wavelength division). The principle of CWDM and DWDM is shown in Fig.1.4 and Fig.1.5. A CWDM system on 20-nm channel is spaced from 1470 nm to 1610 nm [23].

Unlike the CWDM, DWDM system is defined in terms of frequencies as

shown in Fig. 1.4. DWDM involves the process of multiplexing many different wavelength signals onto a single fiber, carrying 40, 80, 96 or up to 160 wavelengths by utilizing a much narrower spacing 0.8/0.4 nm (100 GHz/50 GHz grid) [24].

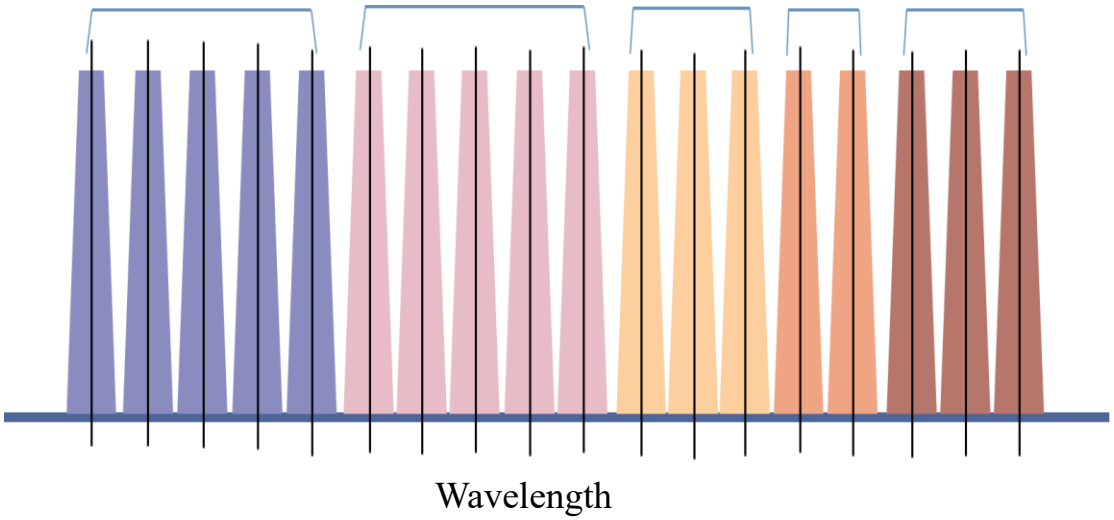

Fig.1.4 Scheme for CWDM system

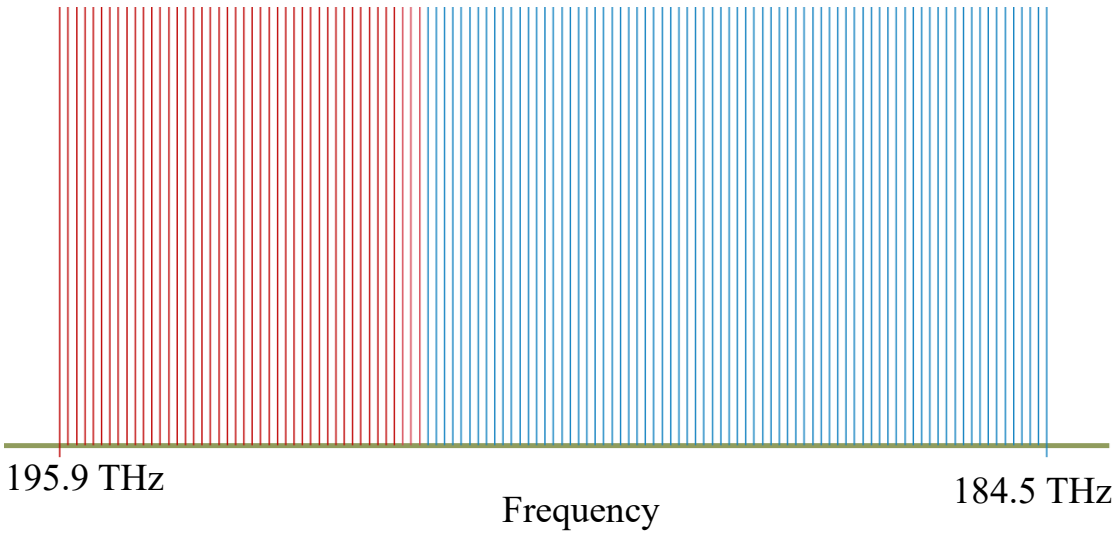

Fig.1.5 Scheme for DWDM system

1.1.3 MDM (Mode Division Multiplexing)

Using space-division multiplexing (SDM) is another concept to increase the capacity of optical fibers. Unlike the principle of WDM, SDM is defined by mode as depicted in Fig.1.6. A multiplexing technique for optical data transmission where multiple spatial channels are utilized. It is considered to be particularly needed for long-haul communications (e.g. through submarine communications cables), but later on also for applications on smaller scales such as regional networks [25-27].

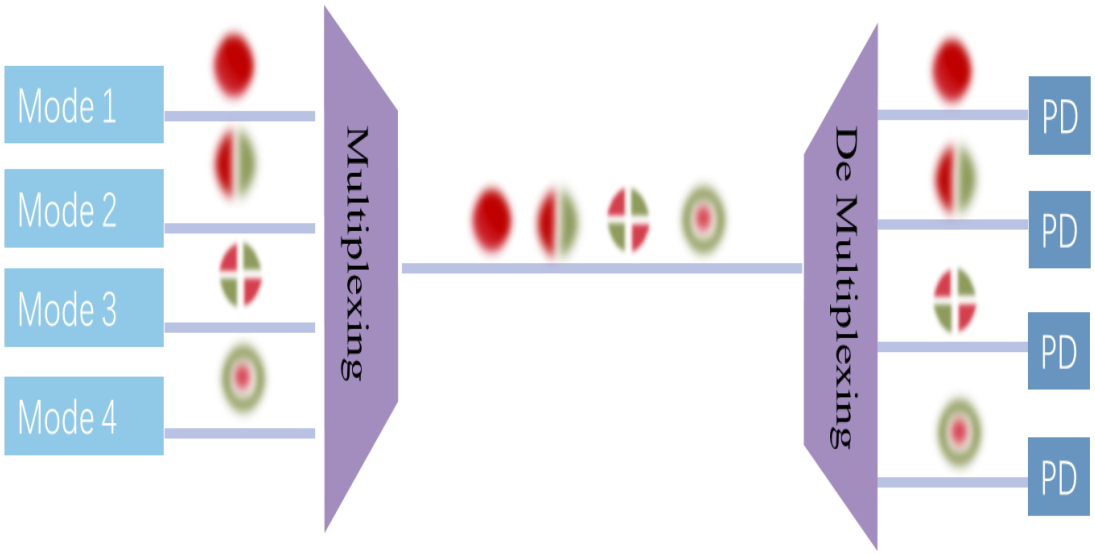

Fig.1.6 Scheme for MDM system

From the explanation above, it is obvious that there are two ways to enhance the capacity of an optic link system. One is increasing the channel to transfer data. By increasing the number of channels (DWDM), more space, and more power are required. What's more, the hardware and

electronics used in that system are expensive. Considering the application to small devices such as smartphones and PC, the promising method is increasing the capacity in each channel. Thus, the fundamental problem is that the data rate of each channel (wavelength/mode) is limited to the modulation speed.

1.2 Directly modulated lasers: State of the art

In optic communication systems, two modulation techniques are widely used: external modulation and direct modulation [28]. The principle of external modulation is shown in Fig.1.7. An External device is incorporated to modulate the intensity/phase of the light source. The external modulator manipulates the optical signal after the laser and ideally, it does not affect the laser operation. Investigation on external modulators has been carried out. Mach-Zehnder modulators (MZMs) based on the free carrier plasma effect [29-32], lithium niobate (LiNbO3) modulators based on Pockels effect [33], electro-absorption (EA) modulators based on quantum-confined Stark effect (QCSE) [34] are the main technologies of the external modulation of optic communication system. Fig.1.8 is the scheme of direct modulation. Without external modulator, the output light is directly modulated by the electric signal. Laser diode used as direct modulation is called directly modulated laser (DMLs).

Except for the modulation techniques, several advanced modulation

formats have been proposed and researched to realize efficient modulation bandwidth: pulse amplitude modulation (PAM) [35-37], carrier-less amplitude phase modulation (CAP) [38] and discrete multi-tone (DMT) modulation [35, 39]. For short-reach applications such as data centers using 100 Gbps per channel, or 400 Gbps in the future [40], the biggest difficulty lies in how to reduce energy per bit [41]. And to our goal that applying high-speed optical link system in PC or smartphone, the issue of energy efficiency is much more critical. Compared to external modulation, DMLs are well known for their high energy efficiency, low cost and compact size. All those features are extremely attractive for short-reach applications. Therefore, to the transmitting speed of over 100 Gbps per channel, DMLs are the promising candidate. Modulation bandwidth over 100 GHz in DMLs has been realized in 2020 [42]. In the following section, the history and the high-speed technology of DMLs are discussed.

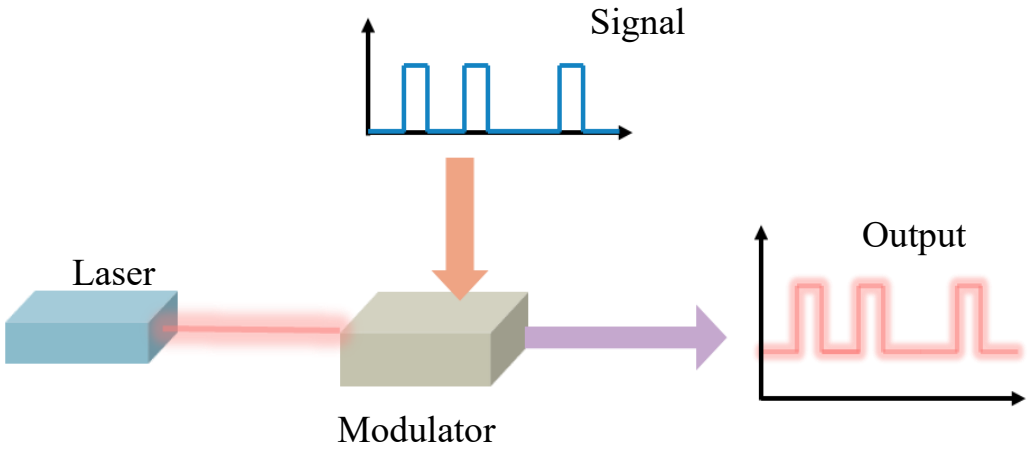

Fig.1.7 Modulation scheme of laser diode used as external modulation.

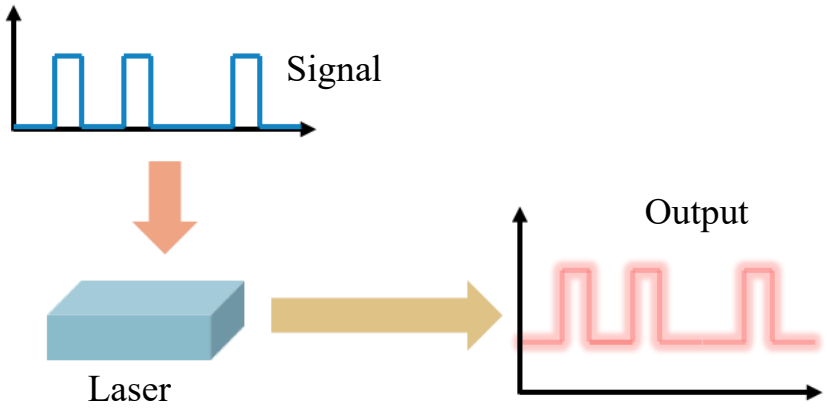

Fig.1.8 Modulation scheme of laser diode used as direct modulation.

Direct modulation of laser diode has long history as the form of a modulation scheme for light. The principle of DMLs is related to the current supply to laser. Carriers in directly modulated laser cavity follow the current modulation. Photons generated through stimulated emission process in the laser cavity rely on carriers [43]. Photons then follow the carriers after some time. The energy conversion in that process is efficient.

This is the reason why DMLs are considered as low power consumption, compact and low-cost devices. Thus, high-speed DMLs are expected to play a critical role in high-capacity transmission systems in the future.

Fig.1.9 shows the modulation bandwidth progress of DMLs. In the middle of the 1960s, the high-speed capability of GaAs semiconductor lasers was demonstrated [44]. Modulation bandwidth rates up to a few GHz. Then, the effects related to modulation bandwidth such as carrier diffusion, multiple transverse and longitudinal mode effects and spectral hole burning effects have been studied and became understood [45-49]. At the beginning of the 1980s, experiment results indicated that modulation bandwidth of semiconductor lasers is able to be extended to 10 GHz by using a short laser cavity [50]. In the late 1980s, researchers were attracted by the multiple quantum wells [MQWs] structure [51-53]. A lot of work associated with MQWs structure has been carried out. Experiment results reveal that the instinct speed of DMLs with MQWs structure is increased. For the shorter wavelength laser, because of few number of wells, superior gain properties were exploited that modulation bandwidths of DMLs over 30 GHz were reported [54-55]. The DMLs in longer wavelength regime (1550 nm) suffer not only from the degraded differential gain but also from the large linewidth enhancement factor. To extend the bandwidth of longer wavelength laser, detuned-loading effect has been utilized. A bandwidth of 37 GHz DML was reported [56]. Though some achievements have been

made, the progress concerning the modulation bandwidth was relatively poor. This is because the maximum current to achieve the MQW laser ultimate limit of the resonance frequency is not possible in many cases in practice [57].

The modulation bandwidth can also be enhanced by the photon-assisted effect through optical injection locking (OIL), integrated grating reflectors, and integrated passive reflectors [58-61]. In 1982, Dr. Lang published the widely accepted standard OIL rate equations by taking into account the linewidth enhancement parameter [62]. In the same year, Kobayashi and Kimura demonstrated optical phase modulation by OIL [63]. After that, the enhancement of resonance frequency was proposed [64-65] as a method for increasing the modulation bandwidth of DMLs. The first frequency enhancement was demonstrated in 1998 [66]. In the 2000s, 80-GHz intrinsic 3-dB bandwidths [67] were demonstrated theoretically. In reality, modulation bandwidths are, however, still limited.

For the purpose of extending the modulation bandwidth of DML, much more attention has been paid to the effect called Photon-Photon resonance (PPR). Utilizing the interaction of two lasing modes inside the laser cavity, resonance higher than the oscillation frequency appears that the modulation response is extended. This phenomenon is called photon-photon resonance. As shown in Fig.1.9, a lot of progress of modulation bandwidth has been achieved [42, 54-56, 68-70,78-79, 89-94, 102] in

DMLs. With the investigation of PPR, modulation bandwidth extends sharply. The current record of DML bandwidth is 108 GHz which is utilized in the PPR phenomenon [42]. The PPR is an ideal candidate to extend the modulation bandwidth of DMLs.

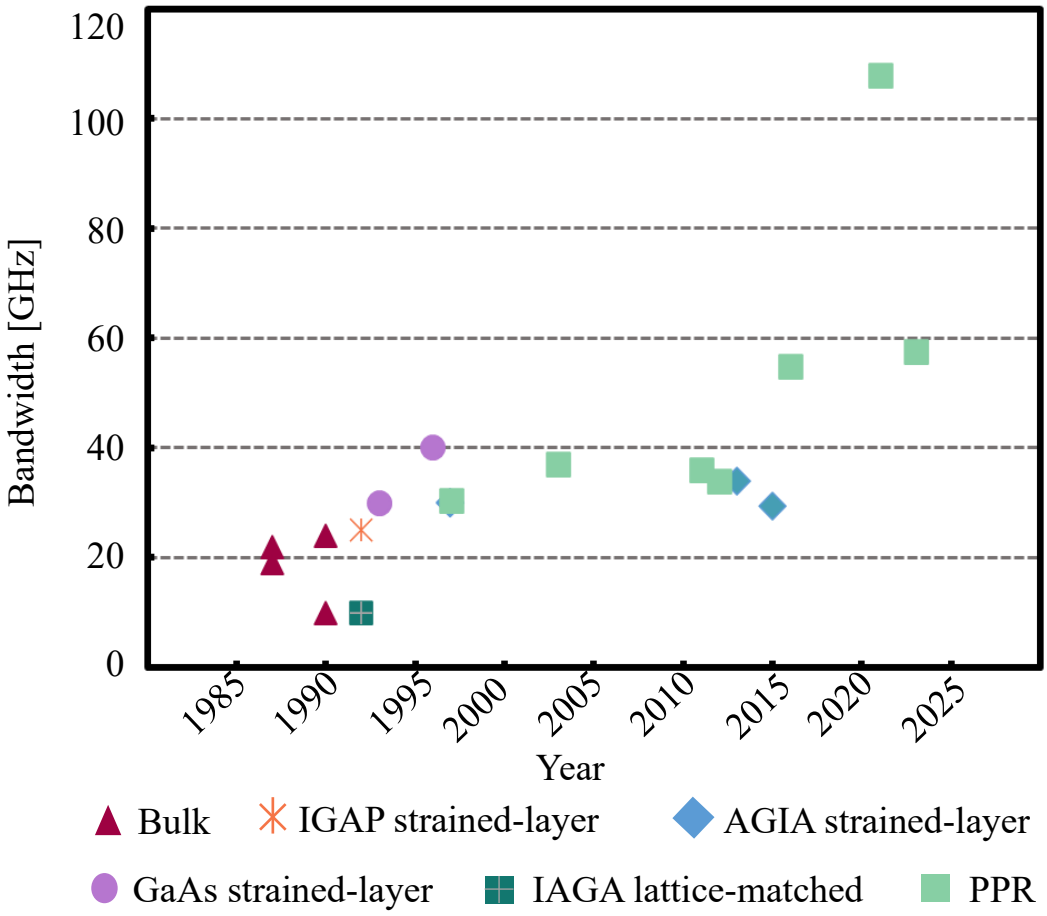

Fig.1.9 Bandwidth progress of DMLs [42, 54-56, 68-70,78-79, 89-94,102].

The bandwidth of DMLs is measured by the modulation of small signal. To the WDM or SDM system, the capacity of one channel is expressed by the large signal modulation speed of DMLs. Though it is related to small signal modulation response, it is better to list the progress of the large signal modulation response of DMLs. The overview of the progress of transition

speed of DMLs is shown in Tab. 1.2.

Tab. 1.2 Progress of DMLs speed

Institute	Material	Structure	Capacity (Gbps)	Year	Reference
Fujitsu	AlGaInAs	DFB	25	2008	Electro.Lett [71]
NTT	AlGaInAs	DFB	25	2009	OFC [72]
Fujitsu	AlGaInAs	DFB	40	2008	ISLC [73]
Finisar	AlGaInAs	DFB	25	2009	OFC [74]
Fujitsu	AlGaInAs	FP	25	2010	CLEO [75]
NTT	AlGaInAs	DFB	40	2011	OFC [76]
Fujitsu	AlGaInAs	DR	25.8	2012	ISLC [77]
NTT	AlGaInAs	DFB	50	2012	ISLC [78]
Hitachi	AlGaInAs	DFB	50	2015	IEEE.PTL [79]
Finisar	AlGaInAs	DR	122	2016	OFC [80]
NTT	AlGaInAs	DBR+DFB	256	2020	Nat.Phot [42]

1.3 Photon-Photon resonance (PPR): state of arts

The modulation bandwidth of DMLs is restricted by the gain compression and transport effect [81-83,87], which is related to the so-called relaxation oscillation (or carrier photon resonance (CPR)). Lots of attempts have been made to extend the modulation bandwidth of DMLs by increasing differential gain of DMLs [84] trying to obtain relatively high CPR. Extending CPR alone, however, is not enough for modulation bandwidth over 100 GHz. In recent research, adding an extra cavity beside the main lasing cavity provides an optical feedback inside the laser forming an additional mode that enhances the modulation bandwidth. Such phenomenon is called PPR as shown in Fig.1.10. PPR phenomena is related to more than one lasing mode inside DMLs cavity. Around the main lasing mode, there will be a side mode that enhances the modulation response at around a frequency corresponding to the frequency difference between the main and the side modes.

In 1993, Dr. AA Tager investigated the effect of external cavity mode beating. He provided the guidelines for designing high-speed laser diodes with integrated passive cavities [85]. In 1994, Dr. D. D. Marcenac also reported his theory of modulation enhancement of modulation bandwidth in push-pull modulated DFB lasers [86]. Since then, lots of endeavors have been made to utilize this effect to extend modulation bandwidth with PPR. DBR lasers, DR lasers, two-section DFB lasers, and so on were proposed

to exploit PPR phenomena. The exploration of PPR has been intensively researched experimentally. Tab 1.3 summarizes the progress of modulation bandwidth of DMLs with PPR effect.

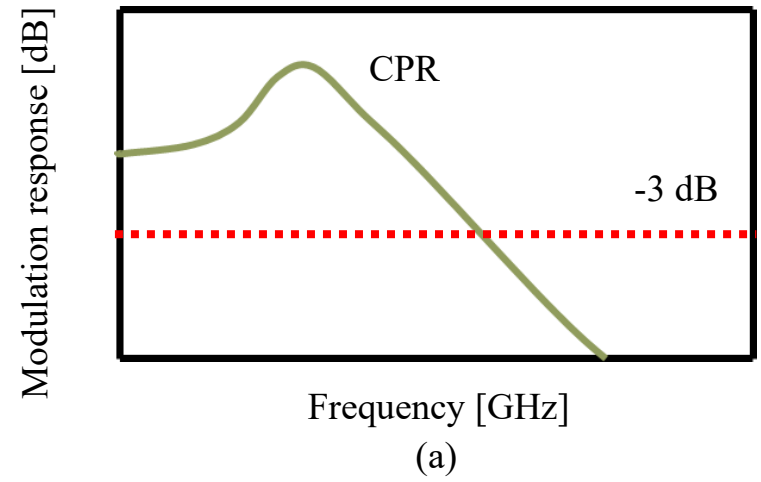

(a)

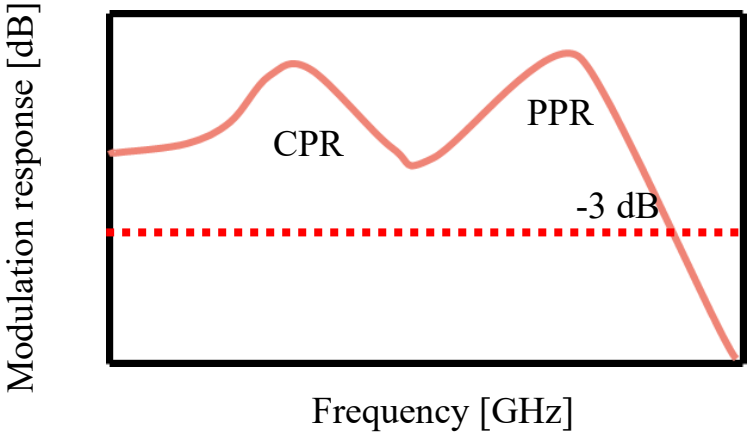

(b)

Fig.1.10 Modulation response: (a) without PPR; (b) with PPR

Tab 1.3 The progress of modulation bandwidth of DMLs with PPR effect.

Institute	Structure	Capacity (GHz)	PPR number	Year	Reference
University Wurzburg	Laterally coupled long cavity DBR	22.8	1	2004	[95]
Weierstrab institute fur angewandte analysis und stochastik	Passive feedback DFB	29	1	2007	[96]
Nanoplus nano system and technoloues GmbH	Quantum dot laser with coupled cavity injection grating	20	1	2008	[97]
Tokyo institute of technology	VCSEL	29	1	2013	[98]
Finisar	Distribute reflected laser	55	1	2016	[99]

Kyushu university	Active-MMI (Multimode Interferometer) laser	10	2	2018	[100]
Tohuku university	DFB with ICLM (intra-cavity loss modulation) section	66	1	2020	[101]
NTT	Membrane DR laser	108	1	2020	[42]
Heinrich-Hertz-Institute	DFB	57.6	1	2023	[102]

As can be seen from Tab 2, though multiple PPRs have not exhibited the ability to extend modulation bandwidth, there is still a lot of potential for multiple PPRs phenomena to exploit as PPR displays the capability. The main problem with utilizing multiple PPRs is the damping problem between resonances. If the PPR phenomenon is in control, the modulation bandwidth will be extended over 200 GHz as the fact that the modulation bandwidth with single PPR is over 100 GHz. The challenge in this work is to explore the PPR control scheme to extend modulation bandwidth.

1.4 Outline of this thesis

This thesis consists of 6 chapters. In Chapter 1, the optical interconnection for supercomputers has been introduced. History, progress and requirements are discussed. Based on the requirements, the key device of optical interconnection system, the high-speed modulation laser diode has been introduced in that chapter. The challenge of utilizing multiple PPRs has been proposed.

In Chapter 2, the multiple PPRs were observed in active-MMI laser, which is contradictory to the theory that PPR phenomenon does not exist in Fabry-Perót (F-P) laser [88]. The principle of the PPR existence in active-MMI laser is explained.

Chapter 3 is mainly about the laser rate equations with PPR for PPR control mechanism. Some key parameters related to PPR in small signal modulation response have been discussed.

In chapter 4, with the theoretical small signal analysis in chapter 3, the large signal affection with PPR has also been clarified. It suggests that the large signal modulation response improved with a high intensity of PPR.

In Chapter 5, as the theoretical analysis of small signal modulation response and large signal modulation response, the design rule of active-MMI laser configuration has been proposed for the optimized PPR utilization.

The last chapter summarized the whole thesis. Future potential and

expectation of active-MMI LD as high-speed modulation device is discussed.

Reference

[1] Clelland, N.L., Lee, J.K., Bimbenet, O.C. and Brantley, W.A, A, "Three-Dimensional Finite Element Stress Analysis of Angled Abutments for an Implant Placed in the Anterior Maxilla, " Journal of Prosthodontics, vol. 4, pp. 95-100 (1995).

[2] N.N. Smirnov, V.B. Betelin, A.G. Kushnirenko, V.F. Nikitin, V.R. Dushin, V.A. Nerchenko, "Ignition of fuel sprays by shock wave mathematical modeling and numerical simulation," Acta Astronautica, vol. 87, pp. 14-29 (2013).

[3] Franziska Michor, Kathryn Beal, "Improving Cancer Treatment via Mathematical Modeling: Surmounting the Challenges Is Worth the Effort, " Cell, Volume 163, Issue 5, pp. 1059-1063, (2015).

[4] T. C. Schulthess, P. Bauer, N. Wedi, O. Fuhrer, T. Hoefler and C. Schär, "Reflecting on the Goal and Baseline for Exascale Computing: A Roadmap Based on Weather and Climate Simulations," in Computing in Science & Engineering, vol. 21, no. 1, pp. 30-41, (Jan.-Feb. 2019).

[5] A.M.M. Leite, C.J.A.P. Martins, E.P.S. Shellard, "Accurate calibration of the velocity-dependent one-scale model for domain walls," Physics Letters B, vol. 718, Issue 3, pp. 740-744, (2013).

[6] A. Hellemans and M. Mukerjee, "Computing the cosmos," in IEEE Spectrum, vol. 41, no. 8, pp. 28-34, (Aug. 2004) .

[7] Michael L. Norman; "Probing Cosmic Mysteries by Supercomputer.

" Physics Today 1, vol. 49, no. 10, pp. 42–48, (October 1996).

[8] A. Acharya, R. Agarwal, M. B. Baker, J. Baudry, D. Bhowmik, S. Boehm, K. G. Byler, S. Y. Chen, L. Coates, C. J. Cooper, O. Demerdash, I. Daidone, J. D. Eblen, S. Ellingson, S. Forli, J. Glaser, J. C. Gumbart, J. Gunnels, O. Hernandez, S. Irle, D. W. Kneller, A. Kovalevsky, J. Larkin, T. J. Lawrence, S. LeGrand, S.-H. Liu, J.C. Mitchell, G. Park, J.M. Parks, A. Pavlova, L. Petridis, D. Poole, L. Pouchard, A. Ramanathan, D. M. Rogers, D. Santos-Martins, A. Scheinberg, A. Sedova, Y. Shen, J. C. Smith*, M. D. Smith, C. Soto, A. Tsaris, M. Thavappiragasam, A. F. Tillack, J. V. Vermaas, V. Q. Vuong, J. Yin, S. Yoo, M. Zahran, and L. Zanetti-Polzi, "Supercomputer-Based Ensemble Docking Drug Discovery Pipeline with Application to Covid-19 J." Chem. Inf. Model. Vol. 60, no. 12, pp. 5832–5852, (2020)

[9] Joux, Antoine. "A tutorial on high performance computing applied to cryptanalysis." EUROCRYPT. Vol. 12. 2012.

[10] Top500, (http://www.top500.org/).

[11] Y. Ajima, T. Inoue, S. Hiramoto, Y. Takagi, T. Shimizu, "The tofu interconnect, " IEEE Micro, vol. 32, no. 1, pp. 21–31, (2012).

[12] D.K. Panda, Designing software libraries and middleware for exascale systems: opportunities and challenges, 2014, Talk at Brookhaven National Laboratory, http://www.iacs.stonybrook.edu/sites/iacs.stonybrook.edu/files/dk_st

onybrook_bnl.pdf.

[13] Mvapich: Mpi over infiniband, omni-path, ethernet/iwarp, and roce, http://mvapich.cse.ohio-state.edu/performance/pt_to_pt/.

[14] D. Chen, N.A. Eisley, P. Heidelberger, R.M. Senger, Y. Sugawara, S. Kumar, V. Salapura, D.L. Satterfield, B. Steinmacher-Burow, J.J. Parker, "The IBM blue gene/q interconnection network and message unit," 2011 International Conference for High Performance Computing, Networking, Storage andAnalysis (SC), pp. 1–10, (2011).

[15] X.-K. Liao, Z.-B. Pang, K.-F. Wang, Y.-T. Lu, M. Xie, J. Xia, D.-Z. Dong, G. Suo, "High performance interconnect network for Tianhe system, " J. Comput. Sci. Technol. 30 (2) (2015) 259–272.

[16] Y. Ajima, T. Inoue, S. Hiramoto, S. Ando, M. Maeda, T. Yoshikawa, K. Hosoe, T. Shimizu, "The tofu interconnect 2, " 2014 IEEE 22nd Annual Symposium on High-Performance Interconnects, (2014) 57–62,

[17] A. Otto, D.H.C. Perez, N. Neufeld, F.P. Rainer Schwemmer, "A first look at 100 gbps LAN technologies, with an emphasis on future DAQ applications, " 21st International Conference on Computing in High Energy and Nuclear Physics, (2015),

[18] Yuichiro Ajima; Takahiro Kawashima; Takayuki Okamoto; Naoyuki Shida; Kouichi Hirai; "Toshiyuki Shimizu; Shinya Hiramoto; Yoshiro Ikeda; Takahide Yoshikawa; Kenji Uchida; Tomohiro Inoue: "The

Tofu Interconnect D," 2018 IEEE International Conference on Cluster Computing (CLUSTER), Belfast, UK, pp. 646-654, (2018).

[19] Khorassani KS, Chen C-C, Ramesh B, Aamir Shaf, Hari Subramoni, Dhabaleswar K. Panda, "High Performance MPI over the Slingshot Interconnect." Journal of Computer Science and Technology, vol. 38, no.1, pp. 128-145, (2023).

[20] https://www.olcf.ornl.gov/olcf-resources/compute-systems/frontier/

[21] E.Rumley, Meisam Bahadori, Robert Polster, Simon D. Hammond, David M. Calhoun, Ke Wen, Arun Rodrigues, Keren Bergman,"Optical interconnects for extreme scale computing systems, "Parallel Computing, vol 64, pp. 65-80, (2017).

[22] H. Ishio, J. Minowa, K. Nosu, "Review and status of wavelength-division-multiplexing technology and its application", IEEE J. Lightwave Technol. Vol. 2 no. 4, pp. 448-463, (1984),

[23] Siddharth Bhatt and Shilen Jhaveri. "A review of dense wavelength division multiplexing and next generation optical internet. " International Journal of Engineering Science and Innovative Technology (IJESIT), vol, no. 2 pp. 404-412, (2013) .

[24] C. A. Brackett, "Dense wavelength division multiplexing networks: principles and applications," IEEE Journal on Selected Areas in Communications, vol. 8, no. 6, pp. 948-964, (Aug. 1990).

[25] S. Berdagué and P. Facq, "Mode division multiplexing in optical fibers,

" ppl. Opt. vol. 21 no. 11, pp. 1950-1955, (1982).

[26] R. W. Tkach, "Scaling optical communications for the next decade and beyond," in Bell Labs Technical Journal, vol. 14, no. 4, pp. 3-9, (2010).

[27] Guifang Li, Neng Bai, Ningbo Zhao, and Cen Xia, "Space-division multiplexing: the next frontier in optical communication," Adv. Opt. Photon. vol. 6, pp. 413-487, (2014).

[28] Anthony E. Siegman: LASERS (University Science Books, California, pp. 187-211, (1986).

[29] S. J. Spector, C. M. Sorace, M. W. Geis, M. E. Grein, J. U. Yoon, T. M. Lyszczarz, E. P. Ippen, and F. X. Kärtner, "Operation and optimization of silicon-diode-based optical modulators, " IEEE J. Sel. Top. Quantum Electron. Vol. 16, no. 1, pp. 165–172 (2010).

[30] M. R. Watts, W. A. Zortman, D. C. Trotter, R. W. Young, and A. L. Lentine, "Low-voltage, compact, depletionmode, silicon Mach Zehnder modulator, " IEEE J. Sel. Top. Quantum Electron. vol. 16, no. 1, pp.159–164, (2010).

[31] D. J. Thomson, F. Y. Gardes, J.-M. M. Fedeli, S. Zlatanovic, Y. Hu, B. P.-P. Kuo, E. Myslivets, N. Alic, S. Radic, G. Z. Mashanovich, and G. T. Reed, "50-Gb/s silicon optical modulator, " IEEE Photon. Technol. Lett. vol. 24, no. 4, pp. 234–236 (2012).

[32] S. Akiyama, T. Baba, M. Imai, T. Akagawa, M. Takahashi, N. Hirayama, H. Takahashi, Y. Noguchi, H. Okayama, T. Horikawa, and

T. Usuki, "12.5-Gb/s operation with 0.29-V·cm VπL using silicon Mach-Zehnder modulator based-on forward-biased pin diode, " Opt. Express vol. 20, no. 3, pp. 2911–2923 (2012).

[33] E. L. Wooten, K. M. Kissa, A. Yi-Yan, E. J. Murphy, D. A. Lafaw, P. F. Hallemeier, D. Maack, D. V. Attanasio, D. J. Fritz, G. J. McBrien, and D. E. Bossi, "A review of lithium niobate modulators for fiber-optic communications systems, " IEEE J. Sel. Top. Quantum Electron. vol. 6, no. 1, pp. 69–82, (2000).

[34] DZ Feng, Wei Qian; Hong Liang, Cheng-Chih Kung, Zhou Zhou; Zhi Li, Jacob S. Levy, Roshanak Shafiiha, Joan Fong, B. Jonathan Luff, Mehdi Asghari, "High-Speed GeSi Electroabsorption Modulator on the SOI Waveguide Platform," IEEE Journal of Selected Topics in Quantum Electronics, vol. 19, no. 6, (pp. 64-73, Nov.-Dec. 2013).

[35] Y Kai, M Nishihara, Toshiki Tanaka, Tomoo Takahara, Lei Li, Zhenning Tao, Bo Liu, Jens C. Rasmussen, Tomislav Drenski, "Experimental comparison of pulse amplitude modulation (PAM) and discrete multi-tone (DMT) for short-reach 400-Gbps data communication," 39th European Conference and Exhibition on Optical Communication (ECOC 2013), 2013, pp. 1-3.

[36] XD Pang, Os Ozolins, Simone Gaiarin, Miguel Iglesias Olmedo, Richard Schatz, Urban Westergren, Darko Zibar, Darko Zibar, Sergei Popov, Gunnar Jacobsen, "Evaluation of High-Speed EML-based

IM/DD links with PAM Modulations and Low-Complexity Equalization," ECOC 2016; 42nd European Conference on Optical Communication, 2016, pp. 1-3.

[37] Roberto Rodes, Michael Müeller, Bomin Li, Jose Estaran, Jesper Bevensee Jensen, Tobias Gruendl, Markus Ortsiefer, Christian Neumeyr, Juergen Rosskopf, Knud J. Larsen, M.-C. Amann, and Idelfonso Tafur Monroy, "High-Speed 1550 nm VCSEL Data Transmission Link Employing 25 GBd 4-PAM Modulation and Hard Decision Forward Error Correction," J. Lightwave Technol. Vol. 31, pp. 689-695, (2013).

[38] Miguel Iglesias Olmedo, Tianjian Zuo, Jesper Bevensee Jensen, Qiwen Zhong, Xiaogeng Xu, Sergei Popov, Idelfonso Tafur Monroy,"Multiband Carrierless Amplitude Phase Modulation for High-Capacity Optical Data Links," in Journal of Lightwave Technology, vol. 32, no. 4, pp. 798-804, (Feb.15, 2014)

[39] S. C. Jeffrey Lee, Florian Breyer, Sebastian Randel, Roberto Gaudino, Gabriella Bosco, Andreas Bluschke, Michael Matthews, Philipp Rietzsch, Rainer Steglich, Henrie P. A. van den Boom, and Antonius M. J. Koonen, "Discrete Multitone Modulation for Maximizing Transmission Rate in Step-Index Plastic Optical Fibers," J. Lightwave Technol. Vol. 27, pp.1503-1513, (2009)

[40] 100 Gb/s, 200 Gb/s, and 400 Gb/s Short Reach Fiber Task Force:

https://www.ieee802.org/3/db/P802d3db_Timeline_Updated_Approved_November_2021.pdf

[41] A. K. Verma, M. Steib, Y. L. Ha, and T. Sudo, "25Gbps 1.3μm DFB Laser for 10-25km Transmission in 100GBE Systems," Optical Fiber Communication Conference and National Fiber Optic Engineers Conference, OSA Technical Digest (CD) (Optica Publishing Group, 2009), paper OThT2.

[42] Suguru Yamaoka, Nikolaos-Panteleimon Diamantopoulos, Hidetaka Nishi, Ryo Nakao, Takuro Fujii, Koji Takeda, Tatsurou Hiraki, Takuma Tsurugaya, Shigeru Kanazawa, Hiromasa Tanobe, Takaaki Kakitsuka, Tai Tsuchizawa, Fumio Koyama and Shinji Matsuo, "Directly modulated membrane lasers with 108 GHz bandwidth on a high-thermal-conductivity silicon carbide substrate. " Nat. Photonics, vol. 15, pp. 28–35, (2021).

[43] Numai, Takahiro. "Fundamentals of semiconductor lasers." Springer Japan, 2015.

[44] K. Konnerth and C. Lanza, "Delay between current pulse and light emission of a GaAs injection laser, " Appl. Phys. Lett., vol 4, Issue 7, 4: pp. 120-121, (1964).

[45] Y. Suematsu and Tchang-Hee Hong, "Suppression of relaxation oscillation in light output of injection lasers by electrical resonance circuit," in IEEE Journal of Quantum Electronics, vol. 13, no. 9, pp.

756-762, (September 1977).

[46] M. Adams and B. Thomas, "Detailed calculations of transient effects in semiconductor injection lasers," in IEEE Journal of Quantum Electronics, vol. 13, no. 8, pp. 580-585, (August 1977).

[47] Kazuhito Furuya, Yasuharu Suematsu, and Tchanghee Hong, "Reduction of resonancelike peak in direct modulation due to carrier diffusion in injection laser," Appl. Opt. vol. 17, pp. 1949-1952, (1978).

[48] K. Seki, M. Yano, T. Kamiya and H. Yanai, "The phase shift of the light output in sinusoidally modulated semiconductor lasers," in IEEE Journal of Quantum Electronics, vol. 15, no. 8, pp. 791-798, (August 1979).

[49] T. Paoli, "Optical response of a stripe-geometry junction laser to sinusoidal current modulation at 1.2 GHz," in IEEE Journal of Quantum Electronics, vol. 17, no. 5, pp. 675-680, (May 1981).

[50] K. Y. Lau, N. Bar-Chiam, I. Ury, C. Harder, and A. Yariv, "Direct amplitude modulation of short-cavity GaAs lasers up to X-band frequencies, " Appl. Phys. Lett., Vol. 43, no. 1, pp, 43.1, (June 1983).

[51] N. Holonyak, R. Kolbas, R. Dupuis and P. Dapkus, "Quantum-well heterostructure lasers," in IEEE Journal of Quantum Electronics, vol. 16, no. 2, pp. 170-186, (February 1980).

[52] Kobayashi, H. Iwamura, T. Saku, K. Otsuka, and H. Okamoto, "Dynamic behavior of a GaAs-AIGaAs MQW laser diode, " Electron.

Lett., vol. 19, pp. 166-167, (1983).

[53] W. T. Tsang, "Extremely low threshold (A1Ga)As modified multi-quantum well heterostructure lasers grown by molecular beam epitaxy, " Appl. Phys. Lett., vol. 39, pp. 786-788, (1981).

[54] Y. Matsui, H. Murai, S. Arahira, S. Kutsuzawa and Y. Ogawa, "30-GHz bandwidth 1.55-μm strain-compensated InGaAlAs-InGaAsP MQW laser," in IEEE Photonics Technology Letters, vol. 9, no. 1, pp. 25-27, (Jan. 1997).

[55] J. D. Ralston et al., "Control of differential gain, nonlinear gain and damping factor for high-speed application of GaAs-based MQW lasers," in IEEE Journal of Quantum Electronics, vol. 29, no. 6, pp. 1648-1659, (June 1993).

[56] U. Troppenz, J. Kreissl, M. Möhrle, C. Bornholdt, W. Rehbein, B. Sartorius, I. Woods, and M. Schell, "40 Gbit/s directly modulated lasers: physics and application", Proc. SPIE 7953, Novel In-Plane Semiconductor Lasers X, pp. 79530F, (16 February 2011).

[57] U. Feiste, "Optimization of modulation bandwidth in DBR lasers with detuned Bragg reflectors," in IEEE Journal of Quantum Electronics, vol. 34, no. 12, pp. 2371-2379, (Dec. 1998).

[58] Zhu, N. H., Shi, Z., Zhang, Z. K., Zhang, Y. M., Zou, C. W., Zhao, Z. P, Li, M. "Directly modulated semiconductor lasers. " IEEE Journal of Selected Topics in Quantum Electronics, vol. 24, no.1, pp. 1-19,

(2017).

[59] Sung, H. K., Lau, E. K., Wu, M. C. "Optical single sideband modulation using strong optical injection-locked semiconductor lasers. " IEEE Photonics Technology Letters, vol. 19, no. 13, pp.1005-1007. (2007).

[60] O. Kjebon, R. Schatz, S. Lourdudoss, S. Nilsson, B. Stalnacke, and L. Backbom, "30 GHz direct modulation bandwidth in detuned loaded InGaAsP DBR lasers at 1.55 μm wavelength, " Electron. Lett., vol. 33, no. 6, pp. 486–489, (1997).

[61] Matsui Y, Schatz R, Pham T, Ling W. A, Carey G, Daghighian H M, Roxlo C. "55 GHz bandwidth distributed reflector laser." Journal of lightwave technology, vol. 35, no.3, pp.397-403, (2017).

[62] R. Lang, "Injection locking properties of a semiconductor laser, " IEEE J. Quantum Electron., vol. 18, no. 6, pp. 976–983, (Jun. 1982).

[63] S. Kobayashi and T. Kimura, "Optical phase modulation in an injection locked AlGaAs semiconductor laser, " IEEE J. Quantum Electron., vol. 18, no. 10, pp. 1662–1669, (Oct. 1982).

[64] C. H. Henry, N. A. Olsson, and N. K. Dutta, "Locking range and stability of injection locked 1.54 μm InGaAsP semiconductor lasers, "IEEE J. Quantum Electron., vol. QE-21, no. 8, pp. 1152–1156, (Aug. 1985).

[65] T. B. Simpson, J. M. Liu, and A. Gavrielides, "Bandwidth

enhancement and broadband noise reduction in injection-locked semiconductor lasers, " IEEE Photon. Technol. Lett., vol. 7, no. 7, pp. 709–711, (Jul. 1995).

[66] X. J. Meng, T. Jung, T. Chau, and M. C. Wu, "Gain and bandwidth enhancement of directly modulated analog fiber optic links using injectionlocked gain-coupled DFB lasers," in Proc. IEEE Int. Top. Meet. Microw. Photon., Melbourne, VIC, Australia, 1999, pp. 141–144.

[67] E. K. Lau, X. Zhao, H.-K. Sung, D. Parekh, C. Chang-Hasnain, and M. C. Wu, "Strong optical injection-locked semiconductor lasers demonstrating > 100-GHz resonance frequencies and 80-GHz intrinsic bandwidths," Opt. Exp., vol. 16, no. 9, pp. 6609–6618, (2008).

[68] R. Olshansky, W. Powazinik, P. Hill; V. Lanzisera, R.B. Lauer, "InGaAsP buried heterostructure laser with 22 GHz bandwidth and high modulation efficiency, " vol .23, No. 16, pp. 839-841, (July 1987).

[69] Bowers, J.E., Koren, U., Miller, B.I., Soccolich, C., Jan, W.Y, "High-speed, polyimide-based semi-insulating planar buried heterostructures, " Electronics Letters, vol.23, no. 24, pp: 1263-1264,

[70] S. Weisser. E.C, Larkins; K. Czotscher; W. Benz; J. Daleiden; I. Esquivias; J. Fleissner; J.D. Ralston; B. Romero; R.E. Sah; A. Schonfeld and J. Rosenzweig, "Damping-limited modulation

bandwidths up to 40 GHz in undoped short-cavity In/sub 0.35/Ga/sub 0.65/As-GaAs multiple-quantum-well lasers," IEEE Photonics Technology Letters, vol. 8, no. 5, pp. 608-610, (May 1996).

[71] K. Otsubo, M. Matsuda, K. Takada, S. Okumura, M. Ekawa, H. Tanaka, S. Ide, K. Mori, T. Yamamoto, "Uncooled 25 Gbit/s direct modulation of semi-insulating buried-heterostructure 1.3 μm AlGaInAs quantum-well DFB lasers," Electronics Letters, Volume 44, Issue 10, pp. 631-633, (May 2008).

[72] T. Tadokoro, T. Yamanaka, F. Kano, H. Oohashi, Y. Kondo, and K. Kishi, "Operation of a 25-Gbps Direct Modulation Ridge Waveguide MQW-DFB Laser up to 85 °C," Optical Fiber Communication Conference and National Fiber Optic Engineers Conference, OSA Technical Digest (CD) (Optica Publishing Group, 2009), paper OThT3.

[73] K. Otsubo, M. Matsuda, K. Takada, S. Okumura, M. Ekawa and T. Yamamoto, "40-Gb/s direct modulation of 1.3-μm semi-insulating buried-heterostructure AlGaInAs MQW DFB lasers," 2008 IEEE 21st International Semiconductor Laser Conference, 2008, pp. 19-20.

[74] A. K. Verma, M. Steib, Y. L. Ha, and T. Sudo, "25Gbps 1.3μm DFB Laser for 10-25km Transmission in 100GBE Systems," Optical Fiber Communication Conference and National Fiber Optic Engineers

Conference, OSA Technical Digest (CD) (Optica Publishing Group, 2009), paper OThT2.

[75] Yu Tanaka, Mitsuru Ishida, Kan Takada, Tsuyoshi Yamamoto, Hai-zhi Song, Yoshiaki Nakata, Masaomi Yamaguchi, Kenichi Nishi, Mitsuru Sugawara, and Yasuhiko Arakawa, "25 Gbps direct modulation in 1.3-μm InAs/GaAs high-density quantum dot lasers," CLEO/QELS: 2010 Laser Science to Photonic Applications, 2010, pp. 1-2.

[76] T. Tadokoro, W. Kobayashi, T. Fujisawa, T. Yamanaka, and F. Kano, "High-Speed Modulation Lasers for 100GbE Applications," Optical Fiber Communication Conference/National Fiber Optic Engineers Conference 2011, OSA Technical Digest (CD) (Optica Publishing Group, 2011), paper OWD1.

[77] T. Simoyama, M. Matsuda, S. Okumura, A. Uetake, M. Ekawa and T. Yamamoto, "4-Wavelength 25.8-Gbps directly modulated laser array of 1.3-μm AlGaInAs distributed-reflector lasers," ISLC 2012 International Semiconductor Laser Conference, 2012, pp. 54-55.

[78] W. Kobayashi et al., "High-speed operation at 50 Gb/s and 60-km SMF transmission with 1.3-μm InGaAlAs-based DML," ISLC 2012 International Semiconductor Laser Conference, 2012, pp. 50-51

[79] K. Nakahara et al., "Direct Modulation at 56 and 50 Gb/s of 1.3-μm InGaAlAs Ridge-Shaped-BH DFB Lasers," in IEEE Photonics Technology Letters, vol. 27, no. 5, pp. 534-536, (March, 2015).

[80] Y. Matsui, T. Pham, W. A. Ling, R. Schatz, G. Carey, H. Daghighian, T. Sudo, and C. Roxlo, "55-GHz Bandwidth Short-Cavity Distributed Reflector Laser and its Application to 112-Gb/s PAM-4," in Optical Fiber Communication Conference Post deadline Papers, OSA Technical Digest (online) (Optica Publishing Group, 2016), paper Th5B.4.

[81] Y. Arakawa and A. Yariv, "Theory of gain, modulation response, and spectral linewidth in AlGaAs quantum well lasers," in IEEE Journal of Quantum Electronics, vol. 21, no. 10, pp. 1666-1674, (October 1985).

[82] S. Kakimoto and H. Watanabe, "Threshold current, differential gain, and relaxation resonance frequency of 1.55-/spl mu/m bulk and MQW DFB laser diodes," in IEEE Journal of Quantum Electronics, vol. 34, no. 7, pp. 1231-1239, (July 1998).

[83] Bowers, J. E. "Modulation properties of semiconductor lasers." Optoelectronic Technology and Lightwave Communications Systems, pp. 299-334, (1989).

[84] R. Tucker and I. Kaminow, "High-frequency characteristics of directly modulated InGaAsP ridge waveguide and buried heterostructure lasers," in Journal of Lightwave Technology, vol. 2, no. 4, pp. 385-393, (August 1984).

[85] A. A. Tager and B. B. Elenkrig, "Stability regimes and high-frequency

modulation of laser diodes with short external cavity," in IEEE Journal of Quantum Electronics, vol. 29, no. 12, pp. 2886-2890, (Dec. 1993).

[86] D. D. Marcenac, M. C. Nowell and J. E. Carroll, "Theory of enhanced amplitude modulation bandwidth in push-pull modulated DFB lasers," in IEEE Photonics Technology Letters, vol. 6, no. 11, pp. 1309-1311, (Nov. 1994).

[87] Coldren, Larry A., Scott W. Corzine, and Milan L. Mashanovitch. Diode lasers and photonic integrated circuits. John Wiley & Sons, 2012, chapter 5.

[88] Laakso, A., Dumitrescu. "M. Modified rate equation model including the photon–photon resonance. " Opt Quant Electron, vol. 42, pp.785–791, (2011).

[89] Aoki, M, M Aoki, K Uomi, T Tsuchiya, M Suzuki, N Chinone, "Enhanced relaxation oscillation frequency and reduced nonlinear K-factor in InGaAs/InGaAsP MQW λ/4-shifted DFB lasers." Electronics Letters, vol. 26, no. 22, pp. 1841-1843, (1990).

[90] Lealman, I. F, DM Cooper, SD Perrin, MJ Harlow. "Effect of Zn doping on differential gain and damping of 1.55 mu m InGaAs/InGaAsP MWQ lasers." Electronics Letters, vol.11, no. 28, pp. 1032-1034, (1992).

[91] Mahgerefteh D, Y. Matsui, B. Johnson, D. Walker, Z.F. Fan, K.

McCallion. "Error-free 250 km transmission in standard fibre using compact 10 Gbit/s chirp-managed directly modulated lasers (CML) at 1550 nm." Electronics Letters, vol. 41, no. 9, pp. 543-544. (2005).

[92] Kjebon, O., Schatz, R., Lourdudoss, S., Nilsson, S., Stålnacke, B., and Bäckbom, L. "30GHz direct modulation bandwidth indetuned loaded InGaAsP DBR lasers at1. 55 μm wavelength". Electronics Letters, vol. 33, pp. 488-489, (1997).

[93] Kreissl, Jochen, V. Vercesi, U. Troppenz, T. Gaertner, W. Wenisch, M. Schell. "Up to 40 Gb/s Directly Modulated Laser Operating at Low Driving Current: Buried-Heterostructure Passive Feedback Laser (BH-PFL). " IEEE Photonics Technology Letters, vol. 24, pp. 362-364, (2012).

[94] Bach, L., Kaiser, W., Reithmaier, J. P., Forchel, A., Berg, T. W., & Tromborg, B. "Enhanced direct-modulated bandwidth of 37 GHz by a multi-section laser with a coupled-cavity-injection-grating design." Electronics Letters, vol. 39, no. 22, pp.1, (2003).

[95] L. Bach; W. Kaiser; J.P. Reithmaier; A. Forchel; M. Gioannini; V. Feies; I. Montrosset, "22-GHz modulation bandwidth of long cavity DBR laser by using a weakly laterally coupled grating fabricated by focused ion beam lithography," in IEEE Photonics Technology Letters, vol. 16, no. 1, pp. 18-20, (Jan. 2004).

[96] Mindaugas Radziunas; Annegret Glitzky; Uwe Bandelow; Matthias

Wolfrum; Ute Troppenz; Jochen Kreissl; Wolfgang Rehbein, "Improving the Modulation Bandwidth in Semiconductor Lasers by Passive Feedback," in IEEE Journal of Selected Topics in Quantum Electronics, vol. 13, no. 1, pp. 136-142, (2007).

[97] Gerschütz, F, M. Fischer, J. Koeth, I. Krestnikov, A. Kovsh, C. Schilling, W. Kaiser, S. Höfling, and A. Forchel. "1.3 μm Quantum Dot Laser in coupled-cavity-injection-grating design with bandwidth of 20 GHz under direct modulation." Optics Express 16.8 (2008): 5596-5601.

[98] Hamed Dalir, Fumio Koyama. "29 GHz directly modulated 980 nm vertical-cavity surface emitting lasers with bow-tie shape transverse coupled cavity. " Applied Physics Letters. vol.103, No.9, pp.091109, (2013).

[99] Matsui, Yasuhiro, et al. "55-GHz bandwidth short-cavity distributed reflector laser and its application to 112-Gb/s PAM-4." Optical Fiber Communication Conference. Optica Publishing Group, 2016.

[100] S. Murakami, B. Hong, H. Jiang and K. Hamamoto, "Observation of 60 GHz and 20 GHz Multiple Photon-Photon Resonances Using Active Multimode Interferometer Laser Diodes," 2019 24th Microoptics Conference (MOC), Toyama, Japan, 2019, pp. 304-305

[101] M. Kanno, N. Yokota and H. Yasaka, "Measurement of Intrinsic Modulation Bandwidth of Hybrid Modulation Laser," IEEE

Photonics Technology Letters, vol. 32, no. 13, pp. 839-842, (2020).

[102] Rajeswari, G. V., Moehrle, M., Ehrensack, F., Troppenz, U., Sigmund, A, Schell, M. Novel> 57 GHz bandwidth O-band InGaAlAs MQW RW DFB. In Novel In-Plane Semiconductor Lasers XXII, vol. 12440, pp. 34-39. SPIE. (2023, March).

Chapter 2

Photon-photon resonance phenomenon in active-MMI laser as Fabry-Perót (F-P) laser

2.1 Introductory overview

The DML's modulation bandwidth is restricted in principle by the so-called relaxation oscillation frequency (or carrier photon resonance (CPR) frequency) [1]. Lots of efforts have been paid to extend DMLs modulation bandwidth [2-10]. One possible way to overcome the restriction of relaxation oscillation is to utilize photon-photon resonance (PPR) which is known to display higher frequency resonance compared to CPR [11-25]. From the previous works, all the configurations that have been utilized to exploit PPR phenomenon share the same characteristics: grating structure. All the reported DMLs with PPR are those DBR lasers or DFB lasers. PPR is known as a resonance caused by the interaction between two lasing modes. Therefore, it is concluded that PPR phenomenon is not able to be observed in Fabry-Perót (F-P) laser because of the mode orthogonality [26-27]. In 2017, however, the existence of PPR phenomenon in F-P laser has been proved [28-31]. By applying active-multimode interferometer (MMI) laser, plural PPRs phenomenon were observed which contradicted the principle. The challenge of this chapter is to explain the existence of PPR in active-MMI laser.

In 2.2, the mode orthogonality in (F-P) laser will be clarified. In 2.3, the non-orthogonality in active-MMI for multiple PPRs is explained. Since active-MMI laser naturally accesses multiple waveguides, different oscillators exist that non-orthogonal mode do exist in active-MMI laser which provides the possibility to exploit PPR.

2.2 Mode orthogonality in F-P laser

To explain the mode orthogonality in (F-P) laser, lasing modes in (F-P) laser need to be clarified first [32]. Figure 2.1 is a schematic diagram of the F-P laser. The F-P cavity whose length is L. It is filled with semiconductor material with refractive index n_r. In the ends, there are two reflection mirrors with reflective index R_1 and R_2. The electromagnetic wave that exists in this cavity is expressed in

$$E = exp\left[\frac{i2\pi n_r z}{\lambda_0}\right] exp[(g - \alpha_i)z] \tag{2.1}$$

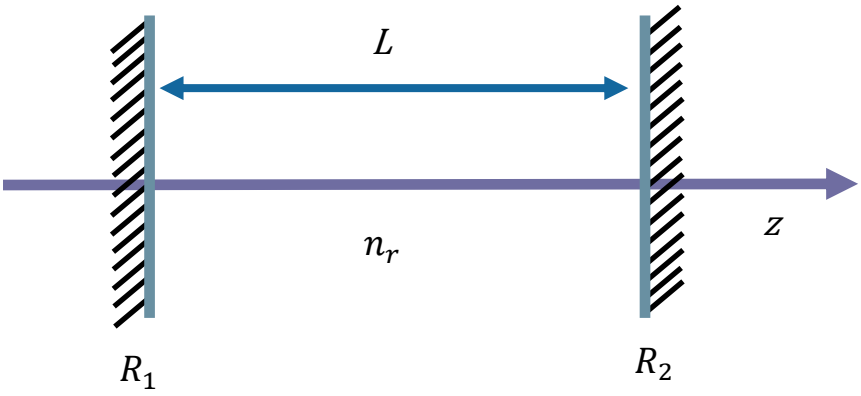

Fig. 2.1 Schematic diagram of F-P laser.

In the expression, λ_0 is the wavelength in free space. α_i is the loss parameter. g is gain parameter. The condition for the existence of an electromagnetic wave is that, when this electromagnetic wave is reflected to its origin, its amplitude has to be at least equal to the starting value.

$$R_1 R_2 exp\left[\frac{i2\pi n_r z}{\lambda_0}\right] exp[(g-\alpha_i)2L] = 1 \tag{2.2}$$

The amplitude condition could be expressed as

$$R_1 R_2 exp[(g-\alpha_i)2L] = 1 \tag{2.3}$$

The phase condition for that electromagnetic wave is

$$2m\pi = \frac{4\pi n_r L}{\lambda_0} \tag{2.4}$$

In Eq. (4), q =1,2,3……. It suggests that the optical path for a photon existing in that cavity has to be integer times its wavelength. Therefore, all the lasing modes in the F-P cavity are orthogonal. This orthogonality is also interpreted as so-called “nodes of wave” as depicted in Fig.2 2.

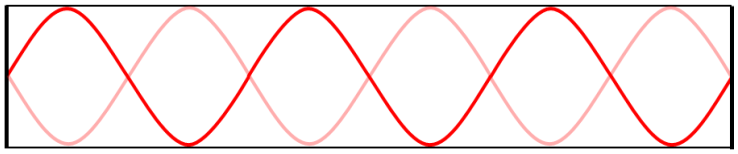

$q = 6$

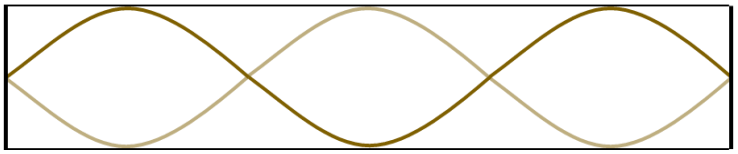

$q = 3$

Fig. 2.2 nodes od wave in F-P laser.

For the lasing modes, the electronic fields are

$$E_m = A_m e^{jm(\frac{z}{L})\pi} \tag{2.5}$$

A_m is the amplitude and m is the order of longitude lasing mode. The PPR phenomenon can enhance the modulation bandwidth as the interaction between two modes increase. The PPR phenomenon enhance the modulation bandwidth as the interaction between two modes increase. The strong lasing mode is called main mode. The weak lasing mode is called sub mode. The coupling efficiency η_z between main and sub modes is important to PPR phenomenon. The coupling efficiency between different

modes is explained as the spatial overlap between different modes as shown in

$$\eta_z = \int_0^{2L} E_a \, E_b dz \tag{2.6}$$

In the Eq. (2.6), a and b mean different lasing modes. Substituting Eq. (2.5) into Eq. (2.6), the longitudinal confinement for Fabry-Perót laser is

$$\begin{aligned}\eta_z &= \int_0^{2L} A_{main} e^{jm_{main}\left(\frac{z}{L}\right)\pi} \; A_{sub} e^{jm_{sub}\left(\frac{z}{L}\right)\pi} dz \\ &= \frac{A_{main}A_{sub}}{j\pi\left(\frac{m_{main}}{L}+\frac{m_{sub}}{L}\right)} e^{j(m_{main}+m_{sub})\frac{z}{L}\pi}\Big|_0^{2L} = 0\end{aligned} \tag{2.7}$$

And the coupling efficiency η_z is to be zero. The result means that all the lasing modes in the Fabry-Perót cavity are orthogonal and thus any PPR phenomenon is not caused any more.

2.3 Non-orthogonality in active-MMI laser diode

The configuration of active-MMI laser [19] reported to observe multiple PPRs is shown in Fig.2.3.

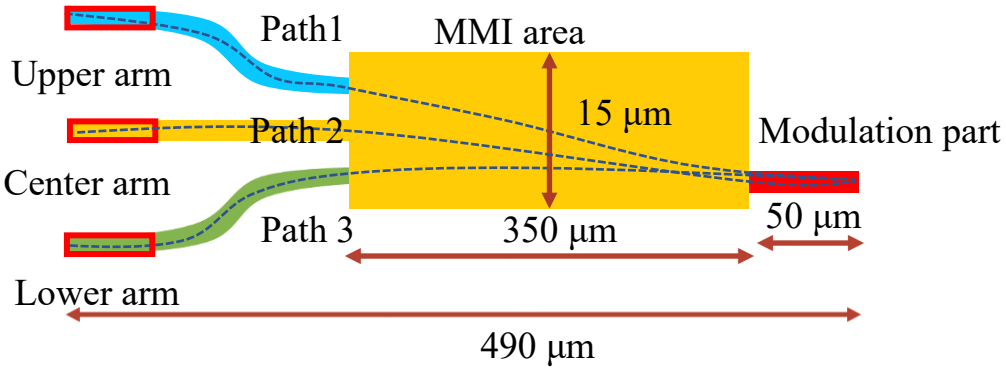

Fig. 2.3 Schematic diagram of active-MMI laser.

The situation of Fabry-Perót resonance in active-MMI LD is slightly different from the above-discussed regular case of Fabry-Perót LD. Even though in a single device, there are several different light-path lengths inside of the device. There are three parts to this device. In the middle is the MMI areas. In the LHS of MMI area are three arm parts, called upper arm, middle arm and lower arm respectively. In the RHS of the MMI area, it is another waveguide working as modulation part. There are three different optical paths named path 1, path 2 and path 3 in that cavity. The coupling efficiency η_z in active-MMI laser diode is

$$\eta_z = \int_0^{2L_{main}} A_{main} e^{jm_{main}\frac{z\pi}{L_{main}}} A_{sub} e^{jm_{sub}\frac{z\pi}{L_{sub}}} dz$$
$$= \frac{A_{main}A_{sub}}{j(\frac{\pi m_{1main}}{L}+\frac{\pi m_{sub}}{L})} e^{j\left(\frac{m_{main}}{L_{main}}+\frac{m_{sub}}{L_{sub}}\right)z\pi} \Big|_0^{2L_{main}} \quad (2.8)$$

As the optical cavity in active-MMI laser diode for different path is

different, the coupling efficiency η_z is

$$\eta_z = \frac{A_{main}A_{sub}}{j\pi(\frac{m_{main}}{L_{main}}+\frac{m_{sub}}{L_{sub}})}\left(e^{j(2m_{main}+2m_{sub}\frac{L_{main}}{L_{sub}})\pi}-1\right)\neq 0 \qquad (2.9)$$

Therefore, non-orthogonal Fabry-Perót resonance exists in active-MMI laser diode. To confirm this path length difference in the active-MMI LD shown in Fig. 2.3, we do simulations by using the following way. For the actual calculation, we utilize the FDTD (finite-division time-domain) method [20].

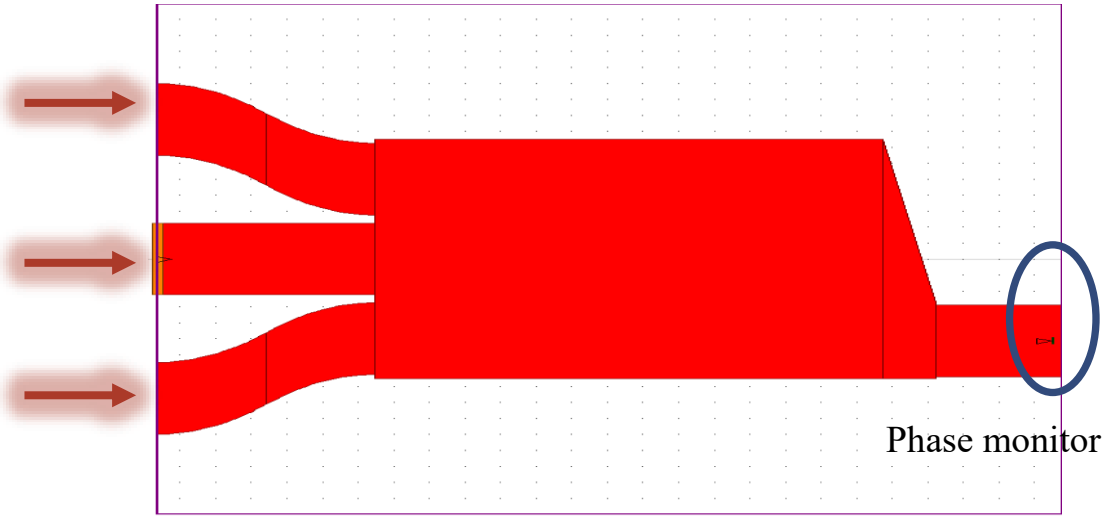

Fig. 2.4 Simulation setting of active-MMI laser.

The initial light is injected from three arms respectively. We monitored the phase of the propagated light at the single output waveguide end. If the path length is the same among three different injection conditions, the

achieved phase as a function of wavelength must be completely matched to each other.

The simulation results are shown in Fig.2.5. The phase conditions for each path are different from each other. This confirms our thought that there are non-orthogonal modes in active-MMI LD.

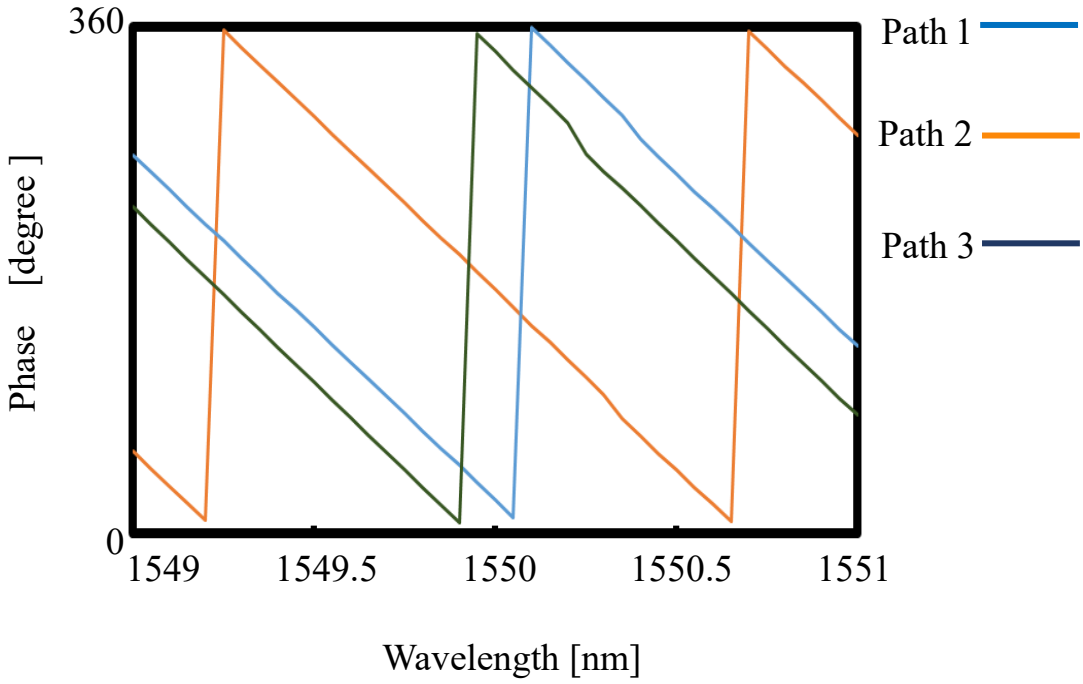

Fig. 2.5 Phase of different paths in active-MMI laser.

Based on the simulation results, the transmittance of each path can be derived from Eq.(4). The transmittance results are shown in Fig.2.5.

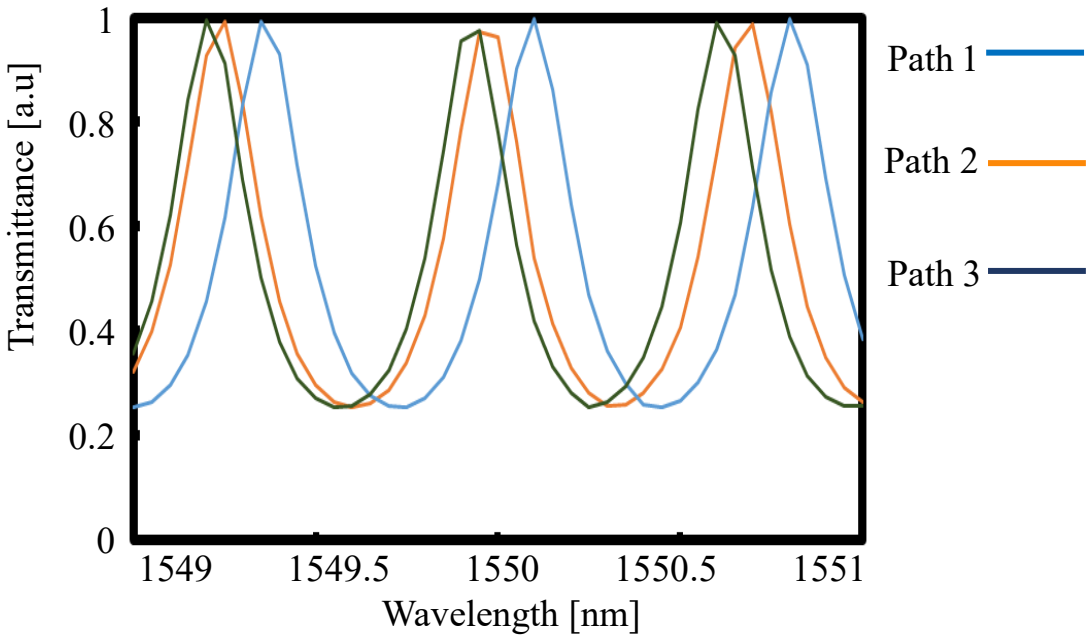

Fig. 2.6 transmittance of different paths of active-MMI laser.

From Fig 2.6, the wavelength whose transmittance is equal to 1 are modes that may exist in the path. Hence, the effective optical path length for each path. For each path, those wavelengths whose transmittance is equal to 1 are called λ_{peak}. It is clear that, in the simulation range, there are three λ_{peak} for each path. With the relationship expressed in Eq.(4), the optical path for each path is achieved and shown in Tab 2.1.

Tab 2.1 Optical path for three paths in active-MMI LD

	λ_{peak1} [nm]	λ_{peak} [nm]	Δλ [nm]	Optical path [μm]
Path 1	1549.35	1550.1	0.75	500.33
Path 2	1549.25	1549.975	0.725	517.52
Path 3	1549.2	1549.925	0.725	517.49

Based on the research on PPR phenomenon, the spectrum of laser is very important information to confirm the PPR phenomenon. From all the work concentrated on PPR phenomenon, experimentally, the spectrum of the laser with PPR phenomenon is similar to Fig.2.7. Except for the main lasing wavelength, there is another weak lasing wavelength. From its spectrum, the location of PPR is derived from

$$f_{ppr} = c(\frac{1}{\lambda_{main}} - \frac{1}{\lambda_{sub}}) \tag{2.10}$$

where λ_{main} and λ_{sub} are wavelengths for the strong lasing mode and weak lasing mode. c is the light velocity in vacuum. It indicates that the location of PPR is related to the spectrum. Thus, the predictable spectrum will help us to utilize PPR to extend the modulation bandwidth.

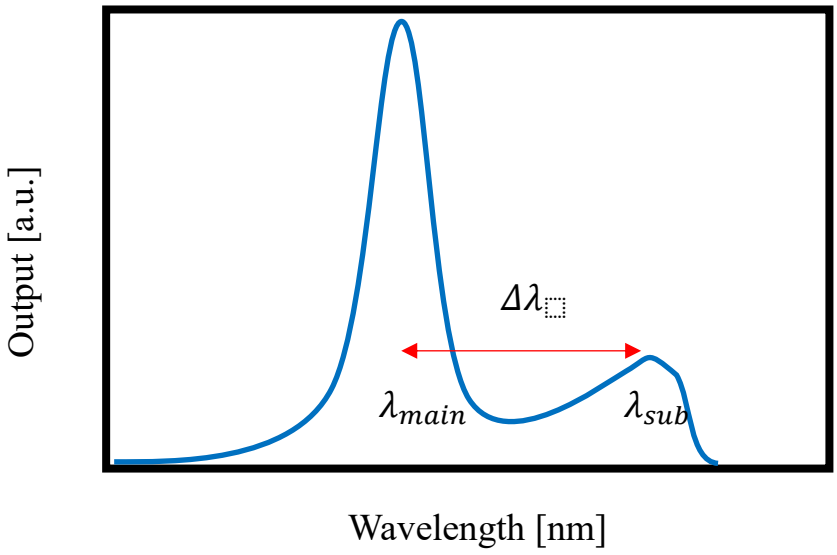

Fig. 2.7 Schematic diagram of active-MMI laser.

To get the spectrum, the intensity ratio of each arm has to be clarified. Because of the self-image phenomenon [33], the ratio of optical power from each path is not the same weight in active-MMI LD. As shown in Fig 2.8, when the light is injected from the single-end side, the percentage of the power in each path is different. The majority of power is propagated through path 1 which is accessed with the upper arm. The second most power is propagated through path 2 connected to the middle arm. Path 3 related to the lower arm contributes the least to light propagation.

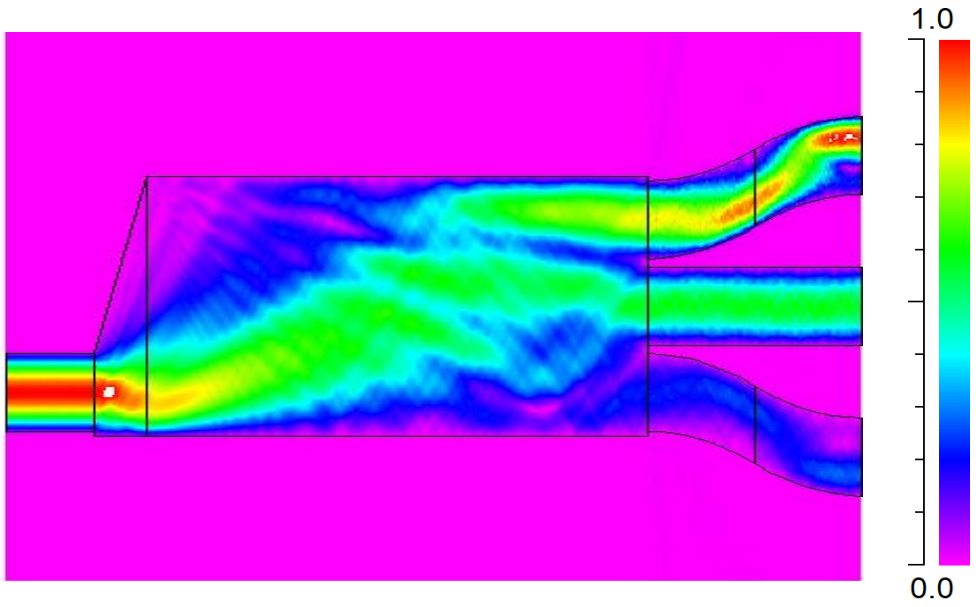

Fig. 2.8 Schematic diagram of intensity distribution of active-MMI laser.

Taking this intensity ratio into account, the transmittance of each arm will be shown in Fig.2.9.

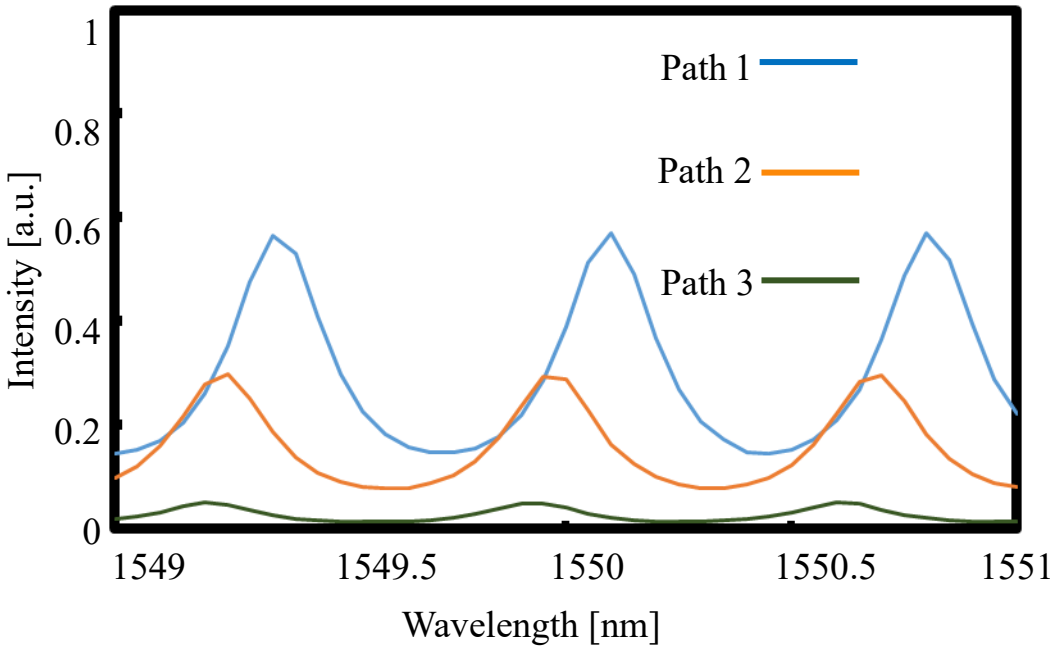

Fig. 2.9 Schematic diagram of intensity of each arm in active-MMI laser.

It is necessary to clarify that, when this configuration is working as an active device, the lasing mode generated by path 1 may not be the main lasing mode, and the lasing mode related to another path may not be the sub-lasing mode either. This is because all the simulations we carried out did not consider the gain. Thus, it is unclear which one is the main lasing mode which one is the sub-lasing mode until the laser is lasing. However, the wavelength difference does not change. From the wavelength difference, the location of PPR is obtained. The spectrum from passive device simulation is calculated. The results are calculated with the condition that lasers have been through 6 times round-trip times. Figure 2.10 displays four possible lasing wavelengths 1549.9 nm, 1550.1 nm,1550.6 nm and 1550.7 nm. Though we don't know which one is the main lasing laser, we assume that the laser with wavelength of 1550.1 as

the main lasing mode. Based on that assumption, there are three possible locations for PPRs. It is 24 GHz, 63 GHz and 75 GHz. The details are listed in Tab 2.2.

Tab 2.2 Wavelength difference and PPR location

Δλ [nm]	0.2	0.5	0.6
PPR location [GHz]	24	63	75

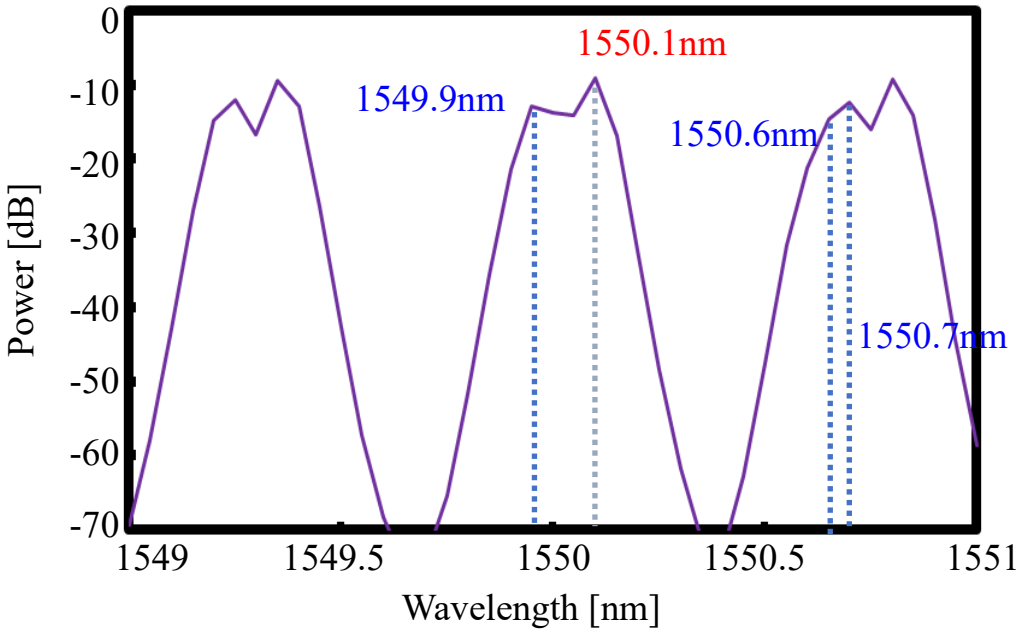

Fig. 2.10 Calculated spectrum of active-MMI laser.

The small signal modulation response of the proposed 1×3 active-MMI LD is shown is shown in Fig 2.11.

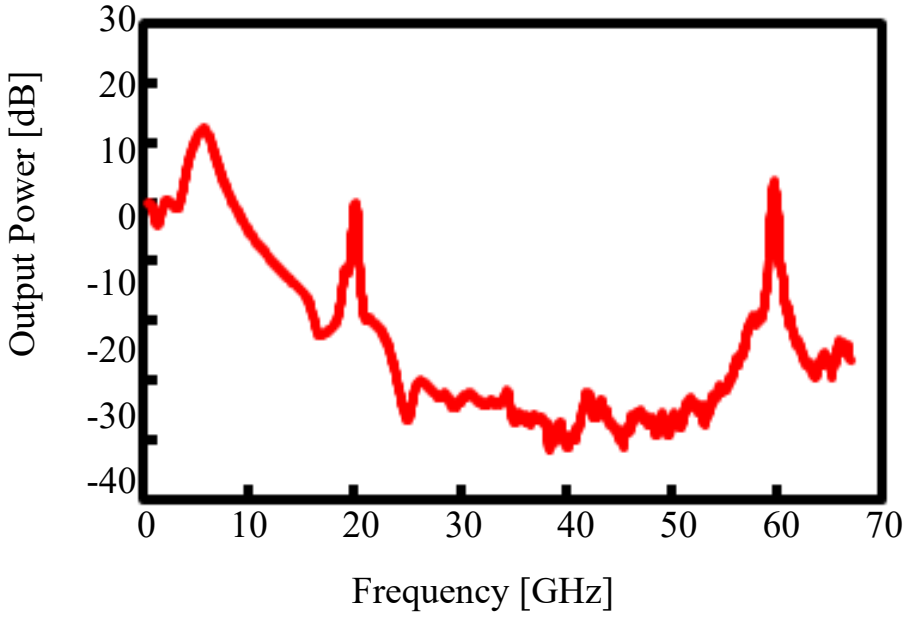

Fig. 2.11 Small modulation of active-MMI laser.

Two PPRs are observed [31]. One is located at 20 GHz and another is located at 60 GHz. The prediction of the spectrum is confirmed by the experiment.

Reference

[1] Coldren, Larry A., Scott W. Corzine, and Milan L. Mashanovitch. Diode lasers and photonic integrated circuits. John Wiley & Sons, 2012. Chapter 2.

[2] Erwin K. Lau, Amit Lakhani, Rodney S. Tucker, and Ming C. Wu, "Enhanced modulation bandwidth of nanocavity light emitting devices," Opt. Express 17, 7790-7799 (2009)

[3] R. S. Tucker, “High-speed modulation of semiconductor lasers,” J. Lightwave Technol. 3, 1180–1192 (1985).

[4] Haglund, Erik, et al. "30 GHz bandwidth 850 nm VCSEL with sub-100 fJ/bit energy dissipation at 25–50 Gbit/s." Electronics Letters 51. (2015): 1096-1098 (2015).

[5] Westbergh, P., Safaisini, R., Haglund, E., Kögel, B., Gustavsson, J.S., Larsson, A., Geen, M., Lawrence, R., Joel, A.: ‘High-speed 850 nm VCSELs with 28 GHz modulation bandwidth operating error-free up to 44 Gbit/s’, Electron. Lett., 48, (18), pp. 1145–1147 (2012).

[6] Fedor Zubov, Mikhail Maximov, Natalia Kryzhanovskaya, Eduard Moiseev, Maria Muretova, Alexey Mozharov, Nikolay Kaluzhnyy, Sergey Mintairov, Marina Kulagina, Nikolay Ledentsov, Lukasz Chorchos, Nikolay Ledentsov, and Alexey Zhukov, "High speed data transmission using directly modulated microdisk lasers based on InGaAs/GaAs quantum well-dots," Opt. Lett. 44, pp. 5442-5445

(2019).

[7] E. Haglund, P. Westbergh, J. S. Gustavsson, E. P. Haglund, A. Larsson, M. Geen, and A. Joel, "High-Speed 850 nm VCSEL with 30 GHz Modulation Bandwidth," in 2015 European Conference on Lasers and Electro-Optics - European Quantum Electronics Conference, (Optica Publishing Group, 2015), paper CB_2_4.

[8] T. H. Wood, C. A. Burrus, D. A. B. Miller, D. S. Chemla, T. C. Damen, A. C. Gossard, W. Wiegmann; High-speed optical modulation with GaAs/GaAlAs quantum wells in a p-i-n diode structure. Appl. Phys. Lett. 1 January; 44 (1): pp.16–18, (1984).

[9] Liu, Zhixin, and Radan Slavík. "Optical injection locking: From principle to applications." Journal of Lightwave Technology 38.,1pp. 43-59 (2020).

[10] C. Sun, D. Liu, B. Xiong, Y. Luo, J. Wang, Z. Hao, Y. Han, L. Wang, and H. Li, “Modulation characteristics enhancement of monolithically integrated laser diodes under mutual injection locking,” IEEE J. Sel. Topics Quantum Electron., vol. 21, no. 6, pp. 628–635, (2015).

[11] Matsui. Y, Murai. H, Arahira. S, Kutsuzawa. S, Ogawa. Y. 30-GHz bandwidth 1.55-μm strain-compensated InGaAlAs-InGaAsP MQW laser. IEEE Photon. Technol. Lett. 9, pp. 25–27 (1997).

[12] Zhao. W, Mao. Y, Lu. D, Huang. Y, Zhao. L, Kan. Q, Wang. W; "Modulation bandwidth enhancement of monolithically integrated

mutually coupled distributed feedback laser." Applied Sciences 10.12 4375 (2020).

[13] Reithmaier. J.P, Kaiser. W, Bach. L, Forchel. A, Feies. V, Gioannini. M, Montrosset. I, Berg. T.W, Tromborg. B: “Modulation speed enhancement by coupling to higher order resonances: A road towards 40 GHz bandwidth lasers on InP”. In Proceedings of the International Conference on Indium Phosphide and Related Materials, Glasgow, Scotland, UK, 8–12 May; pp. 118–123 (2005).

[14] Kreissl J, Vercesi V, Troppenz U, Gaertner T, Wenisch W, Schell, M: “Up to 40-Gb/s directly modulated laser operating at low driving current: Buried-heterostructure passive feedback laser (BH-PFL)”. IEEE Photon. Technol. Lett. 24, pp. 362–364 (2012).

[15] Matsui. Y, Schatz R, Pham T, Ling. W.A, Carey. G, Daghighian. H.M, Adams. D, Sudo. T, Roxlo. C: “55 GHz Bandwidth Distributed Reflector Laser”. J. Lightwave Technol. 35, pp. 397–403 (2017).

[16] Mohrle, M.; Sartorius, B.; Bornholdt, C.; Bauer, S.; Brox, O.; Sigmund, A.; Steingruber, R.; Radziunas, H.; Wunsche, H.J. Detuned grating multisection-RW-DFB lasers for high-speed optical signal processing. IEEE J. Sel. Top. Quantum Electron. 7, pp. 217–223 (2001).

[17] Mao. Y, Ren. Z, Guo. L, Wang. H, Zhang. R, Huang. Y, Lu. D, Kan. Q, Ji. C, Wang. W: “Modulation Bandwidth Enhancement in

Distributed Reflector Laser Based on Identical Active Layer Approach". IEEE Photon. J. 10, pp.1–8 (2018).

[18] Kreissl J, Troppenz U, Rehbein W, Gaertner T, Harde P, Radziunas M: "40 Gbit/s directly modulated passive feedback laser with complex-coupled DFB section". In Proceedings of the 33rd European Conference and Exhibition of Optical Communications, Berlin, Germany, 16–20 September 2007; pp. 1–2.

[19] M. Chacinski and R. Schatz, "Impact of losses in the Bragg section on the dynamics of detuned loaded DBR lasers," IEEE J. Quantum Electron., vol. 46, no. 9, pp. 1360–1367, (2010).

[20] T. Yamamoto, A. Uetake, K. Otsubo, M. Matsuda, S. Okumura, S. Tomabechi, M. Ekawa: "Uncooled 40-Gbps direct modulation of 1.3-μmwavelength AlGaInAs distributed reflector lasers with semi-insulating buried-heterostructure," in Proc. 22nd IEEE Int. Semicond. Laser Conf., 2010, Paper ThB3.

[21] I. Tomkos, I. Roudas, R. Hesse, N. Antoniades, A. Boskovic, and R. Vodhanel, "Extraction of laser rate equations parameters for representative simulations of metropolitan-area transmission systems and networks," Opt. Commun., vol. 194, pp. 109–129, (2001).

[22] Guan S, Zhang Y, Zheng J, Su J, Sun Z, Lu L, Fang T, Li L, Xiao R, Shi Y, and Chen X: "Modulation Bandwidth Enhancement and Frequency Chirp Suppression in Two-Section DFB Laser". Journal of

Lightwave Technology, 40, pp. 7383-7389 (2022).

[23] Matsui, Y., Schatz, R., Che, D., Khan, F., Kwakernaak, M., & Sudo, T. “Low-chirp isolator-free 65-GHz-bandwidth directly modulated lasers”. Nature Photonics, 15(1), pp.59-63 (2021).

[24] Kjebon, O., Schatz, R., Lourdudoss, S., Nilsson, S., Stalnacke, B., & Bäckbom, L. “30 GHz direct modulation bandwidth in detuned loaded InGaAsP DBR lasers at 1.55 /spl mu/m wavelength”. Electronics Letters, 33, pp. 488-489 (1997).

[25] Bach, L., Kaiser, W., Reithmaier, J.P., Forchel, A., Gioannini, M., Feies, V.I., & Montrosset, I. “22-GHz modulation bandwidth of long cavity DBR laser by using a weakly laterally coupled grating fabricated by focused ion beam lithography”. IEEE Photonics Technology Letters, 16, pp. 18-20 (2004).

[26] Laakso, A., Dumitrescu, M. Modified rate equation model including the photon–photon resonance. Opt Quant Electron 42, pp. 785–791 (2011).

[27] Matsui, Yasuhiro. “Directly modulated laser technology: Past, present, and future”. Datacenter Connectivity Technologies. River Publishers, 2022. pp. 149-150.

[28] Mohammad Nasir Uddin, Takaaki Kizu, Yasuhiro Hinokuma, Bingzhou Hong1, Akio Tajima, Kazutoshi Kato and Kiichi Hamamoto. “High intrinsic modulation bandwidth InGaAsP/InGaAsP 1.55 μm

asymmetric active multimode interferometer laser diode by using split pump configuration.” Japanese Journal of Applied Physics 53. 8S2. pp. 08MB09 (2014).

[29] Bingzhou Hong, Takuya Kitano, Tomotaka Mori, Haisong Jiang, and Kiichi Hamamoto, “Bandwidth Enhancement Scheme Demonstration (from 5 GHz to 34 GHz) on Direct Modulation Laser Diode using Multiple PPR (Photon-Photon Resonance) Active MMI,” ECOC 2017, P1.SC2.22, 2017.

[30] Bingzhou Hong, Takuya Kitano, Tomotaka Mori, Haisong Jiang and Kiichi Hamamoto, “Bandwidth enhancement scheme demonstration on direct modulation active-MMI laser diode using multiple photon photon resonance,” Applied Physics Letters, 111, pp.221105, (2017).

[31] S. Murakami, B. Hong, H. Jiang and K. Hamamoto, "Observation of 60 GHz and 20 GHz Multiple Photon-Photon Resonances Using Active Multimode Interferometer Laser Diodes," 2019 24th Microoptics Conference (MOC), Toyama, Japan, 2019, pp. 304-305.

[32] Iniewski, K. (Ed.). (2017). Integrated microsystems: electronics, photonics, and biotechnology. CRC Press. Chapter. 21, pp. 474-478.

Chapter 3

Theoretical analysis of Photon-photon-resonance in active-MMI lasers diode

3.1 Introductory overview

PPR is known as high frequency resonance compared to CPR. Up to now, all the laser diodes that could be observed PPR phenomenon appear with the existence of extra cavities besides the main oscillating cavity in the laser diode (LD) [1-14]. It indicates that an LD with PPR consists of more than one longitudinal mode. As we explained in Chapter 2, non-orthogonal modes exist in active-MMI laser diode, therefore, active-multimode interference laser diode (active-MMI LD) is an ideal structure to utilize PPR phenomenon as it consists of a multimode section and several access waveguides. Moreover, active-MMI LD is capable of exploiting plural PPRs. The experiment result in [15] proved that multiple PPRs exist in active-MMI LD. As we noticed that, though there are two PPRs in the modulation response, the damping problems between CPR and PPR, PPR and PPR are still restricting to the modulation bandwidth. To achieve a higher frequency response without -3 dB degradation in the bandwidth, one important thing is to engineer the peak position, width and height (i.e. the control scheme of PPR peak). However, it seems the investigation into the control scheme is still not sufficient.

In this chapter, the model of PPR in active-MMI LD has been explained. In section 3.2, the rate equation describing the PPR in the laser diode is discussed. Section 3.3 is the control mechanism of PPR. Multiple PPRs design is explained in section 3.4. In the end, the overshoot problem of PPR is discussed.

3.2 Rate equation of PPR in active MMI LD

It has been reported that PPR phenomena were related to multiple longitudinal lasing modes interaction in LD. All the published research about PPR phenomena has shown that there is a pair of lasing modes (a strong lasing mode λ_{main} and a weak lasing mode λ_{sub}) as shown in Fig 3.1. The location of PPR is related to the frequency difference of two lasing modes [16-17], expressed as

$$f_{ppr} = c(\frac{1}{\lambda_{main}} - \frac{1}{\lambda_{sub}}) \qquad (3.1)$$

In other words, to generate PPR, multiple lasing mode is necessary. Therefore, multiple cavities assembled in one device are required. Active-MMI LD is an ideal structure to utilize the PPR phenomenon because it consists of multimode section and several access waveguides as 1×2 active-MMI LD shown in Fig 3.2. In that section, to simplify PPR model, instead of discussing multiple PPRs, one PPR model in 1×2 active-MMI

LD is explained.

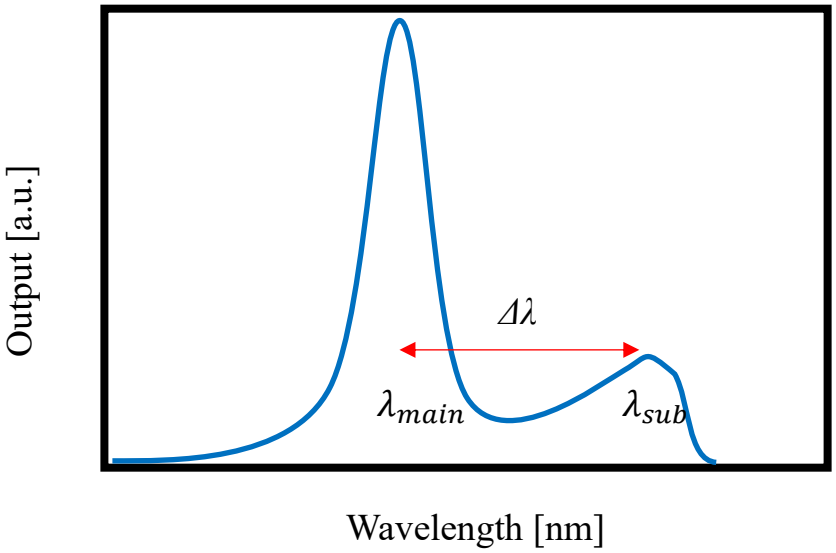

Fig. 3. 1 The spectrum of PPR phenomenon.

Figure 3.2 illustrates the waveguide configuration of this active-MMI LD. It is divided into three sections: section 1: the arm section at which a few waveguides are in LHS, section 2: the MMI section which lies in the middle as the main pumping area, and section 3: the modulation section in which is connected to the RHS of MMI section. All the sections in active-MMI LD are active areas. two longitude modes supported by two different paths are interacting with each other that the PPR phenomena are exploited. There are two different oscillation modes and two different lasing wavelengths in this configuration. In that case, the conventional rate equation described laser activity in cavity is no longer sufficient to be applied to explain PPR phenomena as it only contains photon density and carrier density. rate equations are derived from electro-magnetic wave theory in laser.

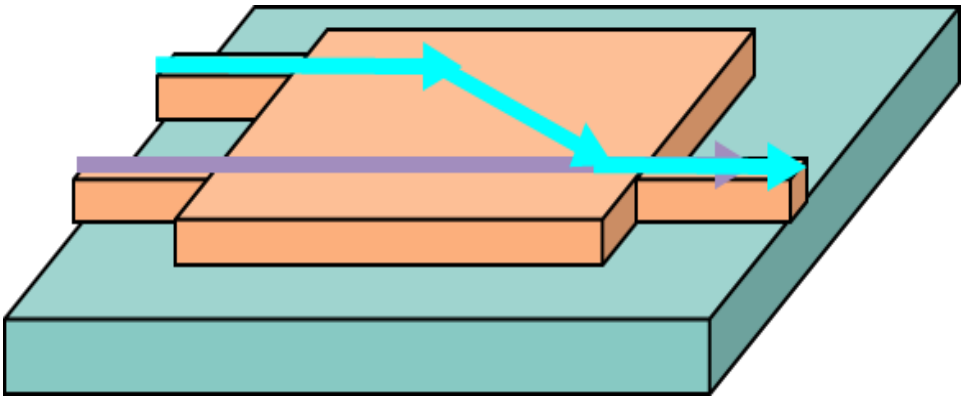

Fig. 3. 2 The structure of 1×2 active-MMI laser.

As explained before, there are two lasing modes in the laser cavity. One is called the main lasing mode (strong lasing mode) whose electric field is

$$E_1(t) = A_1(t)expj\theta_1(t) \qquad (3.2)$$

$A_1(t)$ is the filed magnitude and $\theta_1(t)$is defined as

$$\theta_1(t) = \omega_2 t + \phi_1(t) \qquad (3.3)$$

where ω_1 is the aangularfrequency$\phi_1(t)$ is the initial phase.

The differential equation for the main lasing mode is

$$\frac{dE_1(t)}{dt} = \frac{1}{2}G_1(1 + j\alpha)[N(t) - N_{th}] \times E_1(t) \qquad (3.4)$$

Another one is called sub-lasing mode (weak lasing mode) whose electric field is

$$E_2(t) = A_2(t)expj\theta_2(t) \qquad (3.5)$$

$A_2(t)$ is the filed magnitude. $\theta_2(t)$ is given in eq. (4)

$$\theta_2(t) = \omega_2 t + \phi(t) \qquad (3.6)$$

where ω_2 is the angular frequency and α is the linewidth confinement. $\phi(t)$ is time-dependent phase factor of sub-lasing mode [20]. In that laser cavity, two orthogonal longitude modes exist and synchronization phenomena appear [18]. Based on synchronization theory, the strong resonance will force the weak resonance to oscillate with its frequency. Therefore, the electric field of the sub-mode lasing mode is affected by the main lasing mode. Here we introduce the time-derivative of the electric field which was derived in reference [19-40].

$$\frac{dE_2(t)}{dt} = \left\{\frac{1}{2}(1 + i\alpha)G_2[N(t) - N_{th}] - j\Delta\omega\right\}E_2(t) + \kappa E_1(t) \qquad (3.7)$$

Where, G_2 is gain coefficient of sub lasing mode, κ is coupling efficiency, $\Delta\omega$ is the frequency difference of the main lasing mode and sub-lasing mode is defined as

$$\Delta\omega = \omega_1 - \omega_2 \qquad (3.8)$$

If there is no affection of main lasing mode, the coupling term in amplitude and phase ($\kappa E_1(t)$ and $j\Delta\omega$) will be zero.

We utilize the following relation especially in sub-lasing mode using electric field expression:

$$S_2(t) = E_2(t) \times E_2^*(t) \qquad (3.9)$$

where $E_2^*(t)$ is the conjugate complex of $E_2(t)$, and $S_2(t)$ is photon density. The time-derivate of eq. (3.7) is then:

$$\frac{dS_2(t)}{dt} = \frac{dE_2(t)}{dt}E_2^*(t) + \frac{dE_2^*(t)}{dt}E_2(t) \qquad (3.10)$$

Here we utilize the time-derivative of $E_2^*(t)$ indicated in eq. (3.10):

$$\frac{dE_2^*(t)}{dt} = \left\{\frac{1}{2}(1 - j\alpha)G_2[N(t) - N_{th}]) + j2\pi\Delta\omega\right\} \times E_2(t) + \kappa E_1^*(t) \quad (3.11)$$

Substituting (3.6) and (3.10) into (3.9), we get the following rate equation for sub-lasing mode (The detail is shown in appendix):

$$\frac{dS_2(t)}{dt} = G_2[N(t) - N_{th}] \times S_2(t) + 2\kappa\sqrt{(S_1(t) * S_2(t)}\cos(\theta_2(t) - \theta_1(t)) \quad (3.12)$$

In addition to the differential equation of $S_2(t)$, here we derive the differential equation of $\theta_2(t)$: phase factor for sub-lasing mode. We again utilize eq. (3.7). The time derivation of $E_2(t)$ and $E_2^*(t)$ are rewritten as follows:

$$\frac{dE_2(t)}{dt} = \frac{dA_2(t)}{dt}e^{j\theta_2(t)} + jA_2(t)\frac{d\theta_2(t)}{dt}e^{j\theta_2(t)} \quad (3.13)$$

$$\frac{dE_2^*(t)}{dt} = \frac{dA_2(t)}{dt}e^{-j\theta_2(t)} - jA_2(t)\frac{d\theta_2(t)}{dt}e^{-j\theta_2(t)} \quad (3.14)$$

Then, the equation for $\frac{d\theta_2(t)}{dt}$ is derived by multipling $e^{-j\theta_2(t)}$ and $e^{j\theta_2(t)}$ to eq. (3.13) and eq. (3.14), respectively as follows:

$$\frac{d\theta_2(t)}{dt} = G_2[N(t) - N_{th}] \times S_2(t) + \kappa\sqrt{\frac{S_1(t)}{S_2(t)}}sin(\theta_2(t) - \theta_1(t)) - \Delta\omega \quad (3.15)$$

Overall, four differential equations of the PPR phenomena are

summarized in the following (3.16) – (3.19):

$$\frac{dS_1(t)}{dt} = G_1[N(t) - N_{th}] \times S_1(t) \qquad (3.16)$$

$$\frac{dS_2(t)}{dt} = G_2[N(t) - N_{th}] \times S_2(t) + 2\kappa\sqrt{(S_1(t) * S_2(t)}\cos(\theta_2(t) - \theta_1(t)) \qquad (3.17)$$

$$\frac{d\theta_2(t)}{dt} = \frac{\alpha}{2}[G_2(N(t) - N_{th})] + \kappa\sqrt{\frac{S_1(t)}{S_2(t)}}sin(\theta_2(t) - \theta_1(t)) - \Delta\omega \qquad (3.18)$$

$$\frac{dN(t)}{dt} = J - \frac{N(t)}{\tau_r} - G_1[N(t) - N_{tr}] \times S_1(t) - G_2[N(t) - N_{tr}] \times S_2(t) \qquad (3.19)$$

$S_1(t)$, $S_2(t)$, $N(t)$ and N_{th}, $N_{th}$are the photon density of the main lasing mode, photon density of the sub-lasing mode, carrier density and the threshold carrier density, transparency carrier density respectively.

α is the linewidth-enhancement factor. κ has been historically defined as $1/\tau_p$ (τ_p : photon round-trip time) and its expression is shown in eq. (3.20) [20,38].

$$\kappa = \frac{1}{\tau_p}. \qquad (3.20)$$

The definition of coupling efficiency means that two lasers propagate along

the entire cavity to couple.

The definition of coupling efficiency means that two lasers propagate along the entire cavity to couple.

The small signal analysis approach is applied to solve the fourth rate equation. At the beginning, the steady state of the fourth rate equation is calculated. by setting the LHS of the fourth equation at 0. The steady-state photon density of the main lasing mode and sub-lasing mode are S_1 and S_2. When the laser is modulated by a small signal with frequency ω, the linearized form of Eq. (3.16-3.19) is placed in matrix form:

$$\begin{bmatrix} jw & 0 & 0 & m_{s1n} \\ 0 & m_{s2s2}+jw & m_{s2\phi} & m_{s2n} \\ 0 & m_{\phi s2} & m_{\phi\phi}+jw & m_{\phi n} \\ m_{ns1} & m_{ns2} & 0 & m_{nn}+jw \end{bmatrix} \begin{bmatrix} \Delta S_1 \\ \Delta S_2 \\ \Delta\phi \\ \Delta N \end{bmatrix} = \begin{bmatrix} 0 \\ 0 \\ 0 \\ \Delta J \end{bmatrix} \quad (3.21)$$

Where the matrix terms are:

$m_{s1n} = -G_1 S_1$

$m_{s2s2} = z cos\phi_0$

$m_{s2\phi} = 2zS_2 sin\phi_0$

$m_{s2n} = -G_2 S_2$

$m_{\phi s2} = -\frac{z}{2S_2} sin\phi_0$

$m_{\phi\phi} = z cos\phi_0$

$m_{\phi n} = -\frac{\alpha}{2} G_2$

$$m_{ns1} = \frac{1}{\tau_{p1}}$$

$$m_{ns2} = \frac{1}{\tau_{p2}}$$

$$m_{nn} = \frac{1}{\tau_r} + G_1 S_1 + G_2 S_2$$

Where $z \equiv k\sqrt{\frac{S_1}{S_2}}$. And the parameter $\sqrt{\frac{S_1}{S_2}}$ referring as the photon ratio between the main-mode laser and sub-mode laser is defined as the intensity ratio *R*. All the parameter used in the simulation is listed Tab 3.1.

Tab 3.1 Laser Parameter

Symbol	Value	Units
G_1	7887	1/s
G_2	2090	1/s
α	5	
J_{th}	7.5×10^{17}	1/s
J	$2.13\times J_{th}$	1/s
τ_{p1}	2.77	ps
τ_{p2}	11.6	ps
r	0.3	
L	360	μm
τ_r	3.3	ns
N_{th}	2.5×10^{9}	-
n_g	3.3	-

$\Gamma_{overlap}$	0.7	-

The most convenient solution is to choose a phase value of ϕ_0, knowing that the ϕ_0 is in the range of $-\frac{\pi}{2} - tan^{-1}\alpha \leq \phi_0 \leq \frac{\pi}{2} - tan^{-1}\alpha$.

The change in carrier number must be negative so that the total carrier number can never be higher than the threshold carrier number. Based on that requirement, the locking range is achieved.

$$-z\sqrt{1+\alpha^2} \leq \Delta\omega \leq z \qquad (3.22)$$

The magnitude of the direct modulation frequency response is then written as:

$$H(j\omega) = \frac{\Delta S_1 + \Delta S_2}{\Delta J} = \frac{P(j\omega)^2 + Q(j\omega) + T}{(j\omega)^4 + A(j\omega)^3 + B(j\omega)^2 + C(j\omega) + D} \qquad (3.23)$$

Where

$A = m_{s2s2} + m_{\phi\phi} + m_{nn}$

$B = m_{nn} + m_{s2s2}m_{\phi\phi} - m_{s1n}m_{ns1}$

$\quad + m_{\phi\phi}m_{\phi\phi} - m_{s2\phi}m_{\phi s2} - m_{s2n}m_{ns2}$

$C = m_{ns2}m_{s2\phi}m_{\phi n} - m_{s2n}m_{\phi\phi}m_{ns2} + m_{s2s2}m_{\phi\phi}m_{nn} - m_{nn}m_{s2\phi}m_{\phi s2}$

$D = m_{s1n}m_{ns1}(m_{s2\phi}m_{\phi s2} - m_{s2s2}m_{\phi\phi})$

$P = -(m_{s1n} + m_{s2n})$

$$Q = -m_{s1n}(m_{s2s2}+m_{\phi\phi}) - m_{s2n}(m_{s2\phi}m_{\phi n} - m_{s2n}m_{\phi\phi})$$

$$T = m_{s2s2}m_{\phi\phi} - m_{s2\phi}m_{\phi s2}.$$

The frequency resonance is easily determined by eq. (3.23). The determinant of the resonance frequency is lying in the denominator in the eq. (3.23),

$$E(j\omega) = (j\omega)^4 + A \times (j\omega)^3 + B \times (j\omega)^2 + C \times (j\omega) + D$$
$$\approx E_1(j\omega)\ x E_2(j\omega),$$

And

$$E_1(j\omega) = ((j\omega)^2 + m_{nn}(j\omega) - m_{s1n}m_{ns1}),$$
$$E_2(j\omega) = (j\omega)^2 + (m_{s2s2}+m_{\phi\phi})(j\omega) + (m_{s2s2}m_{\phi\phi} - m_{s2\phi}m_{\phi s2}) \qquad (3.24)$$

From eq. (3.24), it suggests that there are two resonance frequencies. The first resonance frequency lies in $\omega_1 = \sqrt{-m_{s1n}m_{ns1}}$ which is the expression of the relaxation oscillation of the free running laser. And the second one lies in

$$\omega_{ppr} = \sqrt{m_{s2s2}m_{\phi\phi} - m_{s2\phi}m_{\phi s2}} \qquad (3.25)$$

The diagonal matrix terms in eq. (3.21) are typically weak. We can

consider the last nondiagonal terms in eq. (3.25), yielding

$$\omega_{ppr} \approx \sqrt{-m_{s2\phi} m_{\phi s2}} = z sin\phi_0. \quad (3.26)$$

The steady-state condition of (16-19) is

$$\frac{\alpha}{2}[(G_2(N_0 - N_{th})] - z * sin\,\phi_0 - \Delta\omega = 0 \quad (3.27)$$

Considering (13) and (14), we know the relationship between the frequency difference between two lasers and the resonance frequency is

$$\omega_{ppr} = \left| -\frac{\alpha}{2}[(G_2(N_0 - N_{th})] - \Delta\omega \right| \quad (3.28)$$

And in lasering condition, the term $(-\frac{\alpha}{2}(G_2(N_0 - N_{th}))$ is almost zero. Therefore, the final expression of the frequency resonance is

$$\omega_{ppr} \approx \Delta\omega. \quad (3.29)$$

It suggests that the resonance frequency of PPR is equal to the frequency difference between the main mode laser and the sub-mode laser, which is in agreement with the experimental result carried out by former research.

Back to the direct modulation frequency response $H(j\omega)$, it consists of

the direct modulation frequency response of main laser $H_1(j\omega)$ and sub-laser $H_2(j\omega)$:

$$H(j\omega) = H_1(j\omega) + H_2(j\omega) = \frac{\Delta S_1}{\Delta J} + \frac{\Delta S_2}{\Delta J}.$$

The $H_1(j\omega)$ is

$$H_1(j\omega) = \frac{\Delta S_1}{\Delta J}$$

$$\approx \frac{-m_{s1n}((j\omega)^2 + (m_{s2s2} + m_{\phi\phi})(j\omega) + m_{s2s2}m_{\phi\phi} - m_{s2\phi}m_{\phi s2})}{E_1(j\omega) \times E_2(j\omega)}$$

$$= \frac{-m_{s1n}}{E_1(j\omega)} \tag{3.30}$$

This means that the direct modulation to the master laser mostly attributes to the CPR. In that paper, we are more concerned about the PPR, which leads us to the $H_2(j\omega)$:

$$H_2(j\omega) = \frac{\Delta S_2}{\Delta J} \approx \frac{-m_{s2n}((j\omega)^2 + (m_{s2\phi}m_{\phi n} - m_{s2n}m_{\phi\phi})(j\omega))}{E_1(j\omega) \times E_2(j\omega)} \tag{3.31}$$

Mathematically, the $H_2(jw)$ can be split into two terms in form of

$$H_2(j\omega) \approx \frac{W}{E_1(j\omega)} + \frac{Q}{E_2(j\omega)} \tag{3.32}$$

It indicates that the direct modulation of sub-mode laser results in the PPR. According to the analysis, if there are more than two cavities, ignoring the interaction between sub-cavities, all the lasers supported by the sub-mode are forced to oscillate with laser supported by the main cavity, multiple PPRs might be observed. This provided the theoretical foundation of multiple PPR phenomena. Multiple PPRs were observed in 1×3 active-MMI LD.

3.3 PPR frequency, width, and height control by using active-MMI laser diode

3.3.1 Coupling efficiency

As is indicated here, the differences from the conventional rate equation are especially as follows:

(1) Equation (16): This equation is the derivative of photon density for the sub-lasing mode, in addition to the one for the main-lasing mode (eq. (15)).

(2) As is indicated, it involves a co-related term between main- and sub-lasing modes as the second term through coupling efficiency, κ. Note that in eq. (15), this co-related term is neglected as the main-lasing mode is strongly associated, rather than sub-mode laser, in a laser cavity. Equation (17): This equation is considered that this phase term relates to the co-relation in longitudinal mode.

(3) To make sure, κ corresponds to the coupling efficiency between main- and sub-lasing modes. Because of this reason, we introduce $\Gamma_{overlap}$ [41] in κ :

$$\kappa = \Gamma_{overlap} \times \frac{c}{2*L*n_{eff}}. \qquad (3.33)$$

(4) It is obvious that this κ directly affects to PPR phenomena. As 1×N active-MMI configuration may offer the possibility to control $\Gamma_{overlap}$ itself, we verify the affection of $\Gamma_{overlap}$ in the following.

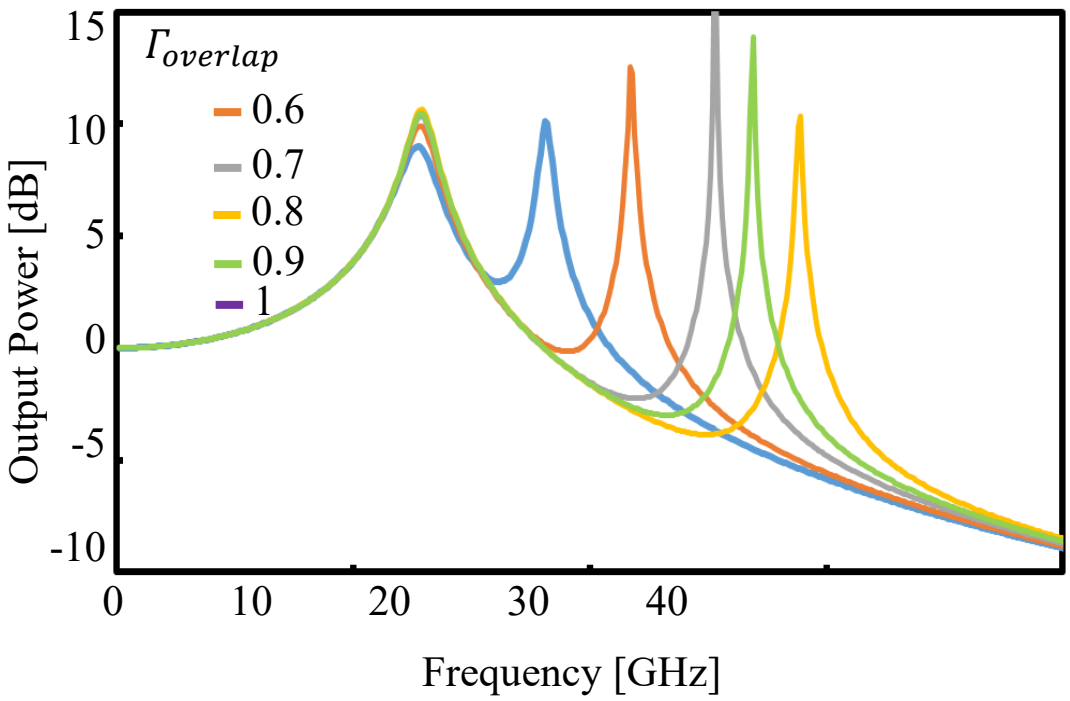

Fig. 3. 3 Calculated small signal modulation response characterized by different coupling ratios.

Figure 3.3 shows modulation response as a parameter of coupling ratios.

Here we use the condition of relaxation oscillation frequency (or CPR: carrier-photon-resonance frequency) f_{CPR} = 12 GHz, and intrinsic PPR frequency of 34 GHz with $\Gamma_{overlap}$ =1. Due to the damping problem between CPR and PPR, the modulation bandwidth only reaches a value of 22 GHz. As $\Gamma_{overlap}$ decreases from 1 to 0.6, the PPR tends to be shifted to lower frequency from 34 GHz to 22 GHz. The width of the PPR tends to become narrower, which has negative impact on modulation bandwidth improvement. Despite this width narrowing effect, the peak height of PPR increases up to $\Gamma_{overlap}$ =0.7. This peak height increase was effective in improving the extension of the modulation bandwidth f_{3dB}.

3.3.2 Phase difference

The phase term $(\theta_2(t) - \theta_1(t))$ in Eq. (14-17) will be discussed in this chapter. The interaction term in the rate equation (14-17) is affected by that phase term. As that phase term is near zero, the value of the interaction term is also close to zero which means that there is no interconnection between two different modes. All those fourth-rate equations degrade to traditional rate equations. it reveals that the phase term is a key parameter in determining the appearance of PPR phenomenon.

The simulation results have been done with PPR which is characterized by different phase terms in a range of (14.75-14.95 /30) π. The results are shown in Fig.3.4. all the parameter used in this simulation is listed in table

I. The CPR is located at 12 GHz with the PPR at 35 GHz. (Coupling ratio is 1). As illustrated in Fig. 3.22, the PPR width remains the same when the phase term is close to -π/2, whereas the intensity tends to be sharp. When the phase term is at (14.75/30) π, the intensity of PPR is -0.5 dB. As the phase changed from (14.75/30) π to (14.95/30) π, the PPR intensity rose from -0.5 dB to 15 dB. Since there is no obvious variation in PPR width, the modulation bandwidth benefits less from the high PPR intensity. What's more, this high PPR intensity would affect the large signal modulation since the overshoot of PPR. In active-MMI LD, by controlling the current injection, the refractive index inside the LD is controlled. The length of the propagation path is influenced by the refractive index, which is the main parameter related to phase difference. Note that laser modulation bandwidth would ultimately limited by the RC parasitics, The benefit of being able to customize the damping factor may be able to compensate by increasing the phase difference between main mode laser and sub-mode laser. However, the PPR phenomenon in active-MMI LD may disappear when we change the current injection , which causes the phase difference between main laser and sub-laser unmatched.

As the prediction the PPR is stronger when the phaser term is close to -π/2. This may explain to us why there is no PPR in lasers sometimes with two non-orthogonal modes existing.

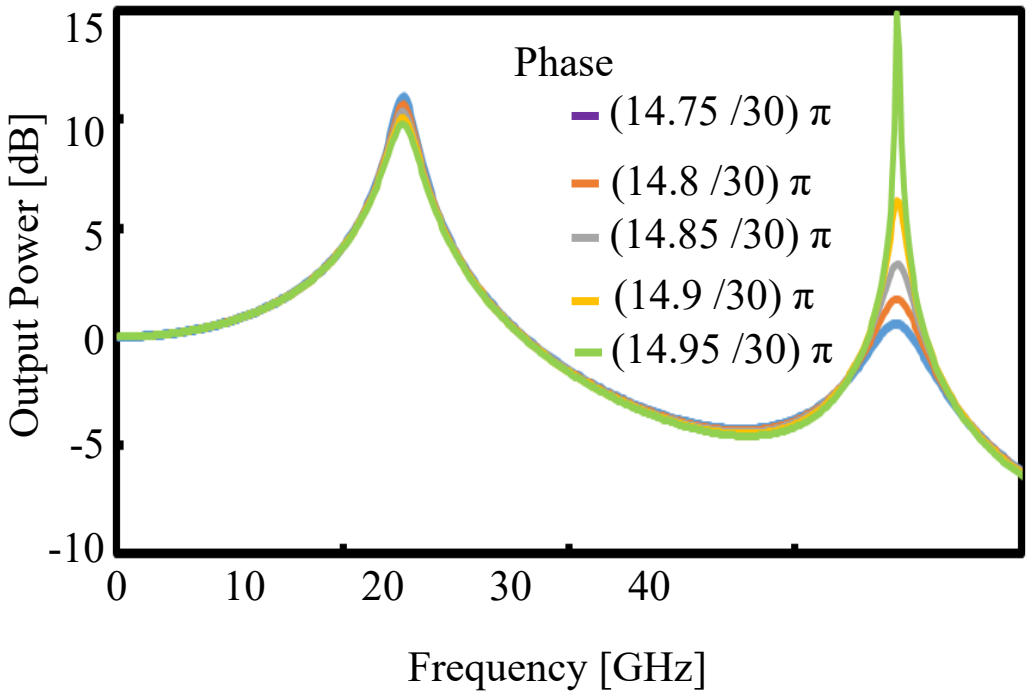

Fig. 3. 4 Calculated small signal modulation response characterized by different phases.

Reference

[1] Y. Matsui, H. Murai, S. Arahira, S. Kutsuzawa and Y. Ogawa, "30-GHz bandwidth 1.55-μm strain-compensated InGaAlAs-InGaAsP MQW laser," in IEEE Photonics Technology Letters, vol. 9, no. 1, pp. 25-27, (1997).

[2] U. Troppenz, J. Kreissl, M. Möhrle, C. Bornholdt, W. Rehbein, B. Sartorius, I. Woods, and M. Schell, "40 Gbit/s directly modulated lasers: physics and application", Proc. SPIE 7953, Novel In-Plane Semiconductor Lasers X, pp. 79530F, (16 February 2011)

[3] K. Otsubo, M. Matsuda, K. Takada, S. Okumura, M. Ekawa, H. Tanaka, S. Ide, K. Mori, T. Yamamoto, "Uncooled 25 Gbit/s direct modulation of semi-insulating buried-heterostructure 1.3 μm AlGaInAs quantum-well DFB lasers," Electronics Letters, Volume 44, Issue 10, pp. 631-633, (2008)

[4] Y. Matsui, T. Pham, W. A. Ling, R. Schatz, G. Carey, H. Daghighian, T. Sudo, and C. Roxlo, "55-GHz Bandwidth Short-Cavity Distributed Reflector Laser and its Application to 112-Gb/s PAM-4," in Optical Fiber Communication Conference Post deadline Papers, OSA Technical Digest (online) (Optica Publishing Group, 2016), paper Th5B.4.

[5] U. Feiste, "Optimization of modulation bandwidth in DBR lasers with detuned Bragg reflectors," in IEEE Journal of Quantum

Electronics, vol. 34, no. 12, pp. 2371-2379, (1998).

[6] D. D. Marcenac, M. C. Nowell and J. E. Carroll, "Theory of enhanced amplitude modulation bandwidth in push-pull modulated DFB lasers," in IEEE Photonics Technology Letters, vol. 6, no. 11, pp. 1309-1311, (1994)

[7] Kreissl, Jochen, V. Vercesi, U. Troppenz, T. Gaertner, W. Wenisch, M. Schell. "Up to 40 Gb/s Directly Modulated Laser Operating at Low Driving Current: Buried-Heterostructure Passive Feedback Laser (BH-PFL). " IEEE Photonics Technology Letters, vol. 24, pp. 362-364, (2012).

[8] Hamed Dalir, Fumio Koyama. “29 GHz directly modulated 980 nm vertical-cavity surface emitting lasers with bow-tie shape transverse coupled cavity.” Applied Physics Letters. Vol.103, No.9, pp. 091109 (2013).

[9] P. Bardella and I. Montrosset, "A New Design Procedure for DBR Lasers Exploiting the Photon–Photon Resonance to Achieve Extended Modulation Bandwidth," in IEEE Journal of Selected Topics in Quantum Electronics, vol. 19, no. 4, pp. 1502408-1502408, (2013).

[10] G. Morthier, R. Schatz and O. Kjebon, "Extended modulation bandwidth of DBR and external cavity lasers by utilizing a cavity resonance for equalization", IEEE J. Quantum Electron., vol. 36, no.

12, pp. 1468-1474, (2000).

[11]M. Vallone, P. Bardella and I. Montrosset, "Enhanced Modulation Bandwidth in Complex Cavity Injection Grating Lasers," in IEEE Journal of Quantum Electronics, vol. 47, no. 10, pp. 1269-1276, (2011).

[12]Mieda S, Shiratori S, Yokota N, Kobayashi W, Yasaka, H. “Intra-cavity loss modulation for ultrahigh-speed direct modulation lasers based on photon–photon resonance.” Applied Physics Express, vol. 8, no. 8, pp. 082701, (2015).

[13]F. Gerschütz, M. Fischer, J. Koeth, I. Krestnikov, A. Kovsh, C. Schilling, W. Kaiser, S. Höfling, and A. Forchel, "1.3 μm Quantum Dot Laser in coupled-cavity-injection-grating design with bandwidth of 20 GHz under direct modulation," Opt. Express, vol.16, no.8, pp. 5596-5601, (2008).

[14]Yokota, N., Nisaka, K., Yasaka, H., and Ikeda, K. “Spin polarization modulation for high-speed vertical-cavity surface-emitting lasers.” Applied Physics Letters, pp.113(17), (2018).

[15]S. Murakami, B. Hong, H. Jiang and K. Hamamoto, "Observation of 60 GHz and 20 GHz Multiple Photon-Photon Resonances Using Active Multimode Interferometer Laser Diodes," 2019 24th Microoptics Conference (MOC), Toyama, Japan, 2019, pp. 304-305

[16]B. Hong, T. Kitano, T. Mori, H. Jiang, K. Hamamoto; Bandwidth

enhancement scheme demonstration on direct modulation active-MMI laser diode using multiple photon photon resonance. Appl. Phys. Lett. vol. 111, no. 22, pp. 221105, (2017).

[17]M. Kanno, N. Yokota and H. Yasaka, "Measurement of Intrinsic Modulation Bandwidth of Hybrid Modulation Laser, "*IEEE Photonics Technology Letters*, vol. 32, no. 13, pp. 839-842, (2020).

[18]Arkady Pikovsky, Michael Rosenblum and Jürgen Kurths: Synchronization: A universal concept in nonlinear sciences (Cambridge Univ. Press, New York 2001) 103

[19]A. Murakami, K. Kawashima and K. Atsuki, "Cavity resonance shift and bandwidth enhancement in semiconductor lasers with strong light injection," in IEEE Journal of Quantum Electronics, vol. 39, no. 10, pp. 1196-1204, (2003).

[20]R. Lang, "Injection locking properties of a semiconductor laser", IEEE J. Quantum Electron., vol. QE-18, pp. 976-983, (1982).

[21]F. Mogensen, H. Olesen and G. Jacobsen, "Locking conditions and stability properties for a semiconductor lasers with external light injection", IEEE J. Quantum Electron., vol. QE-21, pp. 784-793, (1985).

[22]A. Murakami, "Phase locking and chaos synchronization in injection-locked semiconductor lasers", IEEE J. Quantum Electron., vol. 39, pp. 1-10, (2003).

[23]A. Murakami, "Synchronization of chaos due to linear response in optically-driven semiconductor lasers", Phys. Rev. E, vol. 65, pp. 056617, (2002).

[24]T. B. Simpson, J. M. Liu, K. F. Huang and K. Tai, "Nonlinear dynamics induced by external optical injection in semiconductor lasers", Quantum Semiclass. Opt., vol. 9, pp. 765-784, (1997).

[25]E. K. Lau, H. -K. Sung and M. C. Wu, "Frequency Response Enhancement of Optical Injection-Locked Lasers," in IEEE Journal of Quantum Electronics, vol. 44, no. 1, pp. 90-99, (2008).

[26]H.-K. Sung, E. K. Lau and M. C. Wu, "Optical properties and modulation characteristics of ultrastrong injection-locked distributed feedback lasers", IEEE J. Sel. Topics Quantum Electron., vol. 13, no. 5, pp. 1215-1221, (2007).

[27]M. C. Espana-Boquera and A. Puerta-Notario, "Noise effects in injection locked laser simulation: Phase jumps and associated spectral components", Electron. Lett., vol. 32, no. 9, pp. 818-19, (1996).

[28]X. J. Meng, T. Chau and M. C. Wu, "Improved intrinsic dynamic distortions in directly modulated semiconductor lasers by optical injection locking", IEEE Trans. Microw. Theory Tech., vol. 47, no. 7, pp. 1172-1176, Jul. (1999).

[29]J. H. Seo, Y. K. Seo and W. Y. Choi, "Nonlinear distortion

suppression in directly modulated DFB lasers by sidemode optical injection", Proc. IEEE MTT-S Int. Microw. Symp. Dig., vol. 1, pp. 555-558, (2001).

[30][30] H. K. Sung, "Modulation bandwidth enhancement and nonlinear distortion suppression in directly modulated monolithic injection-locked DFB lasers", Proc. IEEE Int. Topical Meeting Microw. Photon., pp. 27-30, (2003).

[31][31] V. Annovazzi-Lodi, "Dynamic behavior and locking of a semiconductor laser subjected to external injection", IEEE J. Quantum Electron., vol. 34, no. 12, pp. 2350-2357, (1998).

[32][32] H.-K. Sung, "Optical generation of millimeter-waves using monolithic sideband injection locking of a two-section DFB laser", Proc. Conf. Lasers Electro-Optics Soc., vol. 2, pp. 1005-1006, (2003).

[33]Z. Liu and R. Slavík, "Optical Injection Locking: From Principle to Applications," in Journal of Lightwave Technology, vol. 38, no. 1, pp. 43-59, (2020).

[34]X. J. Meng, T. Chau, and M. C. Wu, “Improved intrinsic dynamic distortions in directly modulated semiconductor lasers by optical injection locking,” IEEE Trans. Microw. Theory Techn., vol. 47, no. 7, pp. 1172–1176, (1999).

[35]L. Paciorek, “Injection locking of oscillators,” Proc. IEEE, vol. 53,

no. 11, pp. 1723–1727, (1965).

[36]S. Kobayashi and T. Kimura, “Optical phase modulation in an injection locked AlGaAs semiconductor laser,” Electron. Lett., vol. 18, no. 5, pp. 210–211, (1982).

[37]T. Simpson and J. Liu, “Enhanced modulation bandwidth in injection locked semiconductor lasers,” IEEE Photon. Technol. Lett., vol. 9, no. 10,pp. 1322–1324, (1997).

[38]E. K. Lau, X. Zhao, H.-K. Sung, D. Parekh, C. Chang-Hasnain, and M. C. Wu, “Strong optical injection-locked semiconductor lasers demonstrating >100-GHz resonance frequencies and 80-GHz intrinsic bandwidths,” Opt. Express, vol. 16, no. 9, pp. 6609–6618, (2008).

[39]E. K. Lau, H.-K. Sung, and M. C.Wu, “Scaling of resonance frequency for strong injection-locked lasers,” Opt. Lett., vol. 32, no. 23, pp. 3373-3375, (2007).

[40]E. K. Lau, L. J. Wong, and M. C. Wu, “Enhanced modulation characteristics of optical injection-locked lasers: A tutorial,” IEEE J. Sel. Topics Quantum Electron., vol. 15, no. 3, pp. 618–633, (2009).

[41]S. P. Bhooplapur, A. Klee, and P. J. Delfyett, “Line-by-line pulse-shaping at GHz modulation frequencies with an injection-locked VCSEL array,” IEEE Photon. Technol. Lett., vol. 29, no. 15, pp. 1241–1244, (2017).

Chapter 4

Overshoot affection in the frequency response of photon-photon-resonance (PPR) on high-speed laser diode

4.1 Introductory overview

In Chapter 3, rate equations with PPR are discussed. From that rate equation, the modulation response of PPR is able to be calculated and the key parameter of PPR, the coupling efficiency is also found. Based on the simulation results, we notice the existence of an overshoot from PPR in the modulation response. In the communication system, it is large signals that are mainly transferred. So far, however, the discussion for direct modulation laser diode is mostly about the possible modulation bandwidth (small signal modulation response). Thus, too high amplitude of PPR which may degrade large modulation-signal has not been reported yet to our knowledge. Time domain simulation is used to calculate the large signal modulation response with rate equations. In Chapter 3, the rate equations with PPR have been discussed. The output of large signal modulation response, however, is not able to obtain from time domain simulation since there is a phase term in the rate equations. To overcome this problem, we used the signal analysis method in signal and system which could use the small signal modulation response to evaluate the large

signal modulation response directly.

In this chapter, we first propose a calculation method to explain the relationship between small signal modulation response and large signal modulation bandwidth. From this method, the performance of DML is able to be evaluated easily. Then, the affections of overshoot from PPR in small signal modulation response have been evaluated based on that method. In the end, the large signal modulation over 100 Gbps based on our plural PPRs design has also been discussed.

4.2 Numerical calculation of large signal modulation response based on small signal modulation response

The frequency analysis theory is utilized to study the numerical model [1]. The transmitted NRZ signal is generated by pseudo-random binary sequence (PRBS). The frequency of the transmitted NRZ signal is $H_1(\omega)$. When NRZ signal is injected into DML, the frequency modulation response of DML is $H_2(\omega)$. When the signal is output from the DML, its frequency response would be [2-9]

$$H(\omega) = H_1(\omega)H_2(\omega) \tag{4.1}$$

Then, utilizing the inverse Fourier transform, the waveform of the output signal is achieved.

The frequency modulation response of the DML of NRZ signal is the small signal modulation response of the DML. The small signal modulation response of DML is able to be derived from the rate equation in the laser diode. The four rate equations to describe the PPR phenomenon based on electromagnetic waves have been proposed in Chapter 3, Eq (3.16-3.19). Small signal analysis approach is applied that the small signal modulation response $H_2(\omega)$ is obtained.

$$H_2(j\omega) = \frac{P(j\omega)^2+Q(j\omega)+T}{(j\omega)^4+A(j\omega)^3+B(j\omega)^2+C(j\omega)+D} \tag{4.2}$$

For the details, please check the chapter. 3.2 about rate equation with PPR. The scheme of signal transmission is shown in Fig.4.1. As to the output signal, it is expected to be transmitted without error. In other words, the outputted signal from laser diode is expected to be the same as the input signal. Based on that point, if the frequency response $H_2(\omega)$ was equal to 1, the output signal is identical to input signal. It suggests that the flattened modulation response of $H_2(\omega)$ is an advantage to data transmission.

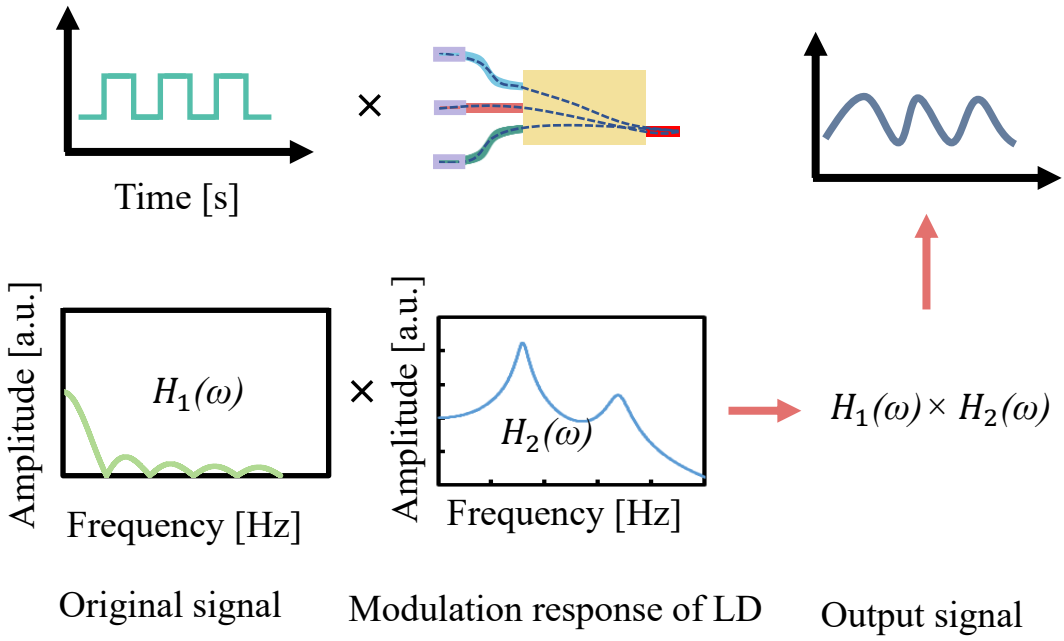

Fig 4.1 Scheme of signal transmission

4.3 Simulation results

In this simulation, the transmitted signal is an ideal 40 Gbps NRZ signal. All the small modulation responses of laser (Fig. 4. 2 (a) series) are with CPR and PPR at 15 GHz and 30 GHz respectively. The -3 dB modulation bandwidths for all simulations are around 38 GHz. The small signal modulation responses given in Fig. 4. 2 are characterized by improved amplitude of PPR. Fig.4.3 are NRZ modulation responses to small signal modulation responses with different amplitudes of PPR. It is necessary to point out that the small signal modulation response with PPR (as shown in Fig.4.2) derived from rate equations by utilizing small signal response approach was used as the frequency modulation response to NRZ signal modulation. It means that, in this simulation, the output of laser is

considered as linear to the input signal. In Fig. 4.2. (a1) and Fig.4.3. (a1), when the amplitude of PPR is 4.2 dB, the extinction ratio (ER) of the eye pattern is 3.36 dB. When the amplitude of PPR increased to 5.3 dB in Fig.4.2 (a2), contradicting our prediction, the ER of the eye pattern increased to 3.65 dB. As the amplitude of PPR rose from 6.8 dB to 9 dB, the ER also increased (not decreased) from 4.1 dB to 4.8 dB. Simulation results also show that the density of the output signal is exceeded 1. According to Eq. 4.1, It suggests that the existence of CPR and PPR is able to magnify the density of signal, which may be considered as an advantage to NRZ modulation because the input signal is magnified.

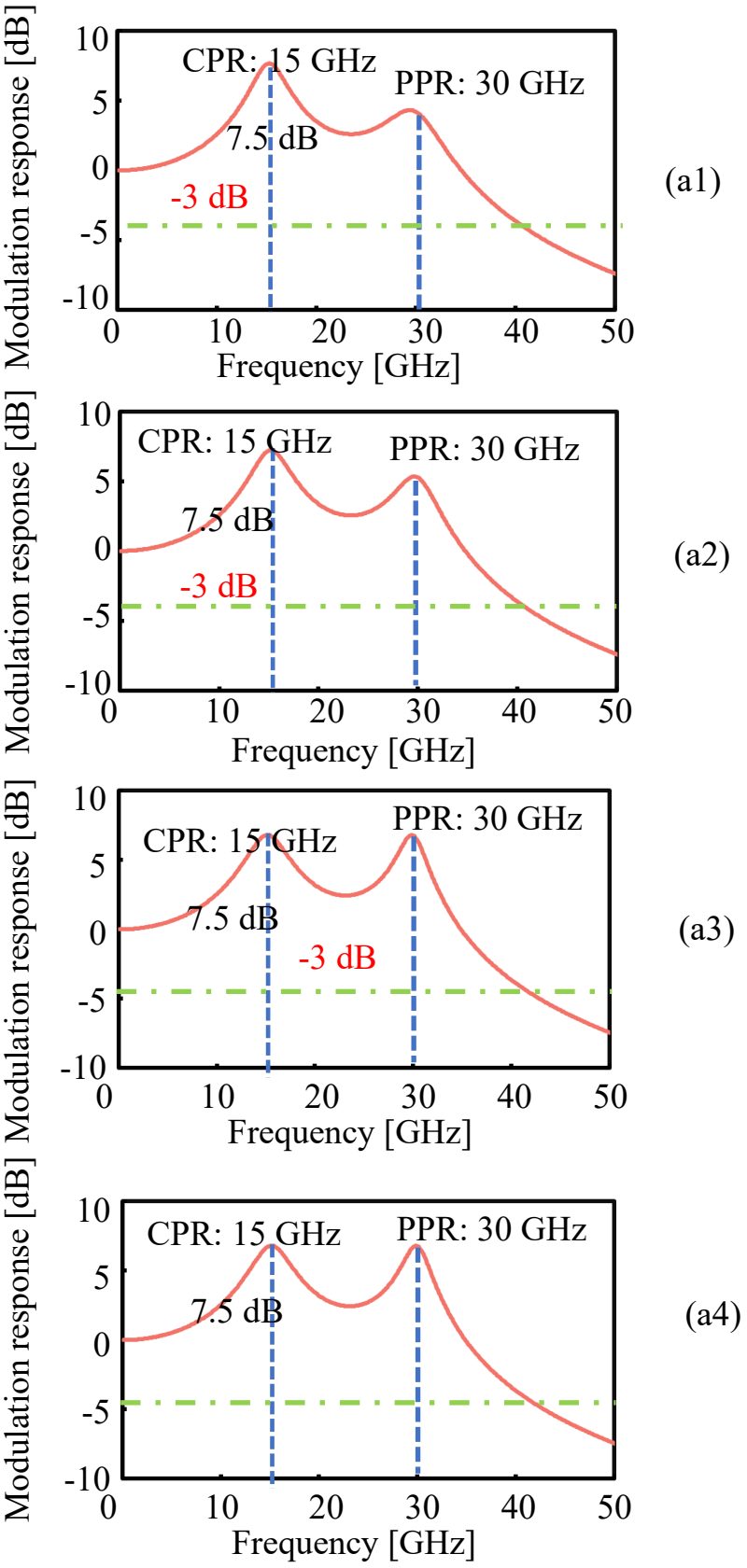

Fig 4.2 small signal modulation response with different amplitudes of PPR

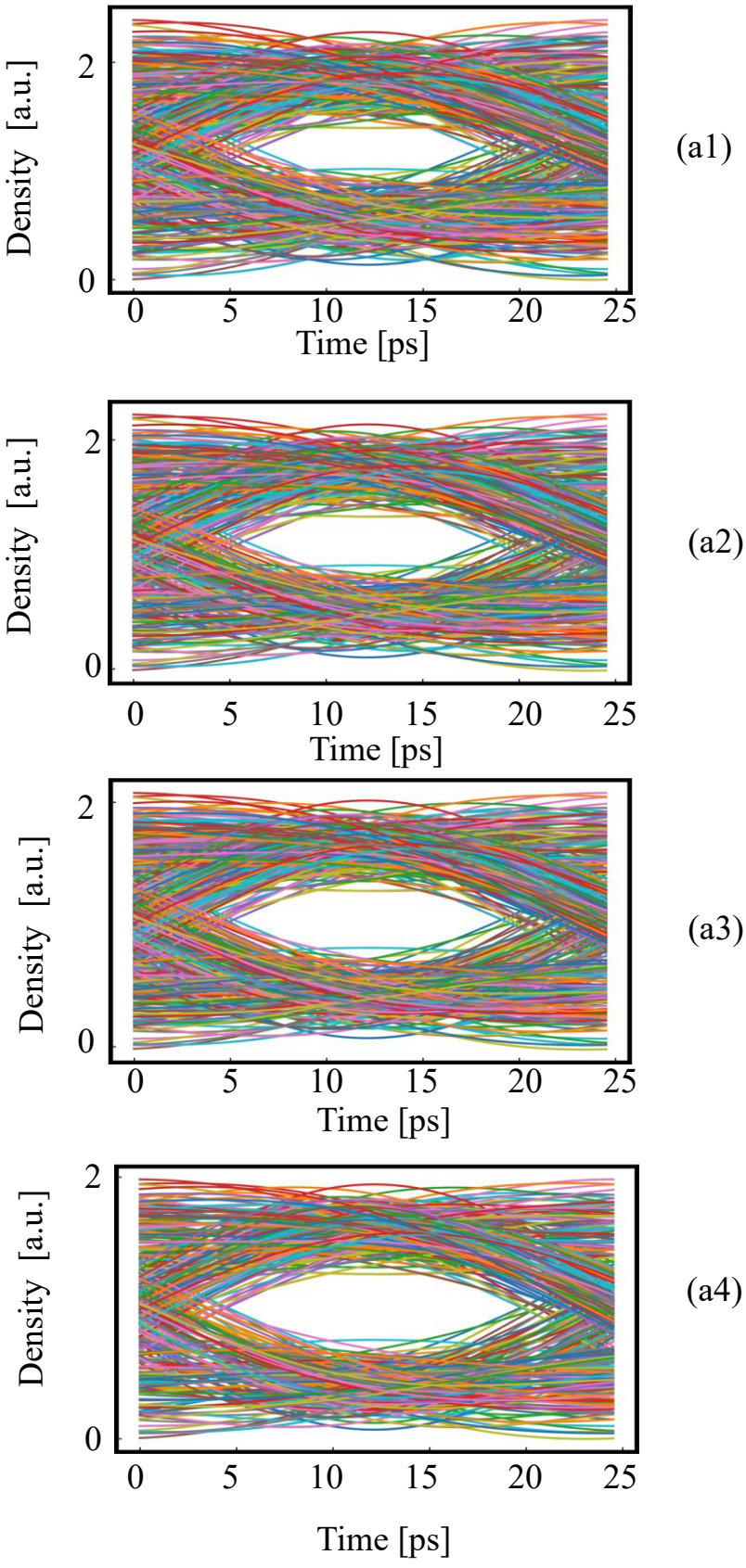

Fig 4.3 NRZ responses corresponding to different amplitudes of PPR

Based on the discussion in Chap. 2, the calculation equation implies that flattened modulation response is an advantage to data transmission. The simulation result, however, reviews that PPR overshoot is an advantage to NRZ modulation. This contradicts the theoretical discussion.

4.4 Discussion of overshoot to large signal modulation

To clarify this problem. The simulation was carried out. Firstly, we designed a flattened modulation response of laser as Fig. 4.4 (a). Utilizing equation (1) to calculate its 40 Gbps NRZ modulation response, the eye pattern is shown in Fig. 4.4 (b). The eye is opened with ER at 3 dB even though the -3 dB modulation bandwidth shown in Fig. 4.4 (a) is 29 GHz. As the prediction, flattening small signal modulation bandwidth does play a positive role in NRZ modulation. Then, we notice that, in laser's small signal modulation response, there is the carrier-photon-resonance (CPR). Figure 4.5 (a) is a modulation response of laser with CPR. The 7 dB peak in the modulation carves caused by CPR at 13 GHz destroyed the flatness of its small signal modulation response. Though in Fig. 4.5 (a), the -3 dB modulation response is still 29 GHz as Fig. 4.4 (a), as shown in Fig 4.5 (b), its eye pattern is almost closed. This explains why the existence of high PPR amplitude an advantage to NRZ modulation is.

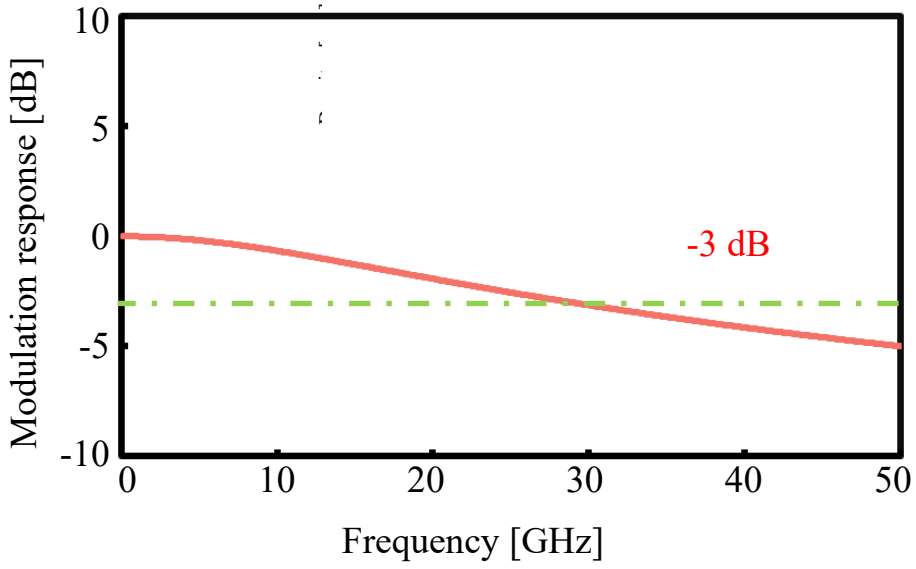

(a)

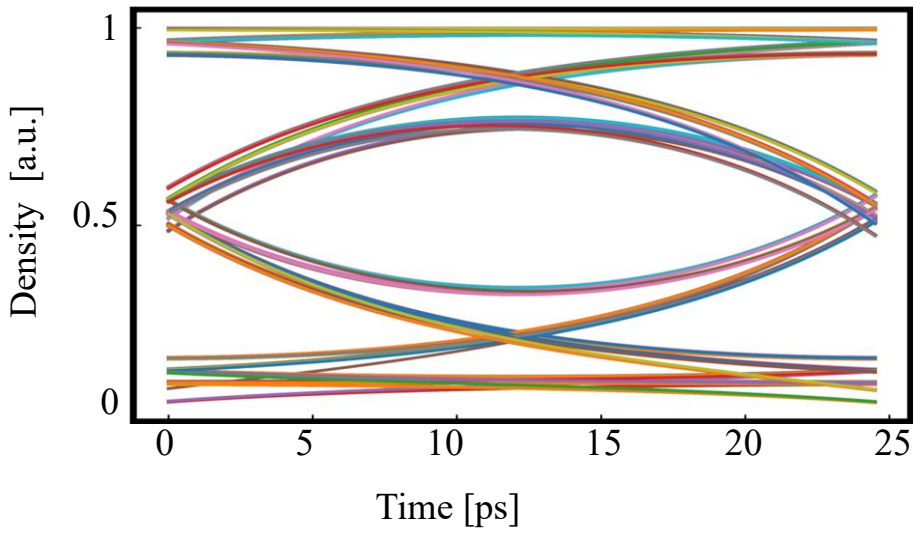

(b)

Fig. 4.4 Simulation results. (a) Small signal modulation response result without CPR; (b) Eye pattern corresponded to small signal modulation response without CPR.

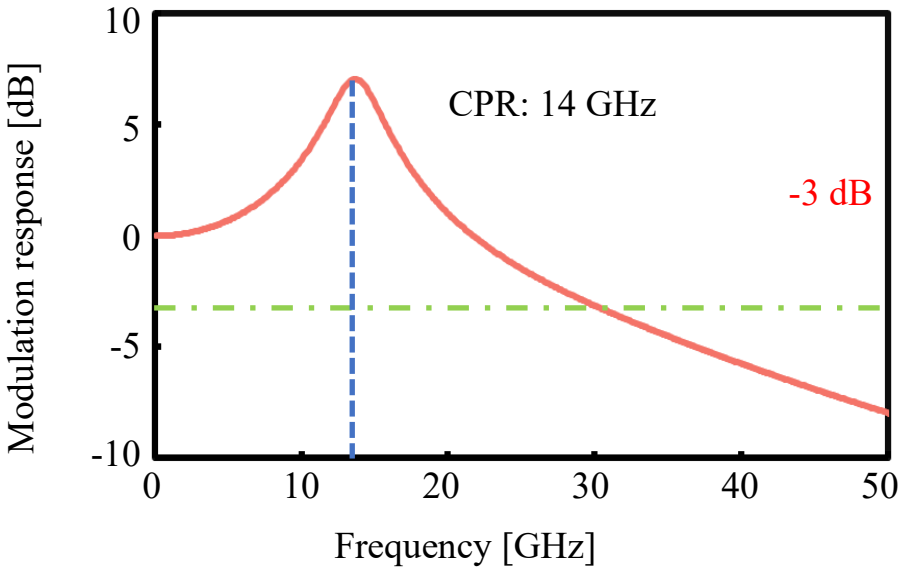

(a)

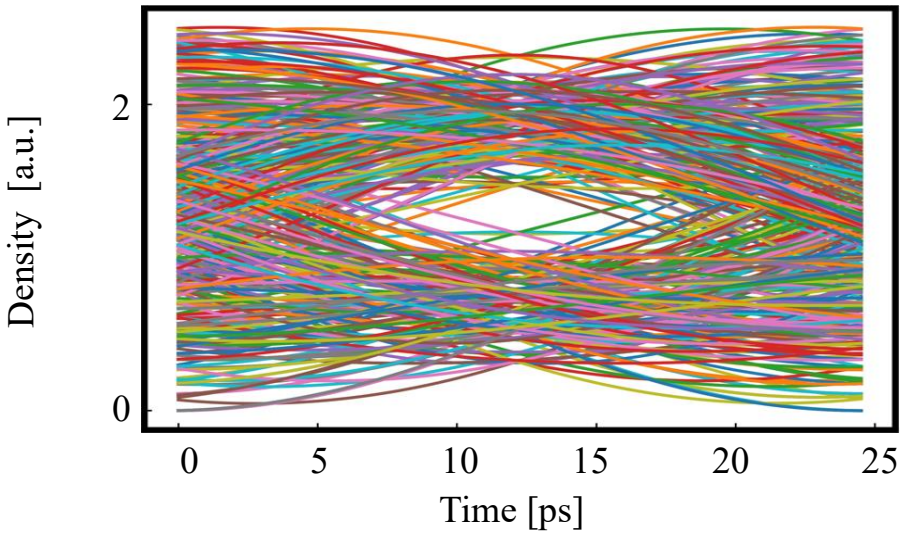

(b)

Fig. 4.5 Simulation results. (a) Small signal modulation response result with CPR; (b) Eye pattern corresponded to small signal modulation response with CPR.

The appearance of PPR is considered as a balance to the high amplitude of CPR. Since CPR is an invertible phenomenon to directly modulated laser, with the existence of PPR, the modulation bandwidth is not only extended, and the flatness distorted by CPR is also compensated by PPR. In that work, to compensate for the affection of 7 dB CPR, 9 dB amplitude of PPR is necessary to achieve ER at 4.8 dB.

It is important to address here that, the traditional large signal analysis method [10] was calculated to prove our large signal modulation method. It is the undesirable results we obtained. When the current injection is changed from $1.1I_{th}$ to $2I_{th}$, as shown in Fig.4. 7, using PPR rate equation with the modulation current, the output of the laser is not stable. This is because the phase term is not able to be divergent. This is the problem that we still need to figure out.

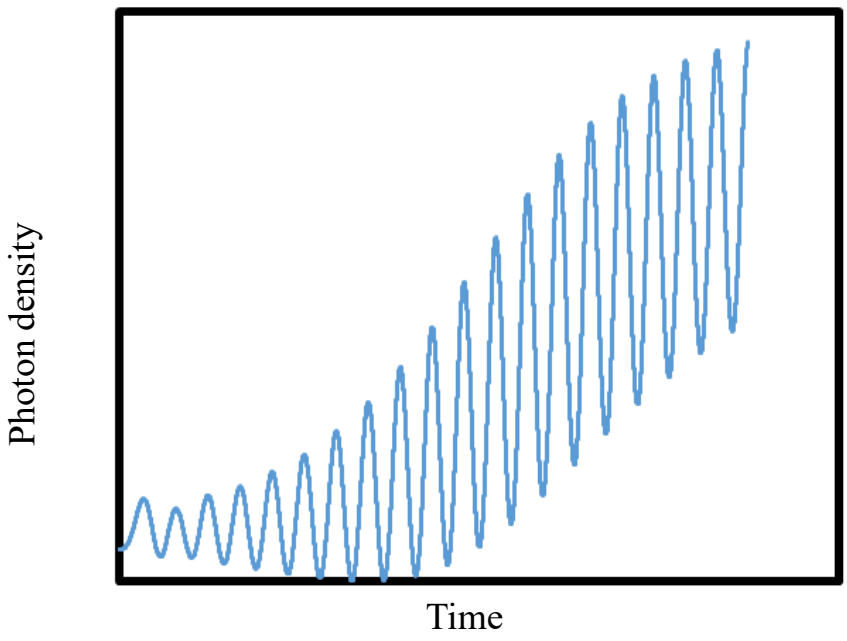

Fig.4.7 Large signal modulation with lager signal analysis methd

Reference

[1] Oppenheim Alan V, Willsky A. S, Nawab S H, *et al*., "Signals and systems. " vol.2. Upper Saddle River, NJ: Prentice hall, chapter 4. (1997).

[2] Lang, Roy. "Injection locking properties of a semiconductor laser. " IEEE Journal of Quantum Electronics, vol. 18, no. 6, pp.976-983, (1982).

[3] Lau, Erwin K, Hyuk-Kee Sung, and Ming C. Wu. "Frequency response enhancement of optical injection-locked lasers." IEEE Journal of Quantum Electronics, vol.44, no. 1, pp. 90-99, (2007).

[4] Lau, Erwin K., Liang Jie Wong, and Ming C. Wu. "Enhanced modulation characteristics of optical injection-locked lasers: A tutorial." IEEE Journal of Selected Topics in Quantum Electronics, vol. 15, no. 3, pp. 618-633, (2009).

[5] Lau, Erwin K., Hyuk-Kee Sung, and Ming C. Wu. "Scaling of resonance frequency for strong injection-locked lasers." Opt letters, vol. 32, no. 23, pp. 3373-3375, (2007).

[6] Simpson, T. B., J. M. Liu, and A. Gavrielides. "Bandwidth enhancement and broadband noise reduction in injection-locked semiconductor lasers." IEEE Photonics Technology Letters, vol.7. no. 7, pp. 709-711, (1995).

[7] Mogensen, Finn, Henning Olesen, and Gunnar Jacobsen. "Locking conditions and stability properties for a semiconductor laser with external light injection." IEEE Journal of Quantum Electronics, vol.21, no. 7, pp. 784-793, (1985).

[8] Henry, C., N. Olsson, and N. Dutta. "Locking range and stability of injection locked 1.54 μm InGaAsP semiconductor lasers." IEEE Journal of Quantum Electronics, vol. 21, no. 8, pp. 1152-1156, (1985).

[9] H. Xiao, Keiichiro K, Yudai K, *et al*., "Affection analysis of frequency response with photon-photon-resonance (PPR) to directly modulated 40 Gbps signal," Tech. Dig. Microoptics Conference, Hamamatsu, Japan, 2021.

[10] Coldren, L. A.; Corzine, S. W.; Mashanovitch, M. L. 2nd ed.; Diode lasers and photonic integrated circuits. John Wiley & Sons, chapter 5.

Chapter 5

Active-MMI LD design for PPR utilization

5.1 Introductory overview

As discussed in chapter.3, coupling efficiency is a key parameter to PPR phenomenon. This parameter is mainly related on the laser's configuration. It is indicted that the damping problem between resonances could be resolved by designing the coupling efficiency of two lasing modes. Hence, The challenge lies in design the PPR with coupling efficiency.

In general laser configuration to explore PPR phenomena, it is difficult to control the PPR phenomena. As depicted in Fig.5.1 (a1), all the lasing mode are propagating in the same direction. The Fig.5.1 (a2) shows the optical field of two lasing mode. It is clear that two lasing modes overlap to each other. In other word, it means that two lasing modes coupling to each other in the whole cavity that the parameter $\Gamma_{overlap}$ will be 1 and is not able to be engineered. Since active-MMI LD naturally accesses different waveguides, it is able to design the coupling efficiency of the lasing mode.

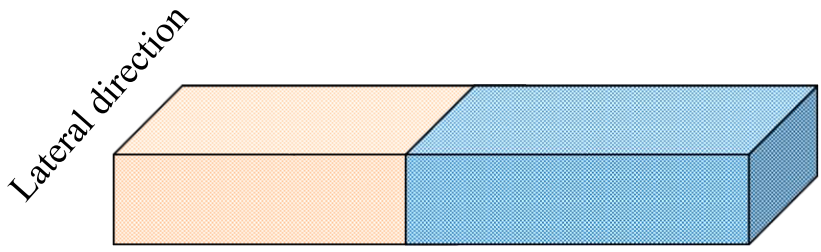

Longitudinal direction [μm]

(a1)

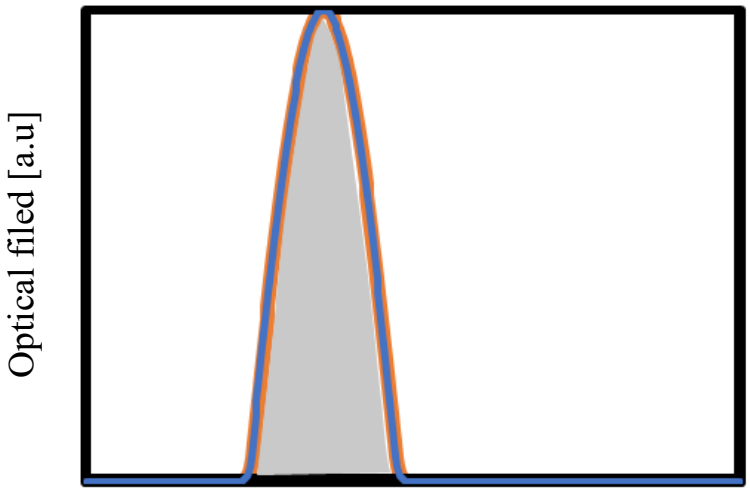

Lateral direction [μm]

(a2)

Fig. 5.1 (a1) Traditional two-section laser configuration;

(a2) optical filed of lasing mode inside LD.

5.2 Theory of Multimode Interferometer

The so-called multimode interferometer (MMI) is based on “self-image” phenomenon when multimode interfere with each other inside the waveguide [1-4]. The very simple configuration of an MMI is shown in

Fig. 5.2. A multimode waveguide section connected with one/several narrower waveguides is the very basic structure. As shown in Fig, the incident light is injected from the narrow waveguide on left side. After propagating into the multimode section, the light excites into a group of modes. Such different modes interfere with each other, as a result at several position of the multimode section, the “self-image” of the incident field will appear periodically. The duplicate field is almost the same as the incident light. The only differences are the amplitude and the phase condition. In Fig. 5.2, duplication of the incident field is illustrated. Be noted that, this duplication always happens whatever the incident modes are.

We care about the position and the phase of duplication in most cases. By delicate arrangement, the duplicated light phase is controlled, and the optical mode converter is designed [5]. The position and the amplitude of the self-image are affected by the mode order, i.e. position or amplitude of self-image are different when incident modes are different. This fact is the most important principle in designing the mode-selective light source.

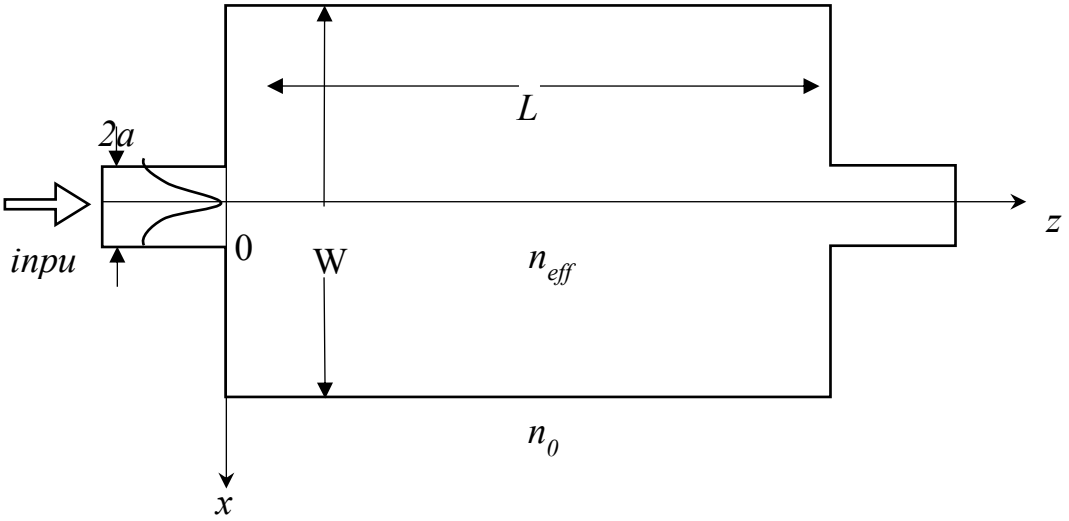

Fig. 5. 2 Two-dimensional representation of an MMI

We discuss the 2-D MMI structure for simple understanding. The width, thickness and length of the multimode region are W, 2d and L. The thickness of the waveguide is ignored here. The width of the access waveguide connected with the multimode section is 2a. Assuming the effective refractive index of the multimode section is n_{eff} and the index of the cladding is n_0. The analysis of the 2-D MMI is as follows:

The description for modes inside the multimode waveguide can be written as:

$$E_y^m(x,y) = \begin{cases} A_m \cos\left(u_m + \frac{m\pi}{2}\right) exp\left[\frac{2\omega_m}{W}\left(x + \frac{W}{2}\right) - j\beta_m z\right] & (x < -\frac{W}{2}) \\ A_m \cos\left(\frac{2u_m x}{W} - \frac{m\pi}{2}\right) exp[-j\beta_m z] & (|x| \le -\frac{W}{2}) \\ A_m \cos\left(u_m - \frac{m\pi}{2}\right) exp\left[-\frac{2\omega_m}{W}\left(x - \frac{W}{2}\right) - j\beta_m z\right] & (x > -\frac{W}{2}) \end{cases} \quad (5.1)$$

where u_m and $\omega_m$denote the transverse wave numbers of the m-th mode inside the core and cladding and A_m is constant.

This equation group can be solved in the form of:

$$\frac{\partial^2 E_y}{\partial x^2} + \frac{\partial^2 E_y}{\partial z^2} + k_0^2 n_{eff}^2 E_y = 0 \tag{5.2}$$

In z direction, for any mode, $\frac{\partial^2 E_y}{\partial z^2} = -\beta^2 E_y$. In x direction, the form of E_y can be expressed as equation 4.2, we can obtain:

$$k_x^2 + \beta^2 = k_0^2 n_{eff}^2 \tag{5.3}$$

For each mode, form fundamental mode to i^{th} (i=0, 1, 2, …) mode, k_x is written in such form as:

$$k_x = \frac{\pi}{W}(i+1) \tag{5.4}$$

Then, β becomes:

$$\beta^2 = k_0^2 n^2 - k_x^2 = k_0^2 n_{eff}^2 - \left\{\frac{\pi(i+1)}{W}\right\}^2 \tag{5.5}$$

$$\beta = \left[(k_0 n_{eff})^2 - \left\{\frac{\pi(i+1)}{W}\right\}\right]^{\frac{1}{2}} \tag{5.6}$$

Here $(k_0 n_{eff})^2$ is much larger than $\left\{\frac{\pi(i+1)}{W}\right\}$, then we can express $[...]^{\frac{1}{2}}$part as:

$$\left[(k_0 n_{eff})^2 - \left\{\frac{\pi(i+1)}{W}\right\}\right]^{\frac{1}{2}} = [a^2 - x^2]^{\frac{1}{2}} = f(x) \quad (5.7)$$

as $f(x)$ can be expressed as:

$$f(x) = [a^2 - x^2]^{\frac{1}{2}}$$

$$f(x)' = \frac{1}{2}(a^2 - x^2)^{-\frac{1}{2}}(-2x) = -x(a^2 - x^2)^{-\frac{1}{2}}$$

$$f(x)'' = -(a^2 - x^2)^{-\frac{1}{2}} - x\left\{-\frac{1}{2}(a^2 - x^2)^{-\frac{3}{2}}(-2x)\right\}$$

Thus,

$$f(x) = f(0) + f(0)'x + f(0)''\frac{x^2}{2} = a - \frac{x^2}{2a} = k_0 n_{eff} - \frac{\pi^2(i+1)^2}{2k_0 n_{eff} W^2} \quad (5.8)$$

then,

$$\beta \approx k_0 n_{eff} - \left\{\frac{(i+1)\pi}{W}\right\}^2 \frac{1}{2k_0 n_{eff}} \quad (5.9)$$

As $k_0 = \frac{2\pi}{\lambda_0}$, the form of β can be wrote as:

$$\beta_m = k_0 n_{eff} - \frac{(m+1)^2 \lambda_0}{4 n_{eff} W^2} \pi \tag{5.10}$$

the total electrical field in the MMI region then can be expressed as:

$$\Psi(x,z) = \sum_{m=0}^{M} E_y^m(x,z) = e^{-jk_0 n_{eff} z} \sum_{m=0}^{M} A_m \cos\left[\frac{(m+1)\pi}{W} x - \frac{m\pi}{2}\right] \times exp\left(j \frac{(m+1)^2 \pi \lambda_0}{4 n_{eff} W^2} z\right) \tag{5.11}$$

Where M denotes the maximum mode number inside the MMI region.

At *z*=0, the electrical field $\Psi(x,0)$ represents the input electrical field $\psi(x)$. Then then electric field amplitude A_m is obtained as:

$$A_m = \frac{2}{W} \int_{-W/2}^{W/2} \psi(x) \cos\left[\frac{(m+1)\pi}{W} x - \frac{m\pi}{2}\right] dx \tag{5.12}$$

In case the input waveguide is at the central part of the MMI region, modes in MMI region become symmetrical modes (m equals to even number, *m=2l*). At the position

$$z = \frac{n_{eff} W^2}{\lambda_0}$$

the phase term in equation 2.11 becomes:

$$exp\left(j\frac{(m+1)^2\pi\lambda_0}{4n_{eff}W^2}z\right) = exp\left(jl(l+1)\pi + j\frac{\pi}{4}\right) = exp\left(j\frac{\pi}{4}\right) \quad (5.13)$$

Here, we can define the characteristic length of L_{MMI} as:

$$L_{MMI} = \frac{n_{eff}W^2}{\lambda_0} \quad (5.14)$$

In such point, the electric field will be:

$$\Psi(x, L_{MMI}) = e^{-jk_0 n_{eff} L_{MMI} + j\pi/4} \sum_{m=0}^{M} A_m cos\left[\frac{(m+1)\pi}{W}x - \frac{m\pi}{2}\right] \quad (5.15)$$

As $\Psi(x, 0)$ in 2.15 equals to the input power field, the equation 2.15 can be written in a further way as:

$$\Psi(x, L_{MMI}) = \psi(x)e^{-jkn_{eff}L_{MMI} + j\pi/4} \quad (5.16)$$

If we consider equation 4.16, when at integral multiple L_{MMI}, the electrical field of input field will be reproduced as such position. Figure 5.3 shows an example of the MMI self-image

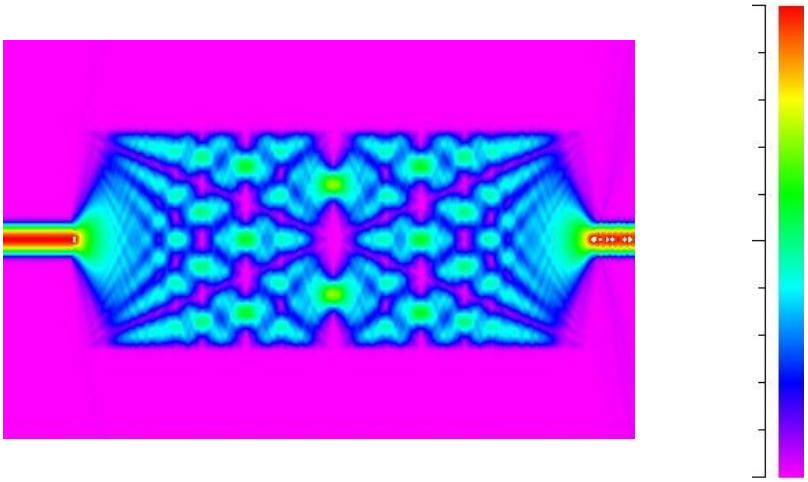

Fig. 5. 3 self-image phenomenon in MMI waveguide

5.3 Coupling efficiency control scheme in active-MMI LD

Utilizing the self-image phenomenon, 1×2 active-MMI LD was proposed. Figure 5.4 shows the waveguide configuration of 1×2 active-MMI LD involving different lasing paths in a cavity for each space-mode. In section 1, when upper arm and lower arm are both designed as fundamental mode waveguide, two different lasing paths do not share the same output port.

As BPM simulation results show in Fig. 5.5 and 5.6, each path for fundamental mode is designed as cross-propagation section 2. The coupling area for two fundamental modes is only the MMI area. Coupling efficiency and its variation are small. To solve this problem, different lateral modes are utilized. As shown in Fig. 5.7, 1st order mode propagates to bar-direction in the same section 3. Thus, two different lasing paths exist whereas the output port has been shared.

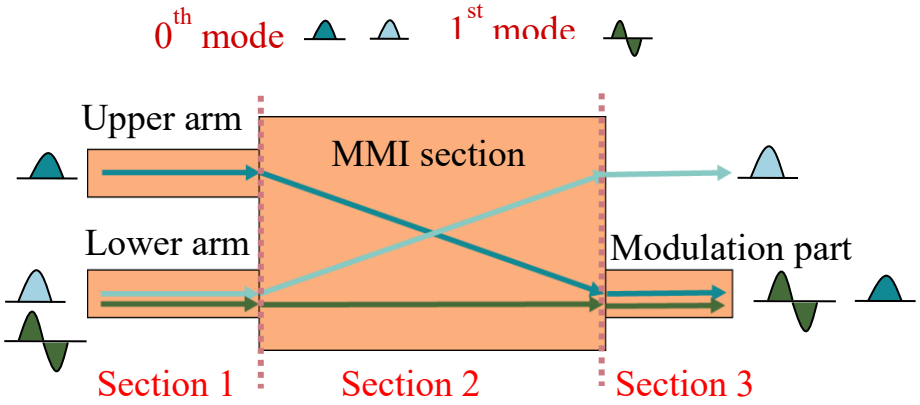

Fig. 5.4 Propogation route of foundemental mode and first mode in 1×2 active-MMI LD.

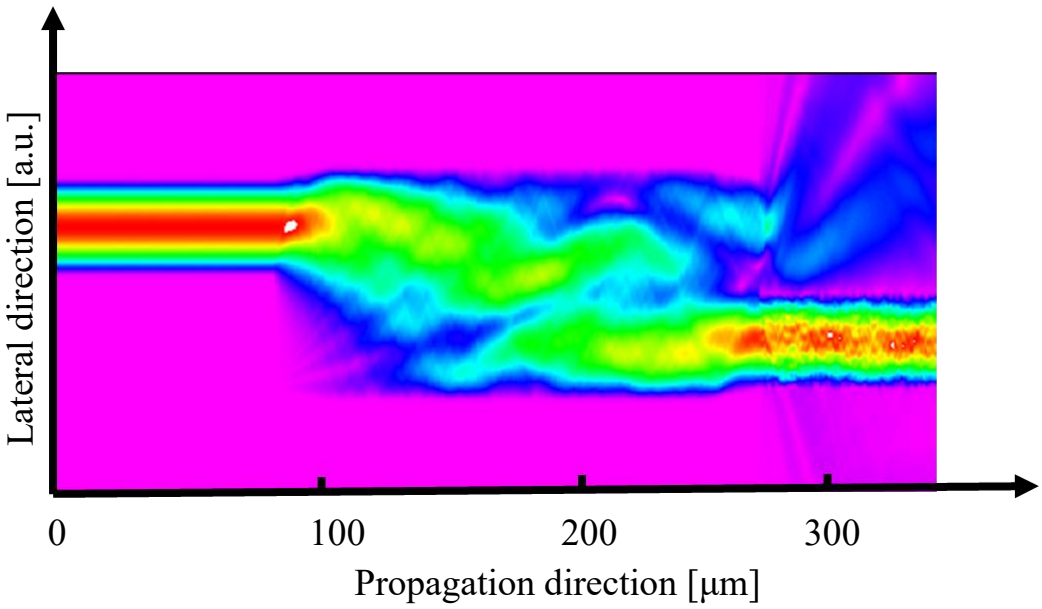

Fig. 5.5 BPM simulation of fundamental mode propagation through upper arm.

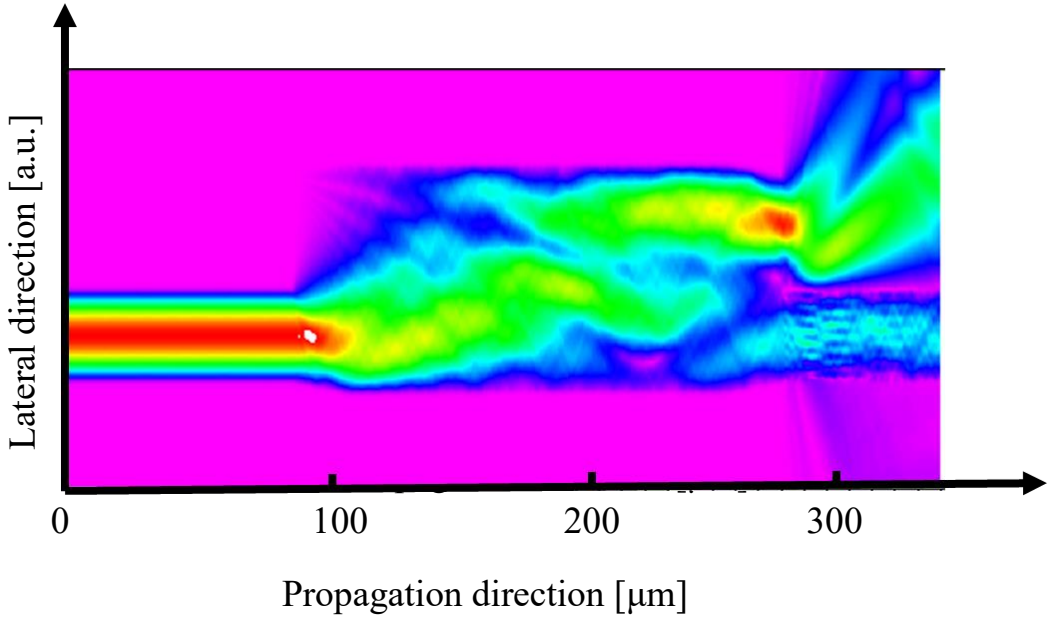

Fig. 5.6 BPM simulation of fundamental mode propagation through lower arm.

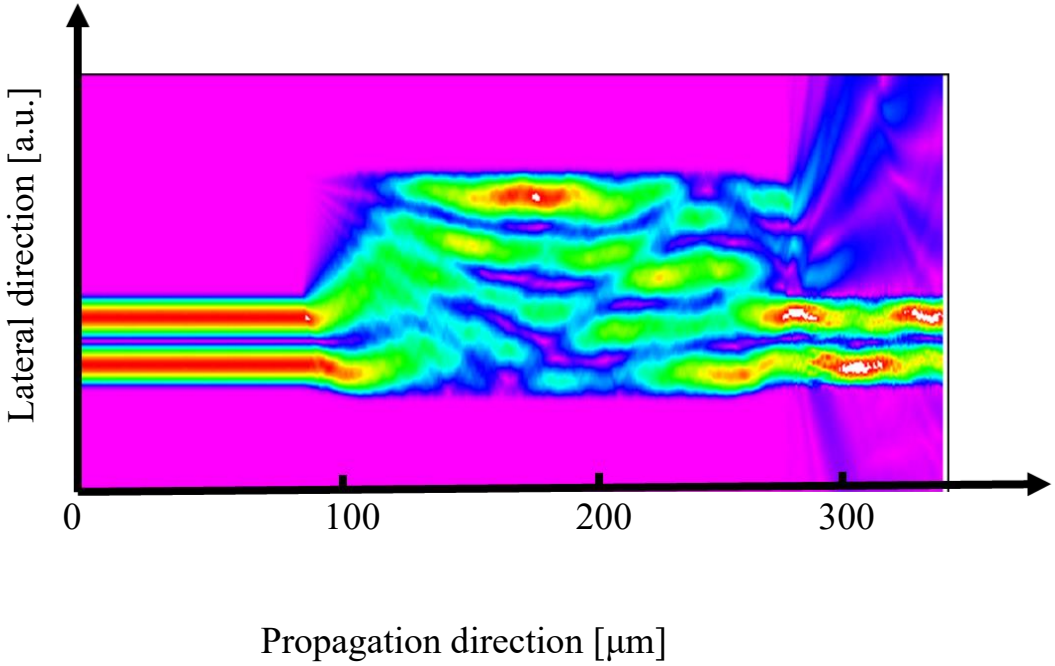

Fig. 5.7 BPM simulation of first mode propagation through lower arm.

Considering that the lasing paths of two lasing modes are different in 1 ×2 active-MMI LD, the coupling efficiency of two lasing modes in each section has to be discussed. When two space modes are lasing in section 1, two lasing modes are separated from each other. In section 2 and 3, two lasing modes overlap. The overlap of two lasing modes is close to 1 in section 3, whereas the lateral optical field overlap of two lasing modes is less than 1 in section 2. The expression of $\Gamma_{overlap}$ in active-MMI LD is:

$$\Gamma_{overlap} = \frac{\Gamma_{Se2} L_{Se2}}{L_{total}} + \frac{L_{Se3}}{L_{total}} \tag{5.17}$$

In that expression, Γ_{Se2}, L_{Se2}, L_{Se3} and L_{total} are respectively the optical filed overlap of two modes in MMI section (section 2), the length of section 2, the length of section 3, and the total length of the whole active-MMI LD. From this definition, it implies that $\Gamma_{overlap}$ is by changing the proportion of the three parts. Thus, the parameter Γ_{Se2} has to be determined.

To do so, the calculation of the optical field overlap of two lasing modes in section 2 is carried out. In the calculation process, we set the length of section 1 at 90 μm and the length of section 3 at 50 μm. The wavelength value in the simulation process is set to 1550 nm. Simulation results of the propagation path of the fundamental mode and first-order mode in Fig 5.6 and 5.7 suggest that the optical filed overlap of two lasing modes is different along the propagation direction. Besides, Fig 5.8 (a2) is an optical profile of two lateral modes in the middle of section 2. As indicated in the

figure, the optical profile of two lasing modes are not totally overlapped. To calculate Γ_{Se2}, from Fig 5.8 (a1), we divided the MMI area into sslicesalong the propagation direction. Hence the overlap of two lasing modes in each slice is calculated. Using the integral menthod, Γ_{Se2} is obtained.

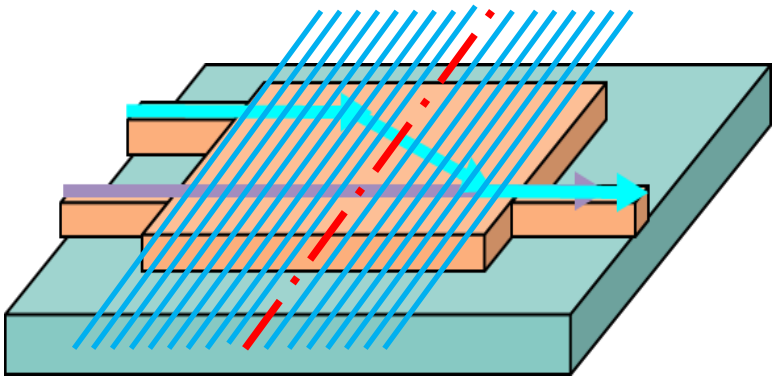

(a1)

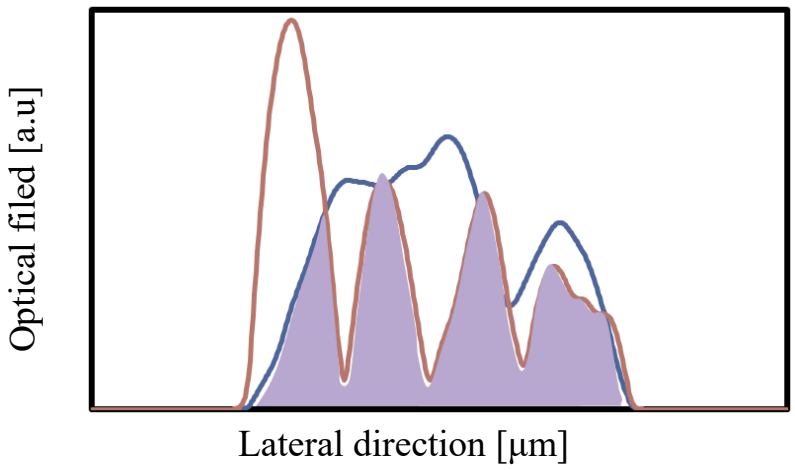

(a2)

Fig. 5.8 (a1) Optical filed overlap of two lasing modes in 1×2 active-MMI LD in the middle of section 2; (a2) scheme of two lasing modes propogation in 1×2 active-MMI LD.

The discussion above suggests that the $\Gamma_{overlap}$ is determined by the

proportion in the acitve-MMI LD configuration. The length of MMI area is set at 240 μm. The relationship between length of arm part and $\Gamma_{overlap}$ is depicted in Fig 5. The $\Gamma_{overlap}$ is able to be controlled from 0.5 to 0.8.

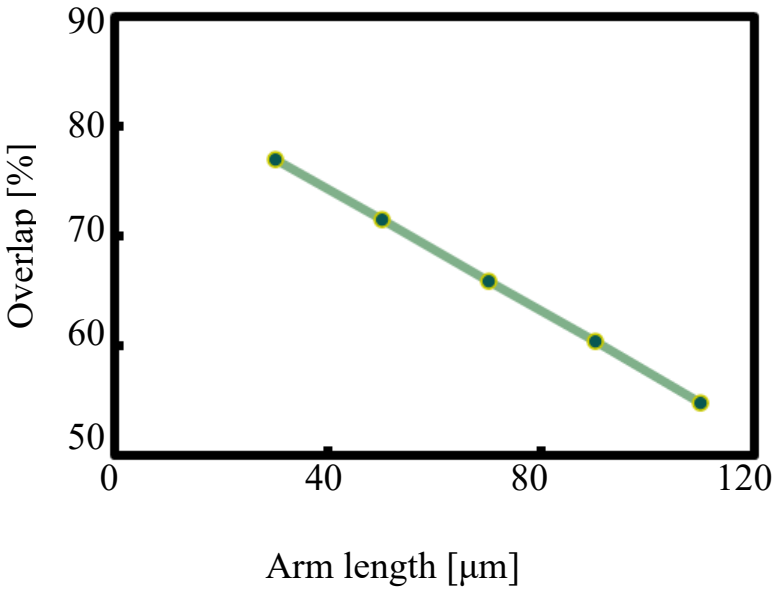

Fig. 5.9 Coupiling ratio of active-MMI with arm-length variation.(@MMI section at 240 μm; Total length at 360 μm; Wavelength at 1.55 μm)

It is necessary to point out that by utilizing different lateral modes in active-MMI LD, the coupling efficiency is tunable. Multimode lights, however, are not commonly used as a light source for optical interconnection because of dispersion loss in long-distance transmission. Active-MMI LD is considered as the optical light source for interconnection in supercomputer or mobile-device. It implies that this device will be applied in short-distance cases for which dispersion loss would not be a problem.

Based on the theoretical analysis discussed above, it is clear that wider

frequency response may occur for $\Gamma_{overlap}$ =0.7. We verified the response in detail, and we derived that $\Gamma_{overlap}$ =0.75 was the optimal value in this case. Figure 5.10 shows the calculated frequency response of $\Gamma_{overlap}$ = 0.75 case. 8 GHz modulation bandwidth improvement was successfully achieved. The control of $\Gamma_{overlap}$ is enabled through the proportion of three parts of active-MMI LD. $\Gamma_{overlap}$ at 0.75 is obtained by setting the section 1, section 2 and section 3 at 40μm, 240μm and 80 μm respectively.

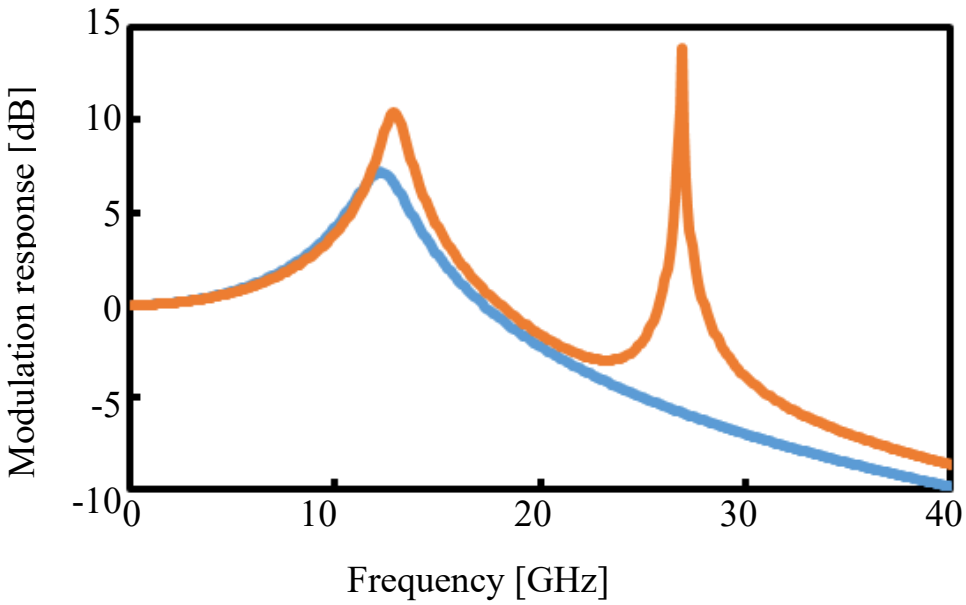

Fig. 5. 10 Calulated modulation response.

The simulation of 40 Gbps NRZ large signal modulation response based on small signal modulation response is carried out. The results are shown in Fig 5.11.

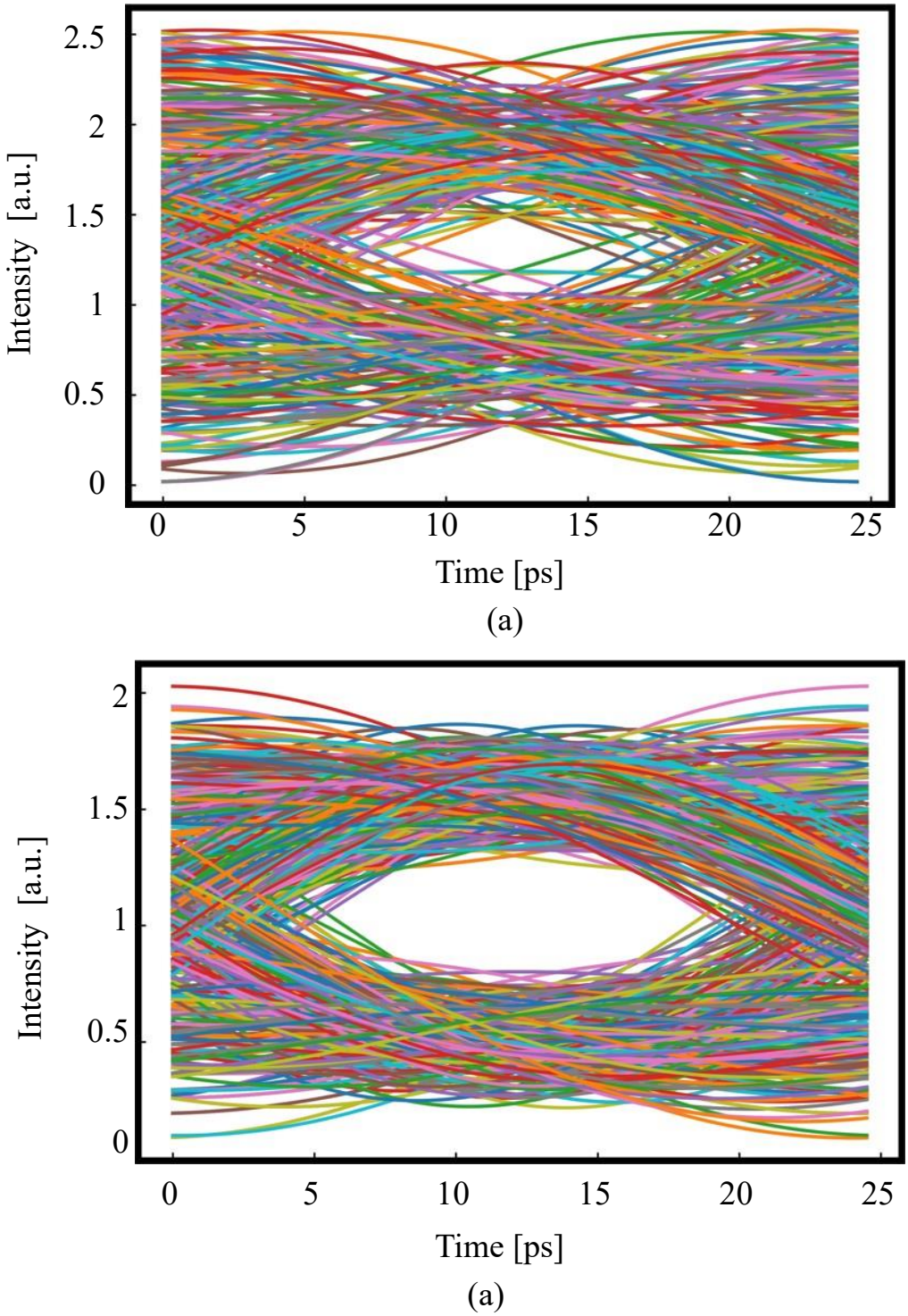

Fig. 5.11 Simulation results. (a) eye pattern corresponded to small signal modulation response with CPR; (b) eye pattern corresponded to small signal modulation response corresponding to optimized PPR

The eye pattern is distorted when the calculated modulation response is without PPR since there is a limitation of -3 dB modulation bandwidth. When the modulation bandwidth is extended with the existence of PPR, the eye pattern is open with an extinction ratio of 4 dB.

5.4 Discussion of designed active-MMI LD

5.4.1 Refractive index change with carrier density

While we have achieved the improvement of modulation response, what we have simulated is under an effective refractive index in the unlasing situation. The effective refractive index, however, varies with current injection because of the so-called carrier plasma effect [6]. In semiconductor field, when laser is lasing, the carrier density inside the active-MMI laser diode accumulates from 0 to its threshold carrier density [7]. The variation of effective index would affect the propagation route of lasing modes that change the overlap of lasing modes. Therefore, the affection of refractive index change caused by the accumulation of carrier density has to be taken into consideration.

When the laser made from InGaAsP is lasing in 1.55 μm, the increase in carrier density results in a reduction of the refractive index. The difference in effective refractive index Δn would be lower than 0.1 [8]. As shown in Table I, the refractive index of our device is 3.24. We conducted calculations to determine the overlap between two light sources across a range of effective refractive indices, spanning from 3.14 to 3.34. The

calculation results are shown in Fig .5.12. Based on the simulation result shown in Fig. 5.12, the stability of overlap is exhibited. Though the overlap between two lights changed with different effective refractive index, it is still kept at the range of 0.74-0.75. This result suggests that, the active-MMI laser diode is able to be lasing in stable with effective refractive index variation caused by the current injection.

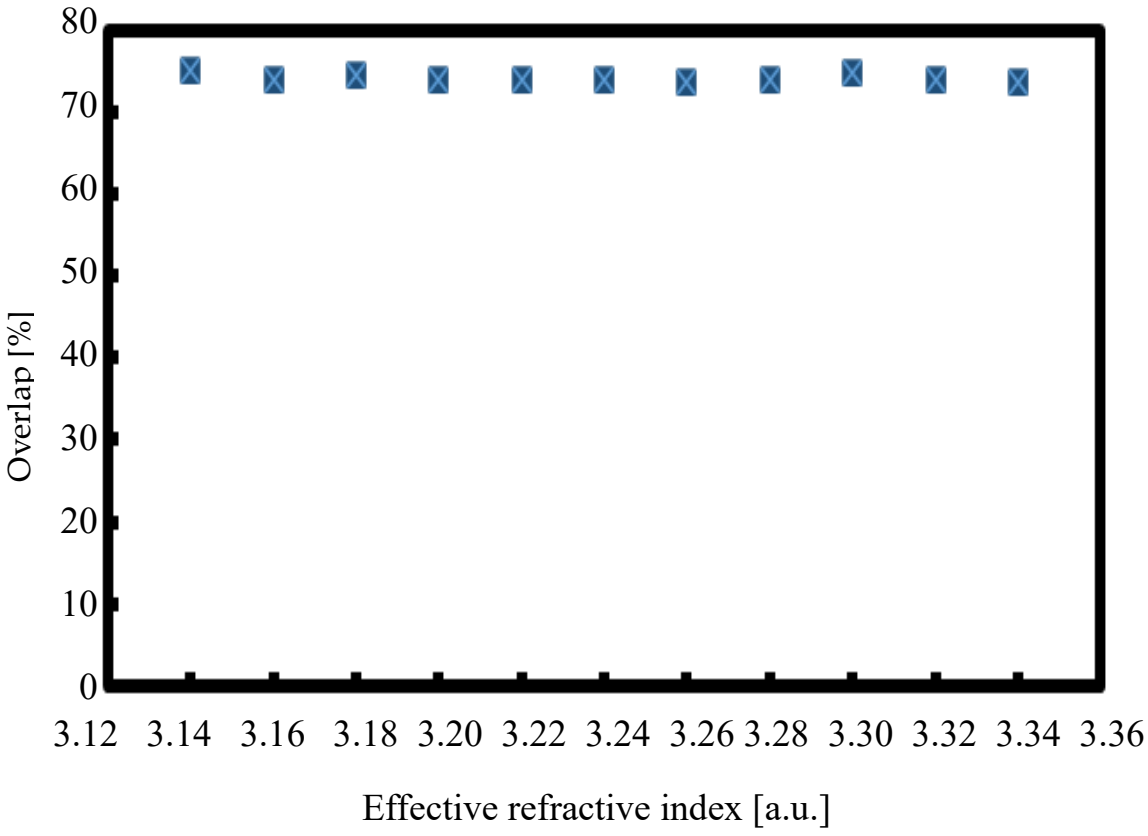

Fig 5.12. overlap ratio of two light with different arm length (@ 360 μm of total active-MMI LD length and 220 μm of MMI area).

5.4.2 Temperature

In addition to the carrier plasma effect, temperature is another factor that needs to be taken into consideration as rising temperatures lead to a narrower bandgap, consequently increasing the refractive index. During experimental procedures, it is essential to employ a temperature controller to maintain and stabilize the operating conditions at room temperature. This ensures that temperature-related effects are controlled and minimized. The real temperature inside active-MMI LD, however, is still different from the setting temperature [9]. The Varshni relation [10] for the temperature dependence of semiconductor band gaps is

$$E_g(T) = E_0 - \alpha T^2/(T + \beta) \tag{5.18}$$

where α and β are fitting parameters characteristic of a given material [44]. Gupta and Ravindra [11] express the refractive index and energy bandgap as

$$n = 4.16 - 1.12E_g + 0.31E_g^2 - 0.08E_g^3 \tag{5.19}$$

Using the eq. (5.18) and (5.19), refractive index variation Δn in active-MMI LD is far less than ±0.1 when the temperature rises from 290 K to 310 K. As the simulation result shown in Fig. 5.11, the desired coupling ratio is kept.

5.4.3 Fabrication tolerance

In the end, the fabrication tolerance is discussed. The single output port in section 3 of active-MMI LD configuration relies on self-image phenomenon in MMI section, which is significantly affected by the width of MMI section [12]. With fabrication error, the overlap between two modes and the optical loss will be affected which affects laser performance. Therefore, the optical loss and the overlap variation with the width difference are calculated and the results are shown in Fig. 5.13. The optical loss of the optimum active-MMI LD is 0.78 dB. It rises with the increase of width difference. When the width difference is within ± 150 nm, the optical loss is below 1 dB. To the overlap, within the width difference at ±150 nm, the overlap is stabilized with the range of 72% to 74%. Given that the overlap and the optical loss within width difference at ± 150 nm remains minimal, the fabrication tolerance of active-MMI LD is ±150 nm. The fabrication tolerance is now about 100 nm to 300 nm, which suggests the active-MMI structure is able to be realized by the fabrication process available now.

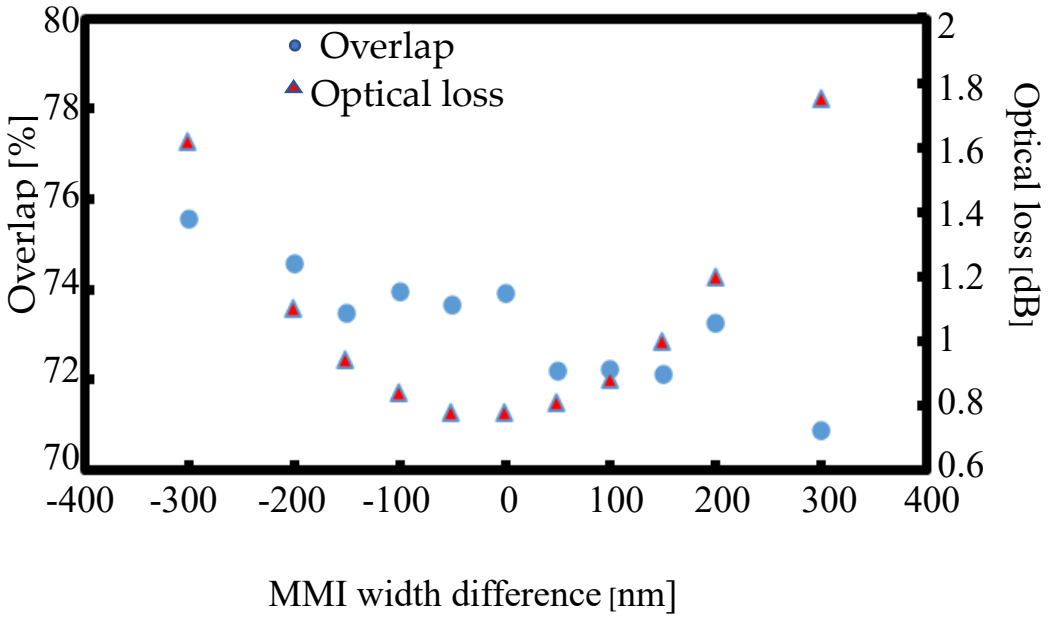

Fig 5.13. Overlap ratio and optical loss with different MMI widths.

5.5 Modulation speeds over 100 Gbps

As is indicated in these rate equations in chapter 3, PPR phenomenon is related to the modulation response of the sub-lasing mode. When there are more than one sub-lasing modes, plural PPRs will be realized, and the modulation bandwidth is able to be extended. It provides the possibility to extend the modulation bandwidth of laser diode by adding lasing modes to generate PPR phenomena. Active-MMI laser diode is an ideal structure to exploit plural PPRs as it is naturally accessed to different waveguides which secure plural lasing modes for the generation of plural PPRs.

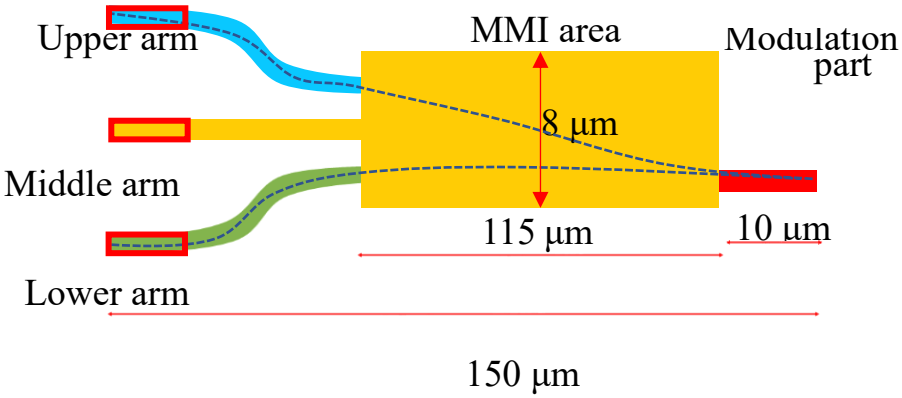

Fig.5.14 1×3 active-MMI laser diode configuration

Figure. 5.14 shows 1×3 active-MMI laser diode configuration for plural PPRs. The active-MMI laser has been divided into three parts. In the middle of the 1×3 active-MMI laser diode is the MMI area. In the LHS, there are two bending waveguides and one straight waveguide connected to the MMI area. In the RHS, there is one straight waveguide accessed to MMI area as the modulation port. As shown in Fig.5.14, three different lasing modes exist in that configuration. A similar configuration has been reported to observe multiple PPRs. The damping problem between CPR and PPR, PPR and PPR, however, is restricted to the modulation bandwidth [13]. It implies that to extend the modulation bandwidth by utilizing plural PPRs, the position of PPRs has to be engineered to avoid the damping problems between resonances.

The first strategy to compensate for the damping problem between CPR and PPR is shortening the length of whole device to achieve relatively high CPR. In the proposed configuration, the length of whole cavity is about

150 μm to achieve a CPR around 20 GHz. Then, the modulation response with plural PPRs was calculated to examine the location of PPRs. The simulation result is shown in Fig 5.15.

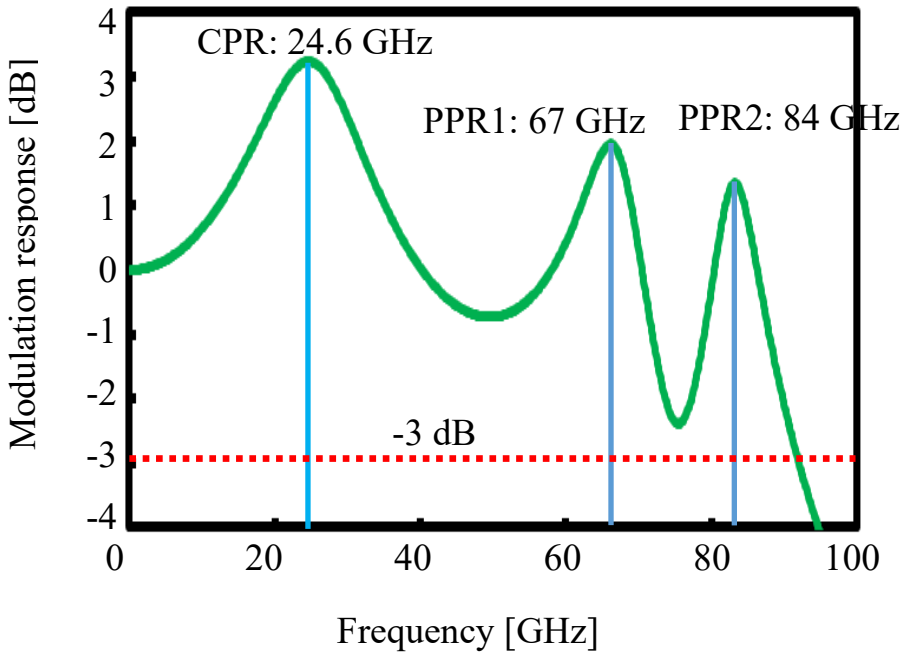

Fig.5.15 Simulation modulation response of plural PPRs

As CPR is located at 24.6 GHz, one PPR located at 67 GHz is observed. The existence of PPR at 67 GHz enables the modulation bandwidth to extend to 76 GHz. Since the modulation response of PPR at 67 GHz declines sharply, to achieve modulation bandwidth over 90 GHz, another PPR is required to compensate for the damping caused by PPR located at 67 GHz. As is shown in Fig 5.15, this damping problem can be conquered to design another PPR at 84 GHz. In that way, the modulation bandwidth is 92 GHz.

To examine the quality of the modulated active-MMI laser diode, the eye

pattern was calculated with 100 Gbps NRZ signal. The result is shown in Fig 5.16. Under the modulation bandwidth over 90 GHz, a clearly opened eye pattern was observed with an extinction ratio at 6 dB.

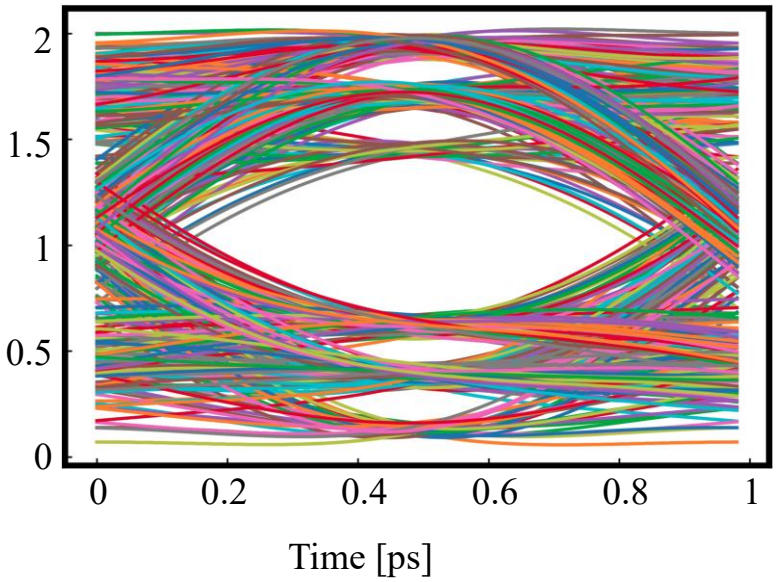

Fig. 5.16 Simulation result 100 Gbps NRZ modulation response under

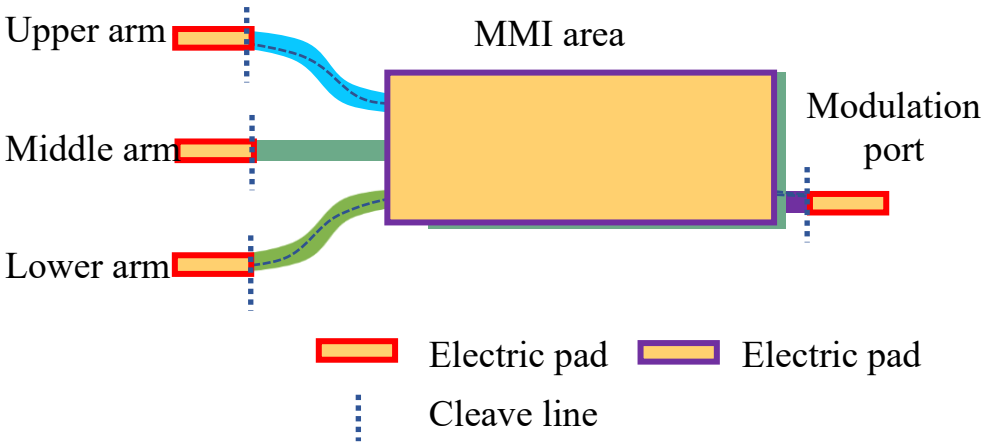

Fig.5.17 1×3 Active-MMI laser diode configuration of electric pad

The distribution of the electric pad of each path is shown in Fig. 5.17. To control the PPR, 5 electric pads are designed. The blue dot line is a cleaving line which is electrically separated from MMI area and arm area. Each electric pad will be connected to a laser driver to obtain current injection. As one may notice, in Chapter 3, only one current injection is in the rate equation that we used to describe the PPR phenomenon. In this actual design, 5 different electric pads suggest that there will be 5 different current injections. The rate equation in Chapter 3 is insufficient to explain PPR in multiple current injections. In fact, for the 3 electric pads in the arm parts (red rectangle), the current injection in these parts is not supposed to generate photons. As shown in Fig.5.18, it is depicted the relationship between the carrier and the current injection. In the phase control, the carrier plasma effect will be utilized. The refractive index of the laser varies with the carrier density. It is in the unlasing phase that the carrier density changes dramatically. When the laser starts to lase, the carrier density almost stays the same. Based on that fact, it is not predicted that the photon density generated in that phase control area has an impact on the PPR phenomenon.

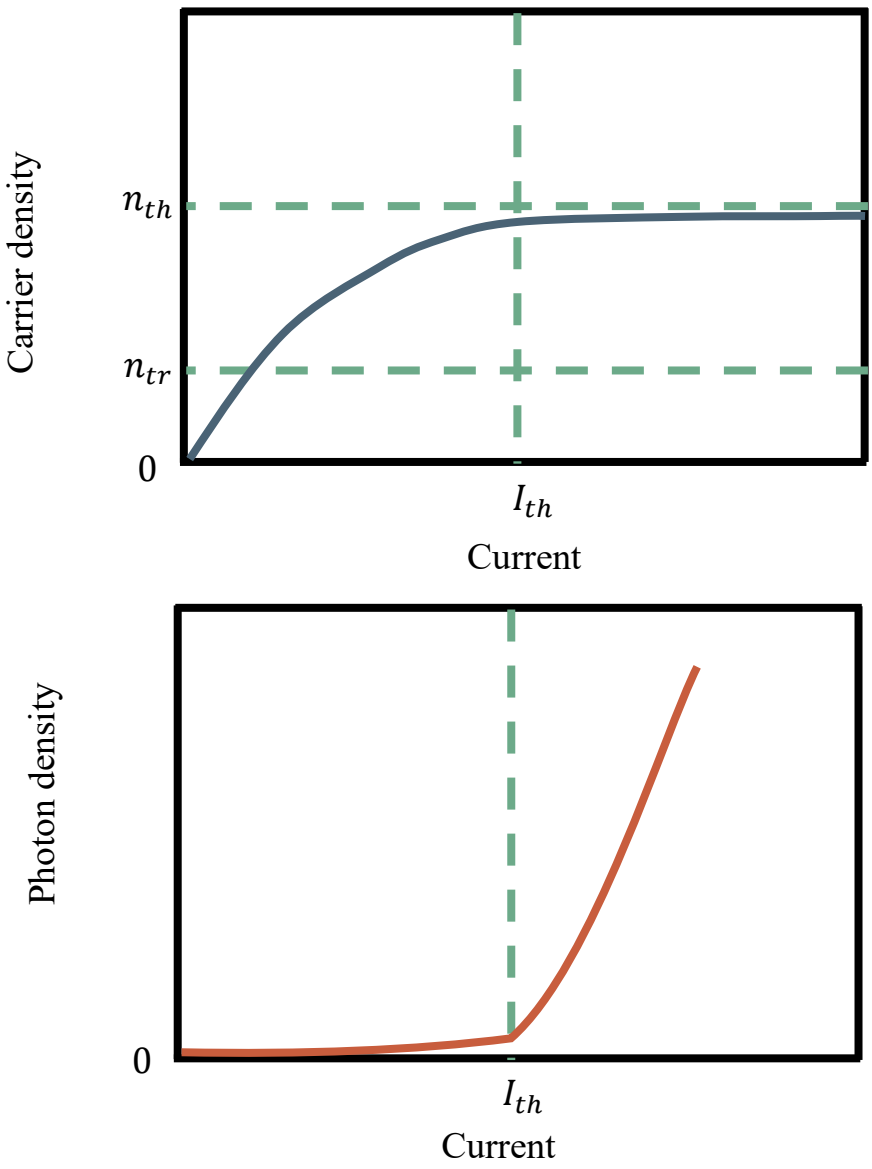

Fig.5.18 Carrier density and photon density vs. the current.

As for the modulation, the carrier density fluctuates with the current injection. The relationship between modulation and carrier density is explained in Fig. 5.19. In the beginning, at the stable current injection of $1.1I_{th}$, the carrier density is kept as the threshold carrier density. From the moment labeled with red spot in Fig. 5.19, the current injection is changed from $1.1I_{th}$ to $2I_{th}$. There is carrier density fluctuation. The variation in

carrier density results in a variation of the refractive index. As shown in Fig. 5. 19. The variation of the carrier density is limited in $\pm 0.003 n_{th}$. The difference in effective refractive index Δn would be lower than 0.1 [8]. As the calculation results shown in Fig. 5. 12, This kind of carrier density fluctuation has less impact on the PPR phenomenon.

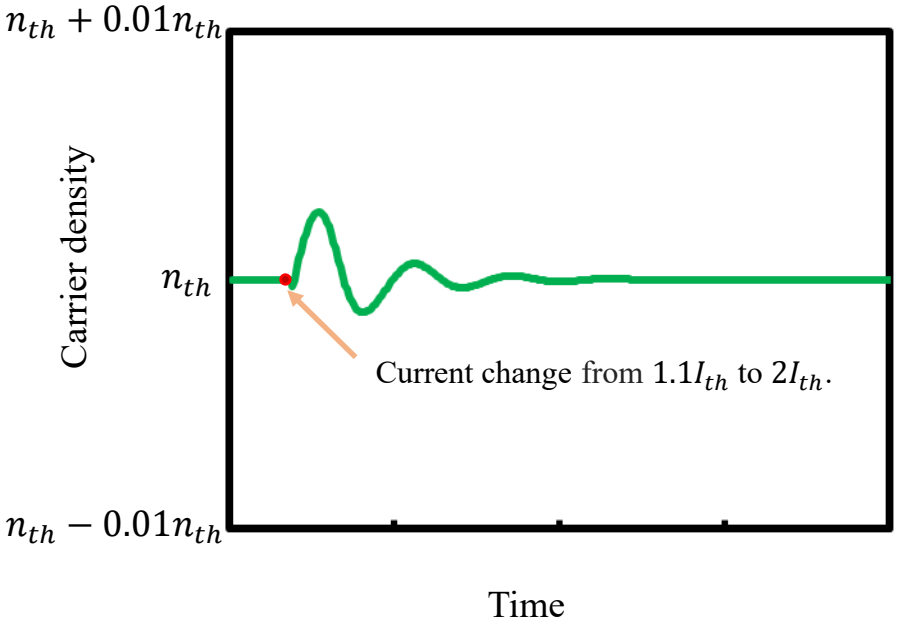

Fig.5.19 Carrier density variation vs. the current change.

The tendency of the intensity of PPR with current change is shown in Fig. 5.20.

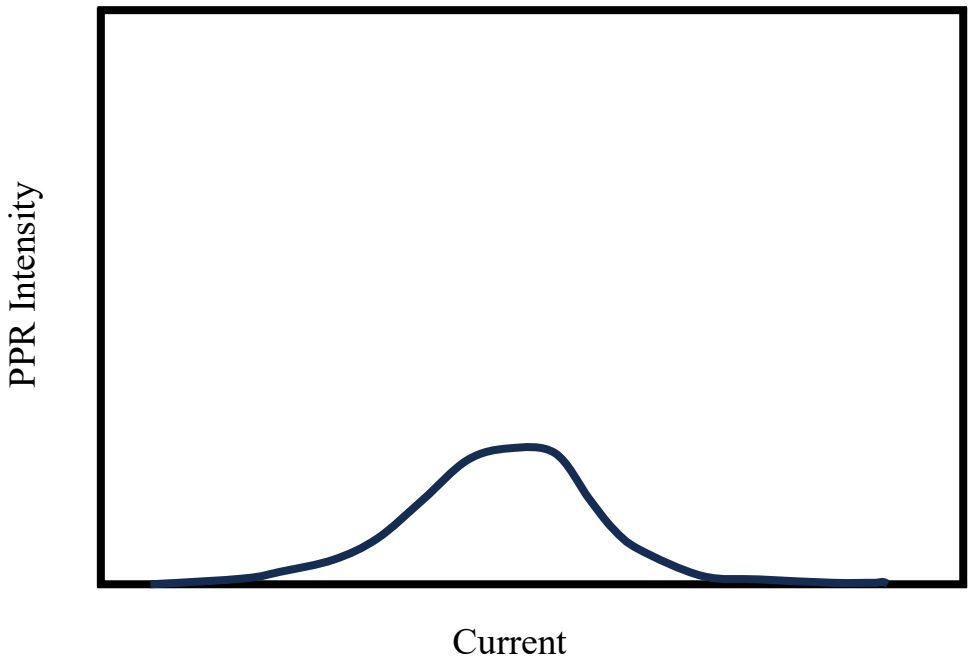

Fig.5.20 PPR intensity vs. the current.

Reference

[1] Soldano, L. B., & Pennings, E. C. Optical multi-mode interference devices based on self-imaging: principles and applications. Journal of lightwave technology, vol .13, no. 4, pp. 615-627, (1995).

[2] Bachmann, M., Besse, P. A., & Melchior, H. General self-imaging properties in N× N multimode interference couplers including phase relations. Applied optics, vol.33, no. 18, pp. 3905-3911, (1994).

[3] Błahut, M., & Opilski, A. Multimode interference structures: new way of passive elements technology for photonics. Opto-Electronics Review, vol. 9, no. 3, pp. 293-300, (2001).

[4] J. Van Roey, J. van der Donk, and P. E. Lagasse, “Beam-propagation method: analysis and assessment,” vol. 71, issue 7, pp.803-810, (1981).

[5] Huang, W. P., Xu, C. L. Simulation of three-dimensional optical waveguides by a full-vector beam propagation method. IEEE journal of quantum electronics, vol. 29, no. 10, pp. 2639-2649, (1993).

[6] Coldren, L. A.; Corzine, S. W.; Mashanovitch, M. L. 2nd ed.; Diode lasers and photonic integrated circuits. John Wiley & Sons, pp.260-279.

[7] J. Manning, R. Olshansky and C. B. Su, "The carrier-induced index change in AlGaAs and 1.3 μm InGaAsP diode lasers", IEEE J. Quantum Electron,Vol. QE-19, pp. 1525-1530, (1983)

[8] B. R. Bennett, R. A. Soref and J. A. Del Alamo, "Carrier-induced change in refractive index of InP, GaAs and InGaAsP," in IEEE J.

Quantum Electron, vol. 26, no. 1, pp. 113-122, (1990).

[9] Zang, Z.; Mukai, K.; Navaretti, P.; Duelk, M.; Velez, C., Hamamoto, K. “Thermal resistance reduction in high power superluminescent diodes by using active multi-mode interferometer.” Appl Phys Lett, vol. 100, no. 3, pp. 031108, (2012).

[10] Varshni, Y. P. “Comparative study of potential energy functions for diatomic molecules.” Reviews of Modern Phys, vol..29, no. 4, pp. 664-682, (1957).

[11] Varshni, Y. P. “Temperature dependence of the energy gap in semiconductors.” Physica, vol. 34, no. 1, pp.149-154, (1967).

[12] Hamamoto, K.; Jiang, H. Active MMI devices: concept, proof, and recent progress. J of Phys D: Appl Phys, vol 48, no. 38, pp. 383001, (2015).

[13] S. Murakami, B. Hong, H. Jiang and K. Hamamoto, "Observation of 60 GHz and 20 GHz Multiple Photon-Photon Resonances Using Active Multimode Interferometer Laser Diodes," 2019 24th Microoptics Conference (MOC), Toyama, Japan, 2019, pp. 304-305.

Chapter 6

Conclusion and outlook

6.1 Conclusion

In the upcoming future, it is predicted that Tbps level devices will be equipped in small devices such as personal computer, smart phone and IoT service. With the purpose of Tbps level, wavelength division multiplexing technology (WDM) and mode division multiplexing technology (MDM) have been proposed. All technologies require high-speed modulation in one channel. According to the requirement of application in small devices, directly modulated lasers (DMLs) are a promising candidate with merits of high-modulation speed, compact size and low energy consumption. The modulation bandwidth of DMLs is limited by the relaxation oscillation, which is also called carrier photon resonance (CPR). To overcome this problem, photon-photon resonance (PPR) phenomenon has been proposed. It suggests that multiple PPRs is a prospective technique to extend modulation bandwidth of DMLs. Active-multimode interferometer (MMI) laser was proposed to explore multiple PPRs. Two PPRs was observed experimentally. The problem limited the utilization of multiple PPRs, however, lies in the damping-issue between resonances (CPR and PPR, PPR and PPR). Besides, as Fabry-Perót (F-P) laser, it is concluded that PPR

phenomenon is not able to be observed in F-P laser as the mode orthogonality.

In this work, firstly, the existence of PPR in active-MMI laser has been clarified. Since active-MMI laser is naturally accessed with different waveguides, non-orthogonal modes exist that multiple PPRs appears. Secondly, aiming to overcome the damping problem, the PPR control scheme is discussed. Electromagnetic wave theory in laser was applied to obtain laser rate equation with PPR phenomenon. Several key parameters related to PPR phenomena have been discussed. With the theoretical small signal analysis, the affection of high intensity of PPR to large signal modulation has been investigated. Contradicted to our prediction, high intensity of PPR is an advantage factor to large signal modulation. Based on the small signal analysis and large signal analysis, the structure of the optimized active-MMI laser diode was proposed. Furthermore, with the purpose of 100 Gbps modulation speed, a 1×3 active-MMI LD with optimized plural PPRs was also proposed.

6.2 Outlook

As all the devices have been designed, the future work mainly resides on the following issues:

1. Fabricating those active-MMI devices to confirm PPR theory and multiple PPRs theory.

2. To realize a Tbps level device, high modulation bandwidth device (over 100 GHz or 200 GHz) is desired. As the indication of the rate equation with PPR, it is possible to generate plural PPRs in one configuration by adding plural sub-modes. with the manipulating scheme proposed in this dissertation, the modulation bandwidth of the directly modulated laser would be extended over 100 GHz. The next step of this research is to study the active-MMI laser structure with plural PPRs. For higher modulation bandwidth, compact configuration is required of configuration-minimized techniques such as nano-pixel are needed to be studied.
3. The ultimate objective of this work is to integrate a chip with a laser diode equipped with smart-photon and IoT devices. Thus, the module of such an application is necessary.

Acknowledgement

It was a long and lonely journey. Because of the pandemic, everything turned to be more difficult. All the connection between each other seemed to be cut all of sudden. One should wear mask every day; One could not come back to its homeland; One could not attend the academic conference in person. In this devastated time, my parents are always there for me. I would like to express my gratitude to my parents, Gejiao He and Yang Xiao, at the first. Though they disagree me to study aboard, they respect my decision and support me after that. Without their support, I might not finish this journey. I am so grateful for being their daughter.

I would also like to thank Dr. Prof. Kiichi Hamamoto, my supervisor, who gave me all the best and most kind guidance. For the past 4 and half years, not only did he support and teach me how to be a researcher, but also how to be efficiency. I benefit a lot from it. I do believe that it would the fortune of my life.

I would like to thank assistant professor Dr. Haisong Jiang. She helped me in my research and my daily life. She is also my “Japanese teacher”. Though I could not speak Japanese as fluent as her, I will do my endeavor to be a female researcher as her in the future.

I would also like to thank Miss. Sara Bruhier for her kind help and encourage. Mr. Shigo Murakami, Keiichiro Shoda, Keiichiro Koudu, Yudai

Kawano and Zhenyu Chu, as my teammates, have worked with me in these 4 years. They supported me in the research and also lent their hand to me when I got trouble in daily life.

Except for help from Hamamoto Lab, I would like to express my gratitude to my friends. Despite we separate to each other by distance, we motivate each other when we feel lost and share the joy when we make progress.

For the past 4 and half years, I've cried and laughed, worked hard, and also experienced moments of despair in Fukuoka. Fukuoka has embraced everything of me. I think she is part of me now. Thank you, Fukuoka.

Yes, it was a long and lonely journey, but I am not alone with all these helps.

To everyone who has helped me, a thousand of emotions and sentences come together in one word: Thank you.